PB-213 902

INITIAL MIXING IN COAGULATION PROCESSES

Richard J. Stenquist, et al

National Environmental Research Center
Cincinnati, Ohio

November 1972

DISTRIBUTED BY:

NTIS
National Technical Information Service
U. S. DEPARTMENT OF COMMERCE
5285 Port Royal Road, Springfield Va. 22151

EPA-R2-72-053
NOVEMBER 1972

W73-03511

PB 213 902

Environmental Protection Technology Series

Initial Mixing in Coagulation Processes

Reproduced by
NATIONAL TECHNICAL
INFORMATION SERVICE
U S Department of Commerce
Springfield VA 22151

Office of Research and Monitoring
U.S. Environmental Protection Agency
Washington, D.C. 20460

167

RESEARCH REPORTING SERIES

Research reports of the Office of Research and Monitoring, Environmental Protection Agency, have been grouped into five series. These five broad categories were established to facilitate further development and application of environmental technology. Elimination of traditional grouping was consciously planned to foster technology transfer and a maximum interface in related fields. The five series are:

1. Environmental Health Effects Research
2. Environmental Protection Technology
3. Ecological Research
4. Environmental Monitoring
5. Socioeconomic Environmental Studies

This report has been assigned to the ENVIRONMENTAL PROTECTION TECHNOLOGY series. This series describes research performed to develop and demonstrate instrumentation, equipment and methodology to repair or prevent environmental degradation from point and non-point sources of pollution. This work provides the new or improved technology required for the control and treatment of pollution sources to meet environmental quality standards.

SELECTED WATER RESOURCES ABSTRACTS
INPUT TRANSACTION FORM

1. Report No.

2.

3. Accession No.
W 73-03511

4. Title
INITIAL MIXING IN COAGULATION PROCESSES

5. Report Date ~~March 1972~~

6.

8. Performing Organization Report No. ~~[illegible]~~

7. Author(s)
Stenquist, R. J., Kaufman, W. J.

10. Project No. EPA Project 17030 DLX

9. Organization
California University, Berkeley,
Sanitary Engineering Research Laboratory.

11. Contract/Grant No.
~~17030 [illegible]NG~~

13. Type of Report and Period Covered

12. Sponsoring Organization

15. Supplementary Notes
Environmental Protection Agency report ~~number~~ EPA-R2-72-053, November 1972. 161p, 40fig, 4tab, 69ref, append

16. Abstract

This investigation was undertaken with the objective of determining the importance of the initial mixing step in water and wastewater treatment processes and determining whether increasing the rapidity of the initial mixing could improve process performance. The principal process considered was alum coagulation-flocculation of a kaolin suspension in water. The initial mixing device under consideration was a biplane, square-mesh grid of bars placed in a turbulent flow, tubular reactor; a 2-in. pipe was used in the present studies. Studies were made using a single electrode "point" conductivity probe and NaCl solution tracer to determine what parameters affect the mixing which occurs in the turbulent flow field downstream from a grid, and from these results a general mixing model was developed. The relation between initial mixing and process performance was studied by using two of the grids from the mixing studies as initial mixing devices in coagulation of a kaolin suspension. (EPA abstract)

17a. Descriptors
*Mixing, *Turbulence, *Coagulation, *Water treatment, Conductivity, Chlorination, Flocculation, *Wastewater treatment

17b. Identifiers
*Initial mixing, Conductivity Probes, *Kaolin suspension

EP 1.23/2:72-53

Copy available [illegible], $2.25 [illegible]
from NTIS as PB 213902, [illegible].

17c. COWRR Field & Group 05F, 05D

18. Availability

19. Security Class. (Report)

20. Security Class. (Page)

21. No. of Pages

22. Price

Send To:
WATER RESOURCES SCIENTIFIC INFORMATION CENTER
U.S. DEPARTMENT OF THE INTERIOR
WASHINGTON, D.C. 20240

Abstractor

Institution

WRSIC 102 (REV. JUNE 1971)

GPO 913.261

EPA-R2-72-053
November 1972

INITIAL MIXING IN COAGULATION PROCESSES

by

Richard J. Stenquist
Warren J. Kaufman

Project 17030 DLX

Details of illustrations in
this document may be better
studied on microfiche

Project Officer

Dr. Sidney A. Hannah
National Environmental Research Center
Environmental Protection Agency
Cincinnati, Ohio 45268

Prepared for

OFFICE OF RESEARCH AND MONITORING
U.S. ENVIRONMENTAL PROTECTION AGENCY
WASHINGTON, D. C. 20460

Ib

For sale by the Superintendent of Documents, U.S. Government Printing Office
Washington, D.C., 20402 - Price $2.25

EPA Review Notice

This report has been reviewed by the Environmental Protection Agency and approved for publication. Approval does not signify that the contents necessarily reflect the views and policies of the Environmental Protection Agency, nor does mention of trade names or commercial products constitute endorsement or recommendation for use.

CONTENTS

Section		Page
I	Summary and Conclusions	1
II	Recommendations	5
III	Introduction	7
IV	Review of Fundamental Theory: Turbulence, Mixing and Coagulation	11
V	Mixing Studies: Apparatus and Methods	47
VI	Mixing Studies: Results and Analysis	71
VII	Initial Mixing and Alum Coagulation — Flocculation	91
VIII	Acknowledgments	115
IX	Appendices	117
X	Glossary	151
XI	References	157

Preceding pages blank

FIGURES

		PAGE
1	MEAN AND FLUCTUATING COMPONENTS OF VELOCITIES	13
2	LONGITUDINAL AND LATERAL CORRELATION FUNCTIONS AND LATERAL MICROSCALE, λ_g, FOR ISOTROPIC TURBULENCE	15
3	DECAY OF TURBULENCE AS MEASURED BY VARIOUS INVESTIGATORS	22
4	INTEGRAL SCALE OF TURBULENCE AS MEASURED BY VARIOUS INVESTIGATORS	23
5	UNIVERSAL FORMS OF SCALAR AND VELOCITY SPECTRA	29
6	CONCENTRATION OF VARIOUS ALUMINUM SPECIES IN EQUILIBRIUM WITH FRESHLY PRECIPITATED $Al(OH)_3$	36
7	EFFECT OF COLLOID CONCENTRATION ON COAGULANT REQUIRED FOR DESTABILIZATION (AT CONSTANT pH)	40
8	FRACTIONAL CONVERSION AS A FUNCTION OF ACCOMPLISHED MIXING	45
9	ILLUSTRATION OF CONDUCTIVITY PROBE	51
10	SINGLE ELECTRODE CONDUCTIVITY PROBE	52
11	PROBE IN PLACE IN TUBULAR REACTOR	52
12	BLOCK DIAGRAM FOR TEKTRONIX TYPE 3C66 CARRIER AMPLIFIER	54
13	AC BRIDGE CIRCUIT	55
14	PROBE CONNECTED IN PARALLEL WITH 120-OHM RESISTOR	57
15	TYPICAL CALIBRATION CURVE FOR SINGLE ELECTRODE CONDUCTIVITY PROBE	59

FIGURES (Continued)

		PAGE
16	ELECTRONIC EQUIPMENT FOR MIXING EXPERIMENTS	60
17	SCHEMATIC ILLUSTRATION OF EXPERIMENTAL SETUP FOR MIXING EXPERIMENTS	61
18	CUTAWAY VIEW OF INJECTION MANIFOLD AND GRID SECTION	63
19	CUTAWAY VIEW OF PROBE SECTION	64
20	MULTIPLE-ORIFICE GRID	66
21	INJECTION MANIFOLD AND GRID SECTION	66
22	HEAD LOSS COEFFICIENTS FOR SQUARE-MESH GRIDS	69
23	DECAY OF CONCENTRATION FLUCTUATIONS DOWNSTREAM FROM A GRID	72
24	a' vs. Q_T FOR GRID WITH $M/d = 4$	75
25	EFFECT OF SCALE OF TURBULENCE ON SCALAR DECAY RATE	77
26	EFFECT OF THE NUMBER OF ORIFICES ON SCALAR DECAY RATE	79
27	INVERSE RELATIONSHIP BETWEEN NUMBER OF SOURCES AND α FOR GRIDS WITH $M/d = 4$	80
28	EFFECT OF CHANGING ORIENTATION OF TRACER INJECTION SYSTEM ON SCALAR DECAY RATE	82
29	RESULTS OBTAINED FROM GEOMETRICALLY SIMILAR GRIDS	84
30	EFFECT OF VARYING M	85
31	GENERAL MIXING MODEL: RESULTS FOR SEVEN GRIDS	90

FIGURES (Continued)

		PAGE
32	EFFECT OF SEGREGATION ON COAGULATION-FLOCCULATION JAR TESTS	95
33	RELATION OF pH AND ALKALINITY AT "OPTIMUM" ALUM DOSAGES	96
34	INITIAL MIXING APPARATUS FOR CONTINUOUS FLOW COAGULATION-FLOCCULATION STUDIES	99
35	EFFECT OF INITIAL MIXING DEVICE ON FLOCCULATION PERFORMANCE: SINGLE COMPARTMENT, T = 5 MIN	106
36	EFFECT OF INITIAL MIXING DEVICE ON FLOCCULATION PERFORMANCE: TWO COMPARTMENTS, T = 10 MIN	107
37	EFFECT OF INITIAL MIXING DEVICE ON FLOCCULATION PERFORMANCE: THREE COMPARTMENTS, T = 15 MIN	108
38	EFFECT OF SEGREGATION ON COAGULATION-FLOCCULATION: CONTINUOUS FLOW TESTS	109
39	EFFECT OF INITIAL MIXING ON FLOCCULATION PERFORMANCE: COMPARISON BETWEEN FLASH MIXER AND NO INITIAL MIXING UNIT, ALKALINITY = 70 mg/ℓ	110
40	SEGREGATION JAR TESTS FOR VARIOUS SEGREGATION TIMES – ALUM COAGULATION OF RAW SEWAGE	113

TABLES

No.		Page
1	Types of Reactions Involved in Hydrolysis of Al(III)	38
2	Grid Characteristics	65
3	Head Loss Through Grids at Various Velocities	70
4	Aggregation Rate Coefficients for Continuous Flow Experiments	109

SECTION I

SUMMARY AND CONCLUSIONS

The purpose of this investigation has been to determine criteria for the design of turbulent flow, tubular reactors for the initial mixing of chemicals in water treatment processes using a biplane grid to inject the chemical and produce the turbulence. Initial mixing is important because certain physical-chemical reactions, if they occur before the mixing of the chemical with the main stream, are detrimental to process performance. Use of a grid initial mixer can provide a more rapid mixing of the chemical with the waste stream. The principal process under consideration was alum coagulation-flocculation of turbid suspensions in the clarification of surface waters. Other processes considered were wastewater chlorination and chemical coagulation of wastewater with alum or ferric chloride.

A salt solution tracer and a single electrode conductivity probe used in conjunction with an AC bridge amplifier and an rms voltmeter were utilized to determine the parameters governing the mixing which occurs when a tracer is injected into a tubular reactor through multiple orifices. An attempt was made to correlate the results to allow prediction of the mixing characteristics for other grids.

Two of the grids used in the mixing studies were then utilized as initial mixing units in a pilot-scale coagulation-flocculation of a kaolin suspension, and the results were compared with those obtained using a flash mixer. It was possible to attain some understanding of the time of mixing necessary to obtain better process performance. It should be emphasized that while the prediction of mixing produced by larger grids may be possible, the larger grids will necessarily produce greater times of mixing and poorer process performance. Part of the prototype design problem will be the construction of a fairly fine grid mesh in relatively large conduits.

Attempts were also made to determine whether the initial mixing step is important in coagulation or chlorination of wastewater. Specific conclusions follow.

MIXING EXPERIMENTS

Sections V and VI describe experiments intended to ascertain the parameters which determine the degree of mixing downstream from a grid in a turbulent flow, tubular reactor. A summary of the results is as follows:

1. Mixing in a grid type tubular reactor takes place in two stages. The first, termed wake-mixing, takes place in a region very close to the grid bars as the tracer spreads out across the cross-section of the reactor. The rms concentration fluctuation just downstream from the wake-mixing region may be less than 1% of the calculated initial rms concentration fluctuation, $a'_o = A_T \sqrt{Q_T/Q_M}$. However, beyond the region of wake-mixing, the "point" concentration may still vary considerably from the spatial mean concentration. The second stage occurs in a region which begins at a point several grid bar diameters downstream from the grid. In this region isotropic turbulence and scalar fields exist, and the decay of rms concentration fluctuations with time or distance from the grid can be plotted as a straight line on log-log paper.

2. The scale of turbulence has a definite effect on the scalar decay rate in the region where isotropic turbulence is present — beyond the region of wake-mixing. For example, small grid bars result in a lower rate of decay than large bars, and the scale of turbulence is proportional to the grid bar diameter.

3. The number of tracer injection orifices per unit area of reactor cross-section does not appear to have a marked effect on the rate of scalar decay. It does, however, greatly influence the extent of wake-mixing and will be important when large conduits are considered for tubular reactors in prototype treatment plants.

4. The direction of tracer injection (upstream or downstream) has a marked influence on the rate of scalar decay (and also on the wake-mixing), it being greatest when the injection orifices face upstream. As the turbulent flow field is essentially independent of the manner in which the tracer is introduced, it must be concluded that the scalar decay rate must be dependent on characteristics of the scalar field — possibly the scale of segregation.

5. Scalar decay downstream from a grid follows the relation

$$\frac{a' n_s}{\bar{A}} = \alpha'' (x/d)^{-a}$$

where a' is the rms concentration fluctuation, $\bar{A}$ is the mean concentration of the tracer mixed with the main flow, n_s is the number of orifices per unit area of reactor cross-section, α'' is a coefficient which depends on the method of scalar injection, x is the distance downstream from the grid, d is the grid bar diameter, and a is the scalar decay rate which is dependent on the method of scalar injection and the grid bar diameter.

6. It appears that head losses incurred by grid mixing devices can be kept to less than 6 in. providing the M/d ratio, the ratio of the center-to-center bar spacing to bar diameter, is greater than about 3.0 (solidity less than approximately 50%). Allowable head loss, of course, will depend on the specific details of each situation.

TREATMENT PROCESSES

The effect of initial mixing in three treatment processes, alum coagulation of a kaolin suspension, chlorination of wastewater, and chemical coagulation of wastewater, was studied. The conclusions for each process are given below:

Alum Coagulation of a Kaolin Suspension

7. The crucial "reactions" which occur are very rapid. This was demonstrated by the fact that in a continuous flow experiment, a high-speed flash mixer produced turbidity removals which were no better than those obtained when the alum feed solution was added directly to the first compartment of the pilot-scale flocculator, a very poor initial mixing situation.

8. Performance was improved by using grid initial mixers (d = 1/8 in., M/d = 4) in a 2-in. diameter tubular reactor. One grid had 24 tracer injection orifices; the other had 4. The value of n_s, the injection orifice density, for each was 7.60 in.^{-2} and 1.27 in.^{-2}, respectively. Improvement in performance over that of a flash mixer was obtained with both grids, and the 24-orifice grid performed better than the 4-orifice grid. From the results obtained, it can be estimated that an orifice density of at least 1.0 in.^{-2} is needed to effect a significant improvement in performance. From both a structual aspect and from consideration of head loss inside the grid bars, this fine a grid for a prototype plant may be somewhat difficult to construct. Such techniques as placing smaller grids within larger grids would probably be necessary.

9. It was found that the alkalinity of the raw water had a strong influence on the importance of the initial mixing step, the effect of rapid mixing increasing with increasing alkalinity. This may be due to the buffering effect of the alkalinity (the reaction rates and products appear to be pH dependent), or it may be due to more direct action of the bicarbonate ion. Jar tests which simulate slow and rapid initial mixing were utilized to demonstrate the effect of the alkalinity. The effect was also seen in the continuous flow experiments.

Chemical Coagulation of Wastewater

10. To determine whether the initial mixing step may be important in chemical coagulation of sewage, segregation jar tests similar to those used with kaolin were done with sewage using alum as the coagulant. It was found that, as with alum coagulation of a kaolin suspension, the rapid initial mixing did provide better results. More importantly, the crucial reactions in sewage are apparently much slower than is the case with kaolin suspensions. This means that it is not necessary to have the high scalar injection orifice density required in the other process, and the resultant design difficulties may not occur.

11. While these results may be extrapolated to include ferric chloride coagulation of sewage, it has been found in other work that in lime coagulation of sewage, the initial mixing step does not appear to be critical.

Chlorination of Wastewater

12. Several experiments (described in Appendices A and B) were done in order to determine if the initial mixing might be a crucial step in that treatment process. The results indicated that while at short contact times an improvement in performance (as measured by coliform survival ratio) can be found, at contact times similar to those found in practice no difference in performance could be discerned. It does appear from the work of others that a tubular (plug flow) reactor, as opposed to a back-mixed reactor, may improve performance.

SECTION II

RECOMMENDATIONS

The recommendations resulting from this study can be divided into two general areas: 1) designing a grid for full-scale plant experiments and 2) continuing studies of the wake-mixing phenomenon.

The present investigation has shown that in pilot-scale operations, initial mixing is an important step in alum coagulation-flocculation of a clay suspension. It remains to be shown that sufficiently rapid mixing can be effected in a full-scale treatment plant to provide a significant improvement in performance. Future studies in initial mixing should be directed toward this objective.

From the present studies it appears that wake-mixing may be critical. From the results obtained it can be estimated that an injection orifice density of at least 1.0 in.$^{-2}$ is needed to obtain a significant improvement in performance. The grid, however, must be fine enough to allow the orifices to be spread evenly across the reactor cross-section. With M/d = 3, 1/2-in. O.D. bars spaced 1-1/2 in. center-to-center would be required for a biplane grid. An orifice would be located halfway between each grid bar intersection. A grid consisting of one row of bars would necessitate 1/2-in. bars spaced 1 in. center-to-center (solidity = 50%).

It would be desirable to have grids with orifice densities greater than 1 in.$^{-2}$. To accomplish this, finer grids will have to be constructed. Placing small grids (e.g., 1/4-in. bars spaced 1/2-in. center-to-center) within larger grids (e.g., 1-1/2-in. bars spaced 6-in. center-to-center) used to feed the coagulant into the smaller bars is one way of attacking the problem.

In such a demonstration it would be desirable to keep the head loss to less than about 6 in. Solidities between approximately 25% and 50% will usually accomplish this.

Since the effect of initial mixing depends upon the alkalinity of the water, any plant-scale projects should be done with a water of high alkalinity, preferably greater than 100 mg/ℓ.

One area of possible exploration is the use of grids at more than one point along a tubular reactor. It should be noted, however, that this simulates backmixing, and if backmixing is detrimental to process performance, the expected improvement may not be realized.

Use of grid initial mixers for other treatment processes should also be considered. It seems that rapid initial mixing can result in a significant improvement in chemical coagulation of wastewater, a process which is often found in advanced waste treatment schemes. It is believed that the injection orifice density need not be as great as that required for coagulation of kaolin suspensions. While it appears from the present investigation that the initial mixing step in wastewater disinfection is not as critical as first believed, the conclusions reached are only tentative, and further research in this area merits consideration.

Improvements in wake-mixing should be developed. For example, it was found that when the tracer injection orifices faced upstream wake-mixing provided less reduction in the concentration fluctuations. Perhaps mixing could be improved by placing the orifices so that the chemical would enter at right angles to the flow. Using square grid bars instead of round bars might improve performance. It appears that wake-mixing is the critical step, and any improvement in this area will probably improve process performance.

SECTION III

INTRODUCTION

In any water or wastewater treatment process which requires the addition of chemicals, the initial mixing step is often a poorly designed aspect of the treatment scheme. This has been largely due to ignorance concerning the importance of initial mixing and the lack of any basic rational design criteria. In some respects it has been "essentially an art" [1], and most designs have been made on the basis of personal experience, intuition, and trial and error.

Much of the contemporary mixing literature in the field of sanitary engineering has been confined to the study of rotating impellor type mixers and development of model laws applicable to them. Most initial mixing units have been flash mixers, short residence time CSTR's utilizing high-speed impellors to produce homogeneous mixtures through convective dispersion and turbulent mixing.

It is believed that a different type of mixer which reduces quickly the segregation between the added chemical and the water stream can be of great importance in improving the performance of water and wastewater treatment facilities. When the chemical is added to the water stream, certain crucial physical-chemical reactions, if completed before segregation is eliminated, can result in less than optimal performance or the use of greater quantities of chemical than actually needed. In many processes a flash mixer cannot provide the required very rapid rate of mixing.

Another feature of the flash mixer is backmixing — mixing between fluid elements which have been present in the reactor for different lengths of time. A result is that reactants entering the mixer may "react" with previously formed "reaction" products rather than with the constituents of the water stream which are of concern. A specific example is aluminum sulfate coagulation-flocculation of a turbid water in which the alum entering the backmixed reactor can react with previously formed flocs instead of with turbidity-producing particles.

A tubular reactor with characteristics close to plug flow would eliminate the backmixing. A type of tubular reactor which is fairly amenable to analysis has a square mesh grid of bars placed normal to the axis. As the flow passes through the grid, turbulence is produced which can be utilized to mix the two fluid streams. Orifices drilled in hollow grid bars can be used to inject chemicals into the water stream. This allows the chemical to be released at many points across the cross-section of the pipe which may be an important consideration in quickly reducing segregation. Grids have been used extensively in studies involving turbulence, and there have been a few studies involving mixing with such devices.

OBJECTIVES

The principal objective of this investigation was to develop criteria for the design of turbulent flow, tubular reactors, utilizing a biplane grid to inject a reactant and to produce turbulence. This objective gives rise to three related questions:

1. What parameters of the turbulent flow field, the scalar (tracer or treatment chemical) field, and the scalar material determine the "goodness of mixing" downstream from a grid initial mixer (e.g., molecular diffusivity and intensity of turbulence may be important factors)? Implicit in this question is the necessity of defining "goodness of mixing."

2. What physical parameters should be used for design and scale-up of such initial mixers (e.g., mean flow velocity, grid bar diameter and grid solidity)?

3. What level of "goodness of mixing" is necessary, and how rapidly must this be achieved in order to attain a given level of performance? It will be necessary to relate the level and rapidity of mixing directly to process performance. This is a question which the present investigation answers only partially. Most of the effort of this study was directed toward objectives 1 and 2. However, certain conclusions will be drawn from experiments performed with three treatment processes: alum coagulation-flocculation of a kaolin suspension in water, chemical coagulation of wastewater (with alum or ferric chloride), and chlorination of wastewater.

ORGANIZATION OF REPORT

Section IV is a review of turbulence, mixing, and coagulation and flocculation theory and experiments pertaining to this investigation. A short review of research involving the initial mixing step in sanitary engineering is also given.

Sections V and VI cover the experiments done to determine the parameters which affect the degree of mixing downstream from a grid in a turbulent flow, tubular reactor (objectives 1 and 2). A single electrode conductivity probe was used to determine the root-mean-square concentration fluctuations produced by various grids. An attempt was made to correlate these results in a manner which allows prediction of the "goodness of mixing" produced by any square mesh grid. Also covered are experiments to determine head or energy loss which results from grids being placed in a tubular reactor. In some instances, the allowable head loss will be restricted to not more than a few inches, while in others several feet may be available.

In Section VII experiments are described which reveal the importance of the initial mixing step in alum coagulation-flocculation of a kaolin suspension in water. Two of the grids studied in experiments described in Sections V and VI were used as initial mixing devices in a pilot-scale study. Results produced by them were compared with results obtained with a flash mixer and with no initial mixing unit. The effect of alkalinity of the raw water on the importance of the initial mixing step was also studied. Jar tests which can be used to determine the significance of initial mixing for a given process and raw water are described. Also covered is alum coagulation-flocculation of wastewater.

Appendices A and B cover the experiments concerned with initial mixing and chlorination of wastewater. This aspect is presented in appendices because the experiments were limited in nature and the conclusions drawn are tentative.

SECTION IV

REVIEW OF FUNDAMENTAL THEORY: TURBULENCE, MIXING AND COAGULATION

ISOTROPIC TURBULENCE

Turbulence is a phenomenon associated with a fluid flowing at a high Reynolds number. This fluid may be the atmosphere or water flowing in a river. The conditions under which turbulence occurs are very diverse. Its defining characteristic is random fluctuations of the fluid velocity. Hinze [2] has defined turbulence in the following way: "Turbulent motion is an irregular condition of flow in which the various quantities show a random variation with time and space coordinates, so that statistically distinct average values can be discerned." This report will be primarily concerned with a particular type of turbulence — that produced by water flowing through a biplane grid of bars placed in the cross-section of the pipe. As will be seen, this type, (isotropic, decaying turbulence) is fairly amenable to theoretical analysis, can be simply produced in the laboratory, and has been extensively studied.

The concept of turbulence in a particular system is very closely associated with the energy being dissipated in that system. In ordinary pipe flow, for example, an energy loss will occur due to wall friction, and this energy is lost from the system through the dissipation of heat. Approximately half of the energy lost from the flow produces heat directly through internal viscous friction associated with gradients in the flow. The other half of the energy goes first to turbulence production and then to heat. In grid-produced turbulence probably most of the energy goes into turbulence production.

Turbulence is a random phenomenon; a Fourier analysis of the instantaneous velocity fluctuations at a point in a turbulent flow field will show that the fluctuations can be associated with a range of frequencies. The lowest frequencies will be determined by the geometry of the physical system, while the highest frequencies will be dominated by viscosity effects. These velocity fluctuations are related closely to the kinetic energy of turbulence. The turbulent kinetic energy is distributed over the range of frequencies with a distribution termed the energy spectrum. It has been found that energy introduced into a system at lower frequencies is dissipated by viscosity at higher frequencies. This results in a transfer of energy from lower to higher frequencies. The form of the energy spectrum and the laws governing the transfer of energy have been studied extensively in order to understand better the phenomenon of turbulence.

A qualitative picture of turbulence has only limited value, and a more detailed quantitative description is necessary. For a more complete

Preceding page blank

coverage of the topics discussed herein, reference is made to Hinze [2], Lee [3], Brodkey [4], and Batchelor [5].

If a grid is placed in a pipe through which water (or any fluid) is flowing, turbulence will be produced downstream. Because energy is added only at one point, the turbulence will decay with time (and distance downstream) because of the action of viscosity. Homogeneous turbulence is that which does not change its character with translation with a set of coordinate axes. Isotropy, a stronger condition which includes homogeneity, occurs if the character of the turbulence is such that its statistical features do not change with rotation or reflection of a set of coordinate axes. While turbulence produced by a grid decays in the downstream direction, isotropic turbulence is closely approximated in these experiments, and comparison between them and isotropic theory shows good agreement.

Root-Mean-Square Velocity and Correlations

If the velocity in the direction of flow downstream from the grid is measured with a hot-wire anemometer, it will be found to consist of a mean and a fluctuating component: $U_1 = \bar{U}_1 + u_1$ (Figure 1).

An important parameter of turbulence is the root-mean-square velocity fluctuation:

$$u_1' = \sqrt{\overline{u_1^2}} \qquad (1)$$

where the overbar indicates averaging. This is called the "intensity of turbulence."

Isotropy requires that all three components of the rms velocity fluctuations be equal, i. e.

$$u' = u_1' = u_2' = u_3' \quad . \qquad (2)$$

The nature of isotropic turbulence also requires that there be no cross-velocity term, that is

$$\overline{u_1 u_2} = \overline{u_1 u_3} = \overline{u_2 u_3} = 0 \quad . \qquad (3)$$

These terms are the Reynold's stresses and are the contribution of the turbulent motion to the total shear stress. In isotropic turbulence there is no shear stress and no gradients of mean velocity.

Taylor [6] first pointed out that in turbulent flow there will be a statistical correlation between the fluctuating velocities at two points

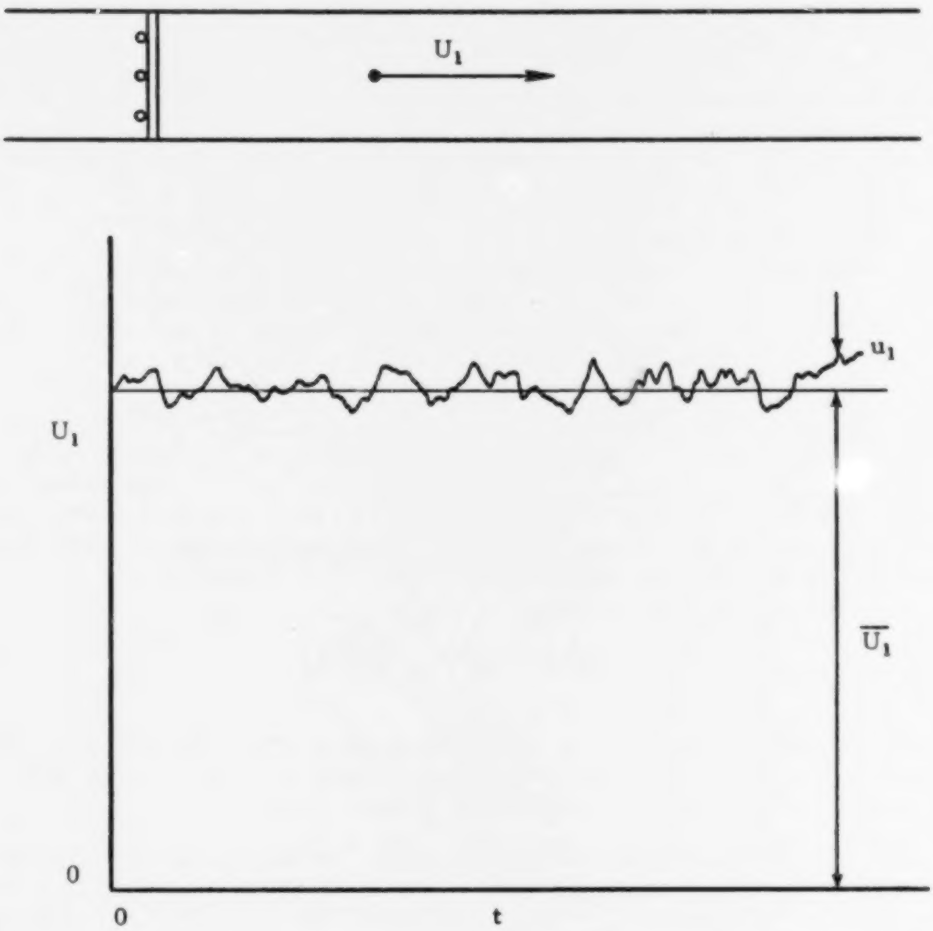

FIGURE 1. MEAN AND FLUCTUATING COMPONENTS OF VELOCITY

a small distance apart, with correlation decreasing as the separation distance increases. A statistical analysis can be made by studing the mean product of the fluctuating velocity components at the two points.

Correlation tensors and correlation functions can be defined by considering the fluctuating velocities at two points separated by a distance $\vec{r}$.

Two correlation functions are widely used in the study of turbulence. The longitudinal correlation function, f(r), and the lateral correlation function, g(r).

$$f(r) = \frac{\overline{u_r(\vec{x})\, u_r(\vec{x}+\vec{r})}}{u'^2} \tag{4}$$

$$g(r) = \frac{\overline{u_n(\vec{x})\, u_n(\vec{x}+\vec{r})}}{u'^2} \tag{5}$$

The subscript r denotes that the velocity fluctuation is measured in the same direction as the vector $\vec{r}$. The subscript n indicates the velocity fluctuation is measured normal to vector $\vec{r}$. Batchelor [5] has shown that only one scalar function is necessary to specify the velocity correlation at two points in isotropic turbulence. Therefore g(r) and f(r) cannot be independent. They are related by

$$g(r) = f(r) + 1/2\ r\left(\frac{\partial f(r)}{\partial r}\right) \tag{6}$$

If the separation distance is reduced to zero, the values of f(r) and g(r) become unity. As the separation distance is increased, the correlation functions decrease (see Figure 2).

In defining the above correlation tensors and functions, a Eulerian viewpoint has been taken with the correlation between velocities at two fixed points in the flow field separated by a distance r considered. It is also possible to define Lagrangian correlation functions which would correlate the velocity fluctuations of a fluid particle at two different times along its path of travel. For a more complete discussion of Lagrangian correlations see Hinze [2] or Brodkey [4].

Scales

The correlation functions given by Equations (4) and (5) can be used to define certain scales of turbulence. The longitudinal and lateral integral scales are defined respectively as

$$L_f = \int_0^\infty f(r)\, dr \tag{7}$$

$$L_g = \int_0^\infty g(r)\, dr \tag{8}$$

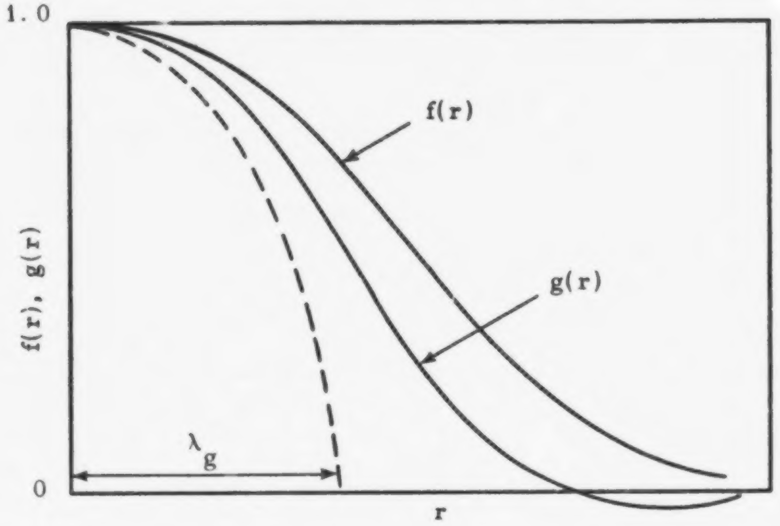

FIGURE 2. LOGITUDINAL AND LATERAL CORRELATION FUNCTIONS AND LATERAL MICROSCALE, λ_g, FOR ISOTROPIC TURBULENCE

These scales can be considered measures of the longest distance which results in a finite correlation between the velocity fluctuations at the two points. In turbulent flow, attempts are often made to relate L_f and L_g to the geometry of the system. For example, in pipe flow L_f may be taken as a certain fraction of the pipe diameter. In grid-produced turbulence attempts have been made to relate L_f to the bar spacing or bar diameter.

Since f(r) and g(r) are related by Equation (6), L_f and L_g must also be related. The equation is

$$L_g = 1/2 \ L_f \quad . \tag{9}$$

Two other important scales can be defined from the functions f(r) and g(r). These scales are related to the shape of the correlation functions near r = 0. It is possible to expand f(r) in a Taylor series:

$$f(r) = 1 + \frac{r^2}{2!}\left[\frac{\partial^2 f}{\partial r^2}\right]_{r=o} + \frac{r^4}{4!}\left[\frac{\partial^4 f}{\partial r^4}\right]_{r=o} + \ldots \qquad (10)$$

For very small values of r, f(r) approaches a parabolic function of r. It is possible to introduce a length λ_f such that

$$f(r) \cong 1 - \frac{r^2}{\lambda_f^2} \qquad (11)$$

Where λ_f is called the microscale of turbulence. Ignoring the higher order terms in Equation (10) and equating Equations (10) and (11), it follows that

$$1/\lambda_f^2 = -1/2\left[\frac{\partial^2 f}{\partial r^2}\right]_{r=o} \qquad (12)$$

A similar scale, λ_g, is defined by

$$1/\lambda_g^2 = -1/2\left[\frac{\partial^2 g}{\partial r^2}\right]_{r=o} \qquad (13)$$

From Figure 2, it can be seen that λ_g is the intercept along the r axis of a parabola whose curvature at r = 0 is the same as g(r). λ_f can be interpreted similarly.

It is known that λ_f is closely related to the velocity fluctuation frequencies at which the most dissipation of turbulent energy into heat takes place. For this reason, it is often called the dissipation scale. The relation between λ_f and λ_g is

$$\lambda_f = \lambda_g\sqrt{2} \qquad (14)$$

Energy Spectrum Functions in Isotropic Turbulence

It was previously qualitatively stated that it was possible to view the kinetic energy of turbulence as being distributed over a range of frequencies. In 1938 Taylor [7] showed that there is a relation between the one-dimensional energy spectrum function — that is, one which considers the velocity fluctuations in one direction only — and the correlation function f(r).

$E_1(k_1)$ is the one-dimensional energy spectrum function associated with the wave number k_1.

$$k_1 = \frac{2\pi n}{\overline{U}_1} \tag{15}$$

where $\overline{U}_1$ is the mean flow velocity and n is the frequency. The sum of $E_1(k_1)$ over all wave numbers (or frequencies) must equal the total turbulent kinetic energy in the x_1 direction, or the mean square fluctuating velocity:

$$\int_0^\infty E_1(k_1)\, dk_1 = \overline{u_1^2} = u'^2 \tag{16}$$

Taylor showed that the longitudinal correlation function f(r) and one-dimensional energy spectrum functions are Fourier cosine transforms of each other, i. e.,

$$f(r) = \frac{1}{u'^2} \int_0^\infty E_1(k_1) \cos(k_1 r)\, dk_1 \tag{17}$$

$$E_1(k_1) = \frac{2}{\pi} u'^2 \int_0^\infty f(r) \cos(k_1 r)\, dr \quad . \tag{18}$$

There is also a three-dimensional energy spectrum function E(k, t), defined such that:

$$\int_0^\infty E(k,t)\, dk = \frac{3}{2}\, u'^2 \quad . \tag{19}$$

The one-dimensional energy spectrum function is related to E(k, t) in the following manner.

$$E_1(k_1, t) = \int_{k_1}^\infty \frac{E(k,t)}{k} \left(1 - \frac{k_1^{\,2}}{k^2}\right) dk \quad . \tag{20}$$

Universal Equilibrium

It is known that the geometry of the physical system in which the flow is taking place strongly affects the character of the low wave number range of the turbulence spectrum. As has been noted, the integral scale has often been related to a physical length involved, e. g., the pipe diameter in pipe flow. An equation can be derived [2] relating $E_1(o, t)$ and L_f. However, it is found that at the higher wave numbers under certain conditions, i. e., high Reynolds number, the form of the spectrum is independent of the conditions in a particular turbulent flow and are universal in character. This theory was first proposed by A. N. Kolmogoroff in 1941 [8–10] and is usually known as the theory of universal equilibrium. It states that at high wave numbers, the turbulence is isotropic (no matter what the character of the overall turbulence may be) and that the spectrum in this universal equilibrium range will depend only on the rate of energy dissipation or input, ε, and on the kinematic viscosity, ν.

Dimensional analysis reveals that a characteristic length and velocity can be defined in terms of ε and ν. They are respectively,

$$\eta = \left(\frac{\nu^3}{\varepsilon}\right)^{1/4} \tag{21}$$

$$v = (\nu\varepsilon)^{1/4} \quad . \tag{22}$$

The length scale, η, is often called the Kolmogoroff microscale of turbulence. It should not be confused with λ_f and λ_g which were discussed earlier and which are associated with G. I. Taylor. $1/\eta = k_K$ can be taken as the wave number at which the maximum of the dissipation spectrum, $k^2\ E(k,t)$, occurs.

A Reynolds number based on Equations (21) and (22) can be defined and its value is equal to unity.

$$\frac{v\eta}{\nu} = 1 \quad .$$

This means that at the Kolmogoroff microscale, the inertial and viscous forces are balanced. A higher wave numbers viscous forces become predominant.

In order for the equilibrium range to exist, the energy input by transfer must equal the energy dissipated by viscosity, or

$$\varepsilon = -\frac{3}{2}\left(\frac{d\ u'^2}{d\ t}\right) = 2\ \nu \int_0^\infty k^2\ E(k,t)\ dk \quad . \tag{23}$$

This will occur only if the wave numbers associated with the scale L_f do not overlap with the wave numbers associated with the maximum dissipation, or $\eta \lll L_f$.

In terms of Reynolds number, this condition [2] is:

$$N_{Re_\lambda}{}^{3/2} = \left(\frac{u'\lambda_g}{\nu}\right) \ggg 1 \quad . \tag{24}$$

In the universal equilibrium range, a dimensionless function can be found to relate $E(k,t)$ to v and η. Dimensional analysis shows that

$$E(k,t) = v^2 \ \eta \ E_e(k\eta) \qquad (25)$$

or, substituting in Equations (21) and (22),

$$E(k,t) = \nu^{5/4} \ \varepsilon^{1/4} \ E_e(k\eta) \quad . \qquad (26)$$

Thus, spectra, $E(k,t)$, can be plotted in universal form by dividing by $\nu^{5/4} \ \varepsilon^{1/4}$ and plotting against $k\eta$. The same holds for the one-dimensional energy spectrum [11],

$$E_1 (k_1 \ t) = \nu^{5/4} \ \varepsilon^{1/4} \ E_{1 \ e}(k_1 \ \eta) \quad . \qquad (27)$$

An important corollary to the theory of universal equilibrium is that for Reynolds numbers much higher than that given by Equation (24), there is a subrange of wave numbers for which the form of the spectrum no longer depends on viscosity, but only on ε. In other words, energy is transferred in at the lower end of the wave number range and is transferred out at the higher end of the range. No production or dissipation of energy takes place. This is called the inertial subrange.

Hinze [2] concludes that the requirement for an inertial subrange to occur is

$$N_{Re_\lambda}{}^{3/4} \ >>> 1 \quad . \qquad (28)$$

Gibson [11] derived the following criterion for the existence of an inertial subrange:

$$\frac{u'L_f}{\nu} > 3.3 \times 10^5 \quad . \qquad (29)$$

It has been found that these criteria are essentially impossible to meet with laboratory produced turbulence. Experiments have been done in the ocean [12], however, with a Reynolds number, based on the channel depth, of 10^8. It was found that an inertial subrange did exist and extended over a wave number range of two orders of magnitude.

This conclusion was made by comparing measured spectra with the form of spectra derived through dimensional analysis for the inertial subrange.

$$E_1 (k_1 \ , \ t) = A_1 \ \varepsilon^{2/3} \ k_1{}^{-5/3} \quad . \qquad (30)$$

A similar equation exists for the three-dimension spectrum,

$$E(k,t) = A\ \varepsilon^{2/3}\ k^{-5/3} \quad . \tag{31}$$

It is widely accepted that this is the form of spectrum in the inertial subrange.

For values of $k > k_K$ in the universal equilibrium range, the dependency on k is much greater. A relation [13] which agrees fairly well with experiment is:

$$E(k,t) = \frac{c\varepsilon}{4\nu^2}\ k^{-7} \quad . \tag{32}$$

Hinze [2] has noted certain errors in the derivation of Equation (32). A summary of the above spectra forms and the wave number ranges is given in Figure 5 in the section on Review of Mixing Theory.

Decay of Isotropic Turbulence

The mixing which occurs downstream from a grid is in part governed by the decay of the intensity of turbulence and the variation in the scales of turbulence with increasing distance from grid. For this reason it is important to review the theoretical and experimental work in this field. As noted, isotropic turbulence is easily produced by passing a fluid through a grid of bars. Development of the hot-wire and hot-film anemometer have led to a great deal of experimentation, most of which has been done in air.

As the fluid passes through a grid with a center-to-center bar spacing, M, and a bar diameter, d, turbulent wakes are produced behind the grid bars as a result of vortex shedding.

This initial turbulence is highly anisotropic. However, these wakes gradually coalesce and the resulting turbulence is reasonably close to isotropic. The distance downstream at which this occurs is approximately 20 M.

Between 20M and 100 M to 150 M downstream, the initial period of decay occurs. In this period, inertial forces are predominant in determining the decay. At distances greater than approximately 500 M downstream, the Reynolds number of turbulence is very low, and viscous forces predominate. As has been noted, the Kármán-Haworth equation is soluble in this case, and the decay of the intensity of turbulence has been found to follow the solution,

$$u'^2 = \text{const} \times t^{-5/2} \tag{33}$$

where t is the time.

In the initial period of decay, which is of greater interest, the most well-known decay law is that proposed by Batchelor and Townsend [14]:

$$\frac{u_1'^2}{\overline{U}_1^{\,2}} = \frac{C_D}{c}\left[\frac{x - x_o}{M}\right]^{-1} \tag{34}$$

where c is a constant depending on grid geometry, C_D is the drag per unit area of the grid, x is the distance downstream from the grid, and x_o is the distance from the grid of the apparent origin of the intensity of turbulence. For round-bar, square-mesh grids, C_D can be obtained from [2].

$$C_D = \frac{(d/M)\,(2 - d/M)}{(1 - d/M)^4} \quad . \tag{35}$$

Van der Hegge Zijnen [15] has reviewed the experimental work of several experimental investigators, including Batchelor and Townsend. He found that no general law such as Equation (34) holds for all experiments. The rate of decay of u' (i. e., the exponent in an equation of the form $u' = Kx^{-r}$) with distance varied from 1/2 as proposed by Batchelor and Townsend to - 5/7, a value derived by Frenkiel [16]. Van der Hegge Zijnen found that it was possible to obtain a reasonable correlation between the data of five different investigations by plotting, $u_1'/\overline{U}_1$ against $(x-x_o)/d$. There is considerable scatter which makes it difficult to rely on the graph to predict actual values of u' for application under a particular set of circumstances. The data are shown in Figure 3.

It should be noted that, strictly speaking, it is inconsistent to plot results as shown in Figure 3. It implies that there should be no dependence of u' on M/d. This ratio strongly influences the head loss through the grid which determines the turbulent kinetic energy produced. Inspection of Figure 3, however, shows no consistent dependence of u' on M/d. The conclusion which must be drawn is that other factors such as experimental error must have produced differences in the results which hide the dependence on M/d.

Van der Hegge Zijnen also compared results of six separate investigations of the variation of the integral scale, L_f, downstream from a grid. L_f/d is plotted against $(x-x_o)/d$. M is the other parameter often related to the scale of turbulence. Examination of Figure 4 shows no apparent dependence on M/d.

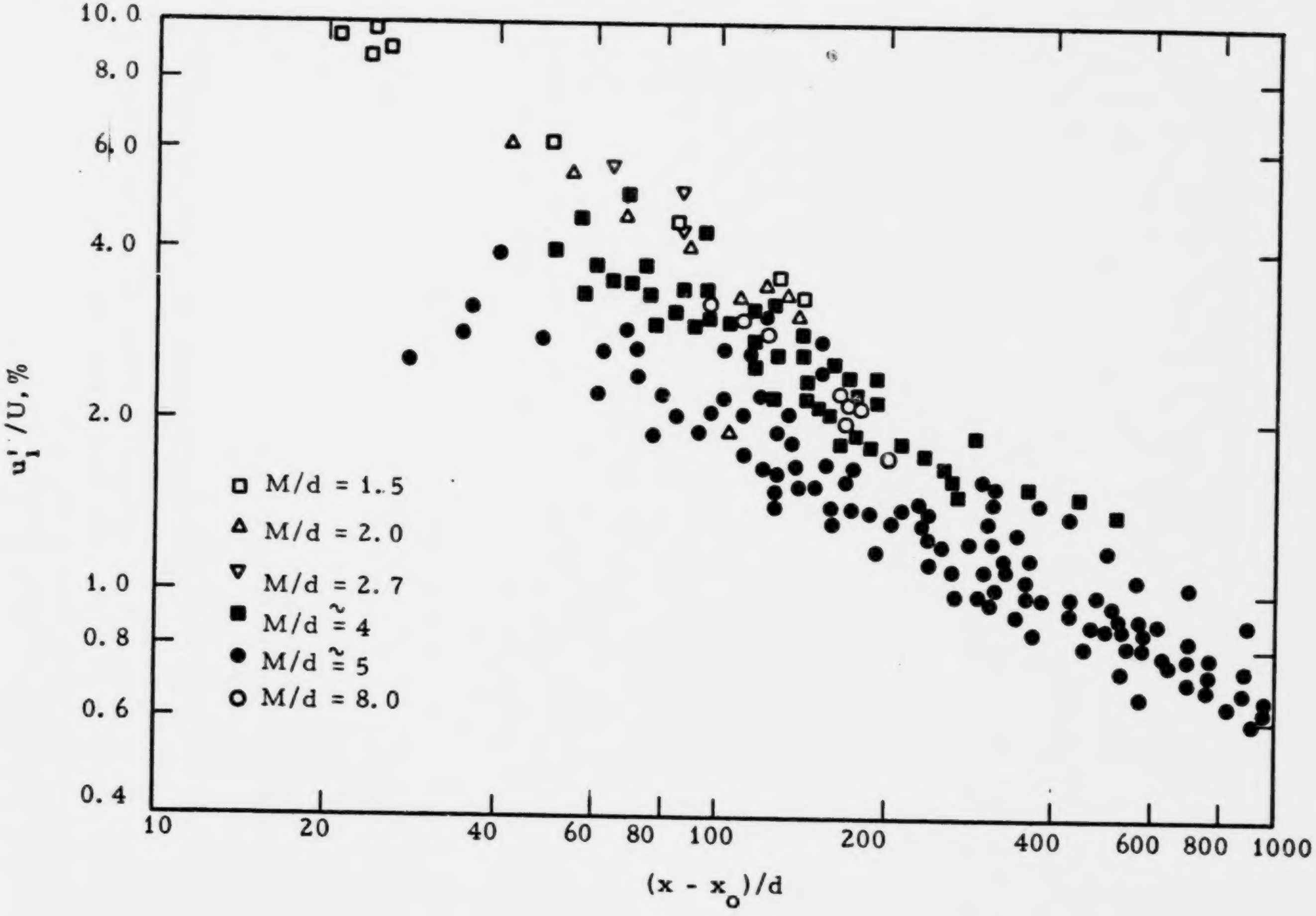

FIGURE 3. DECAY OF TURBULENCE AS MEASURED BY VARIOUS INVESTIGATORS (FROM VAN DER HEGGE ZIJNEN [15])

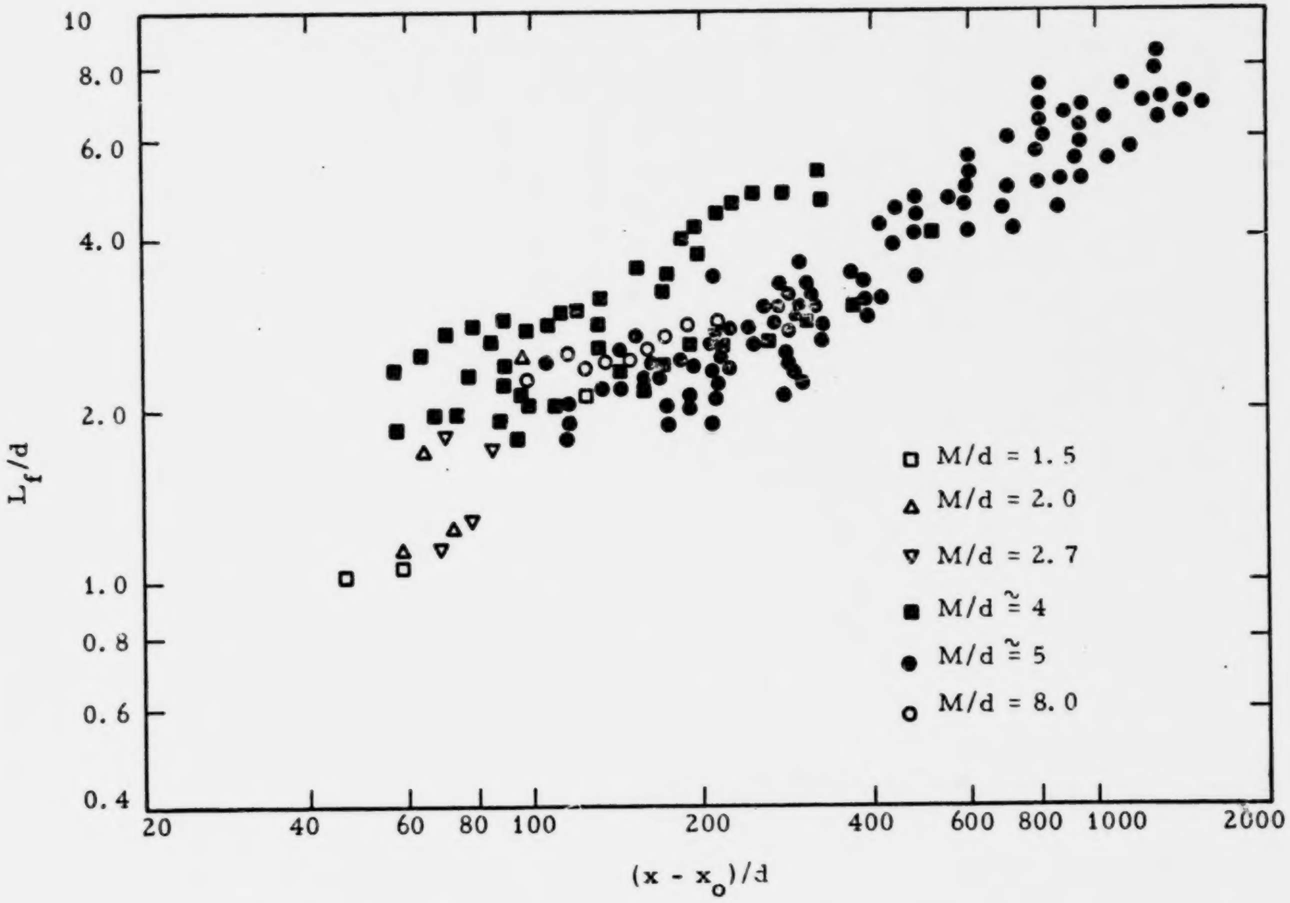

FIGURE 4. INTEGRAL SCALE OF TURBULENCE AS MEASURED BY VARIOUS INVESTIGATORS (FROM VAN DER HEGGE ZIJNEN [15])

REVIEW OF MIXING THEORY

Criteria for Mixing

In a study of mixing it is first necessary to define the terms involved. Brodkey [4] defines mixing to mean a blending into one mass "a complex of two or more ingredients . . . which, however thoroughly commingled, are conceived as retaining a separate existence." This definition, however, does not allow visualization of the mixing process. Consider, for example, the addition of a small amount of salt water to a beaker of fresh water. If the water is stirred, the salt will become spread throughout the beaker. Soon the salt concentration at all "points" throughout the beaker will be the same. The mixing can then be said to be complete. By a "point" is meant the smallest volume which is still very much larger than the dimensions of the molecules. How small this volume must be is not easily defined. Brodkey [4] states that it must be submicroscopic, i. e., smaller than that which can be seen with the best microscope. Gibson [11] states that it must be smaller than that volume associated with microscale of scalar fluctuations, a term which will be defined later. The term scalar is used to denote any tracer, contaminant, or chemical which is added to and mixed with the fluid. All correlations defined with a scalar are also scalars whereas correlations defined with velocities (a vector or a first-order tensor) become higher-order tensors. A scalar is a zero order tensor.

Before proceeding further, it is necessary to differentiate between the terms mixing, diffusion, and dispersion or bulk diffusion. Diffusion should be more precisely termed molecular diffusion. It is due to the Brownian motion of individual molecules. Molecular diffusion is very important in the mixing process with which this project is concerned. The turbulence can act to create very small blobs of scalar material, but even the smallest scales of turbulence cannot act to eliminate all variations in "point" concentration. Molecular diffusion must function in conjunction with the turbulence to accomplish complete mixing. If turbulence were not present, the mixing would eventually be completed by diffusion. However, the time required would be quite long. The random motions of turbulence break large blobs of scalar material down into the smallest blobs upon which molecular diffusion can act with greater effectiveness. A slightly different interpretation by Corrsin [17] is that the turbulence causes an increase in the local, instantaneous concentration gradients which allows molecular diffusion to act more effectively.

The term dispersion is used to describe the spreading of a scalar in a flow field due to steady state spatial variations in the flow velocity. The terms diffusion, bulk diffusion, or Taylor diffusion are often used, but these are misleading because they tend to be confused with molecular diffusion. Consider for example, turbulent flow in a pipe. If a tracer is released from a point source in the center of the pipe, the turbulence will tend to spread the tracer across the cross-section. Near the walls, the velocity will be lower which will cause the tracer to disperse longitudinally to a greater extent than would be produced by the turbulence alone in a uniform velocity field. This type of phenomenon also occurs in laminar flow. Molecular diffusion, rather than turbulence, causes the lateral spreading in this case.

This project is concerned with the mixing which takes place downstream from a turbulence-producing grid. Only in the region very close to the grid bars will gradients of temporal mean velocity exist. The scalar field will be inhomogeneous in this region as there will exist gradients of mean concentration. The processes which occur here are very complex and difficult to treat mathematically. Considerable experimental work has been done on the turbulent wake produced by a circular cylinder [18, 19]. Mixing and chemical reactions in the wake of a cylinder have been studied for the case of two-dimensional spreading [20, 21]. Such results might be expected to apply to a grid in the limit as the spacing of the bars increases. They clearly do not apply to the situation encountered in this study where the maximum M/d ratio was 4.0 and where the spreading is three-dimensional. Therefore, as has been done by previous investigators [11, 22], the problem of turbulence and transport in the vicinity of the grid bars will be treated empirically and, consequently, somewhat superficially. That it is done in this manner does not mean that the mixing which takes place in this region is unimportant. In fact, it will be found that most of the decay of concentration fluctuations occurs in this region.

Further downstream, the temporal mean value of the tracer concentration will become constant across the cross-section, even though the rms concentration fluctuations at a given point will not be zero. The scalar field will become isotropic and will become amenable to theoretical analysis.

Basic Definitions in Mixing

It will be seen that the basic equations used in mixing will bear a close resemblance to equations used to describe turbulence. An isotropic scalar field is very similar to an isotropic turbulent field, with the exception that scalars rather than vectors are involved. It is possible to view the mixing process as being analogous to the dissipation of turbulent energy. When large blobs of scalar material are added to a fluid, in terms of the scalar spectrum, these large blobs represent the low wave number range. The turbulence then acts to create smaller blobs which correspond to higher frequency, or higher wave number, fluctuations. Finally, at the highest wave numbers, molecular diffusion acts to spread out the smallest blobs in a manner analogous to the way viscosity damps out the highest frequency velocity fluctuations.

Consider an isotropic scalar field downstream from a grid. No spatial variations in temporal mean concentration exist. At a particular point, the instantaneous concentration can be taken equal to the sum of the mean value plus a fluctuating value.

$$A = \bar{A} + a \quad . \tag{36}$$

This is similar to the expression for instantaneous velocity with the exception that vector notation is no longer required.

As with velocity, the rms value of the concentration fluctuations can be defined:

$$a' = \sqrt{\overline{a^2}} \quad . \tag{37}$$

Dankwerts [23] defined the mean square concentration fluctuation divided by the initial mean square concentration fluctuation to be the intensity of segregation, i. e. ,

$$I_s = \frac{a'^2}{a_o'^2} \quad . \tag{38}$$

This parameter, or its square root, will be used to indicate the "goodness of mixing" obtained in a given system. When the scalar is completely unmixed with the fluid to which it has been added, $I_s = 1$. When the mixing is complete, and there are no deviations from the mean concentration, $I_s = 0$. $1 - \sqrt{I_s}$ is sometimes defined as the "degree of mixing" [24].

Dankwerts has defined another important parameter of mixing — the scale of segregation.

$$L_s = \int_0^\infty C(r)\, dr \tag{39}$$

where

$$C(r) = \frac{\overline{a(\vec{x})\, a(\vec{x} + \vec{r})}}{a'^2} \quad . \tag{40}$$

C(r) is the Eulerian concentration correlation. It is analogous to the Eulerian correlation function for velocity fluctuations. L_s may be considered to be indicative of the size of the largest scalar blobs.

A scalar microscale, λ_s, can also be defined from the C(r) vs. r curve.

$$\frac{1}{\lambda_s^2} = -\frac{1}{2}\left[\frac{\partial^2 C(r)}{\partial r^2}\right]_{r=o} \quad . \qquad (41)$$

Again, this is analogous to the Taylor microscales, λ_g and λ_f.

As with velocity spectra, considerable effort has gone into determining the shape of the spectral curve in different wave number ranges. This investigation will be concerned with the case where the scalar material is added to a liquid. Under these conditions, the Schmidt number, N_{Sc}, $= \nu/D_m$ the ratio of kinematic viscosity to molecular diffusivity is much greater than unity. Under conditions of mixing in a gas, $\nu/D << 1$ and the spectral curve has a different shape. The reason for the difference in shape is related to the fact that under conditions of high and low Schmidt numbers, the wave number at which molecular diffusivity becomes important is either much higher or much lower than the Kolmogoroff wave number. Thus, for $\nu/D << 1$, molecular diffusivity becomes effective in a wave number range $k < k_K$ where viscosity is not important. For $\nu/D >> 1$, scalar transport due to convection is important at the higher wave numbers where viscosity has a strong effect on the velocity spectra.

Considering turbulence in a liquid with a fully developed inertial subrange, for wave numbers $k_{o,s} << k << k_K$ the form of the scalar spectra has been found to be

$$E_s(k) = B\,\varepsilon_s \varepsilon^{-1/3} k^{-5/3} \qquad (42)$$

where B is a constant coefficient, and ε_s is the time rate of "dissipation" of the mean square concentration fluctuation.

This is called the inertial-convective subrange because inertial forces dominate the velocity spectra and convective transport dominates the scalar spectra for corresponding wave numbers. Batchelor [25] showed that scalar transport due to convection and transport due to diffusion become of the same order of magnitude at a wave number,

$$k_B = \left(\frac{\varepsilon}{\nu D_m^2}\right)^{1/4} \quad . \qquad (43)$$

This is analogous to the Kolmogoroff wave number k_K. If $D_m << \nu$, it follows from Equations (21) and (43) that $k_B >> k_K$.

For wave numbers $k_K << k << k_B$, Batchelor determined that the spectrum should take the form:

$$E_s(k) = A \left(\frac{\nu}{\varepsilon}\right)^{1/2} \varepsilon_s k^{-1} \quad . \qquad (44)$$

This is called the viscous-convective subrange, because while convective transport is still dominant, viscous dissipation becomes important in the corresponding velocity spectrum.

Figure 5 shows the form of the scalar spectra discussed above as well as that of the universal equilibrium range for turbulence. It should be noted that the shape of the scalar spectrum depends on that of the velocity spectra and if the Reynolds number is not high enough to produce the complete universal spectrum shown in Figure 5, then the scalar spectrum will also be altered. As was noted previously, a fully developed inertial subrange cannot be expected to be found in laboratory-produced turbulence. Therefore, the resulting universal scalar spectrum of Figure 5 cannot be expected to be found either. However, this should not prevent these concepts from being used. The Reynolds number necessary for universal equilibrium to occur can be easily obtained. Several investigators [2, 11, 26] have examined velocity spectra and found a universal form. Usually, a line with a -5/3 slope, corresponding to the inertial subrange, can be drawn tangent to the experimentally-determined spectrum curve. Therefore, as a first approximation, the characteristic spectra of Figure 5 can be used in the study of laboratory-produced turbulence and the mixing resulting therefrom.

Decay of an Isotropic Scalar Field

When an isotropic scalar field is superimposed on a decaying isotropic turbulent velocity field, it will decay in a manner at least partially dependent upon the velocity field. Only recently has this rate of decay been studied experimentally or theoretically.

Usually the rate of decay of the intensity of segregation in isotropic decaying turbulence has been represented by an equation of the form:

$$I_s = \alpha_1 \left(\frac{x}{M}\right)^{-2a} \tag{45}$$

$$\sqrt{I_s} = \alpha \left(\frac{x}{M}\right)^{-a} \tag{45a}$$

where α, α_1 are coefficients, a is the decay rate. Only two investigations [11, 22, 26, 27] have been made concerning the decay of an isotropic scalar field in water (high N_{Sc} case). The resulting data were shown to fit such a curve although the relationship of the coefficients α and a to the physical parameters involved remained uncertain.

Hinze [2] derived a relation for scalar decay based upon the Kármán-Howarth correlation equation for a scalar field, the assumption that the form of the scalar correlation function maintains its shape during decay,

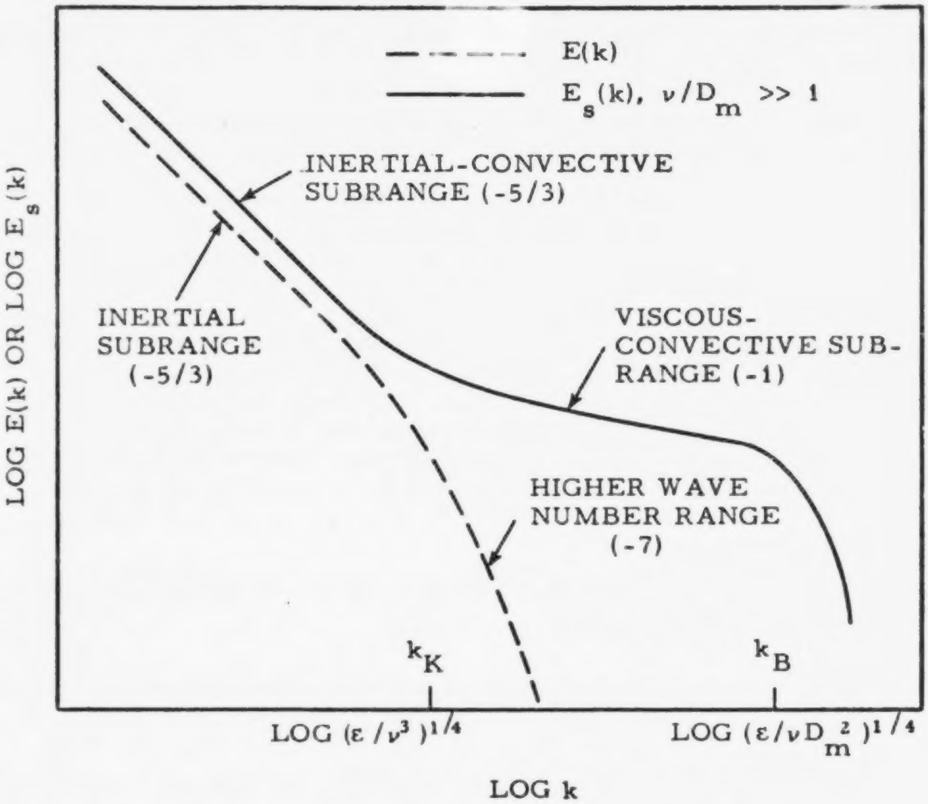

FIGURE 5. UNIVERSAL FORMS OF SCALAR AND VELOCITY SPECTRA. (FROM BRODKEY [4])

and Batchelor and Townsend's linear decay law for isotropic turbulence (Equation 34). His equation is

$$I_s = C\left(\frac{x-x_o}{M}\right)^{-3/2} \quad . \tag{46}$$

Note that a value for C is not given in this derivation.

Gibson [11] derived Equation (45) by dimensional analysis, assuming that the rate of decay of a'^2 was dependent only on $\overline{U}$, M, t, and $a_o'^2$.

Recently, Corrsin [17, 28] has attempted to derive relations for the rate of decay of scalar fluctuations in decaying and nondecaying isotropic turbulence for different values of Schmidt numbers. The case of interest here is high Schmidt number and decaying turbulence [17].

The mass transfer equation for the case of a homogeneous scalar field with a conservative tracer (i.e., $\overline{A}$ = constant) is

$$\frac{\partial a}{\partial t} + u_i \frac{\partial a}{\partial x_i} = D_m \nabla^2 a \quad . \tag{47}$$

One can convert this equation to a more useful form [2] by multiplying by a, averaging, and putting u_i inside the derivative.

$$\frac{d\overline{a'^2}}{dt} = -2 D_m \overline{\left(\frac{\partial a}{\partial x_j}\right)\left(\frac{\partial a}{\partial x_j}\right)} \quad . \tag{48}$$

The scalar microscale is related to the derivative products in such a way that

$$\frac{d a'^2}{dt} = -12 D_m \frac{a'^2}{\lambda_s^2} \quad . \tag{49}$$

A corresponding equation can be derived for the mean square velocity fluctuations from the Navier-Stokes equation:

$$\frac{d u_1'^2}{dt} = -20 \nu \frac{u_1'^2}{\lambda_f^2} \quad . \tag{50}$$

Dividing (49) by (50), one obtains the relative decay equation:

$$\frac{u_1'}{a'} \frac{da'}{du_1'} = \frac{3}{5} \frac{1}{N_s} \left(\frac{\lambda_f}{\lambda_s}\right)^2 \quad . \tag{51}$$

Equations for λ_f and λ_s in terms of the three-dimensional velocity and scalar spectra can be developed

$$\frac{1}{\lambda_f^2} = \frac{1}{10} \frac{\int_0^\infty k^2 E(k)\, dk}{\int_0^\infty E(k)\, dk} \tag{52}$$

$$\frac{1}{\lambda_s^2} = \frac{1}{6} \frac{\int_0^\infty k^2 E_s(k)\,dk}{\int_0^\infty E_s(k)\,dk} \quad . \tag{53}$$

Corrsin's method was to use the characteristic spectral form shown in Figure 5 to obtain values for λ_f and λ_s. These in turn were substituted into Equation (61). Corrsin did make one deviation from the spectra shown in Figure 5 in that he ignored the higher wave number range of the velocity spectrum and used a purely inertial spectrum. His assumption was that the higher wave number range would not contribute significantly to either integral in Equation (52).

Corrsin's final equation, bypassing the intermediate steps, is

$$\frac{u_1'}{a'} \quad \frac{da'}{du_1'} = \left[\frac{2 + N_{Sc}^{-1}}{3(\frac{3}{2})^{2/3} \left(\frac{L_s}{L_f} \right)^{2/3} + 2(\frac{5}{3})^{3/2} \frac{\log N_{Sc}}{N_{Re_\lambda}}} \right] . \tag{54}$$

All the terms in the equation have been defined previously.

It is instructive to examine the influence of the various parameters on Equation (54). The Schmidt number appears in two places. In the numerator, if $N_{Sc} > 10$, its effect becomes insignificant. This is the situation with which this project shall be concerned. In the denominator, log N_{Sc} appears. The rate of decay is weakly dependent on N_{Sc}, but note that if $N_{Sc} = \nu / D_m \rightarrow \infty$, log $N_{Sc} \rightarrow \infty$ also, and the rate of decay of a'goes to zero. This means that if the molecular diffusivity is zero, mixing will not occur. This effect of no molecular diffusivity was noted earlier.

It is important for this project that the dependence on N_{Sc} should be weak. The tracer used in the mixing experiments necessarily has a molecular diffusivity different from the chemicals to be used in the treatment processes. In fact, since the chemicals will be undergoing reactions during the mixing process, their diffusivity will probably be undergoing changes as mixing occurs. Very weak dependence of the mixing rate on the molecular diffusivity means that results obtained from the mixing experiments can be reasonably applied to the treatment process experiments.

Since Equation (54) was developed on the assumption of an inertial subrange, it applies only to cases where $N_{Re\lambda}$ is large. Under those circumstances and if log N_{Sc} is not too large, the second term in the denominator of Equation (54) will be small and dependence on N_{Re_λ} will be weak. At lower values of N_{Re_λ} where, strictly speaking, Equation (54) does not apply, it is possible that a dependence on N_{Re_λ} may be discerned.

The other parameter in Equation (54) is (L_s/L_f), the ratio of the scalar and velocity integral scales. There is a physical interpretation of the manner in which this parameter affects the rate of decay [22]. L_f represents the largest scale of turbulent motion. L_s represents the largest scale of tracer blobs. If L_f is small with respect to L_s, then the turbulent motion cannot be as effective in breaking up the blobs of tracer. If, however, L_f is large with respect to L_s, the turbulence can be much more effective in mixing and a more rapid decay of the concentration fluctuations results.

It is possible that by changing the physical characteristics of the grid or the tracer injection system, (L_s/L_f) can be made smaller and the decay rate greater. It was noted previously that L_f seems to be a function of the grid bar diameter, d. This means that an increase in d, with other factors held constant, should result in an increase in the decay rate.

It has been assumed by some [22, 29] that the scale of segregation is a function of the number of tracer sources, L_s decreasing when the number of sources is increased. According to Equation (54), this would cause an increase in the rate of scalar decay. There seems to be no rational reason for assuming that L_s is a function of the number of sources. The assumption seems to be based mostly on analogy with the dependence of L_f on d or, as some investigators claim, M.

It is possible, assuming that the right-hand side of Equation (54) remains constant during the period of decay, to integrate Equation (54) and obtain Equation (45). The right-hand side becomes essentially the decay rate, a, of Equation (45). The coefficient, α, is dependent on the initial conditions at a time, t_0. It should be noted that the derivation depends on the assumption that $u' = f(x/M)$. If $u' = f(x/d)$, then d will appear in Equation (45).

Since Equation (54) was derived for high N_{Re_λ}, there is the implication that it cannot be applied to laboratory experiments. Strictly speaking, this is true. However, it may be possible to qualitatively relate Equation (54) to experimental results obtained under the conditions of low Reynolds number. In particular, it may be possible to relate certain physical characteristics of the experimental apparatus to L_s/L_f and, consequently, the scalar decay rate.

Previous Experimental Investigations

There have been two previous investigations into the rate of decay of concentration fluctuations of an isotropic scalar field in isotropic decaying turbulence produced by a grid: one by Gibson [11, 26, 30] and the other by Keeler [22, 27]. Both used single electrode conductivity probes to attempt to determine "point" values of tracer concentrations.

Gibson worked with a 6 in. x 6 in. water tunnel in which the flow was recycled. For grids, he used 3/16 in. and 1/8 in. O. D. lucite tubes in a square mesh grid with the bar spacing chosen such that M/d was 16/3. The tubes were perforated by drilling 12 mil holes on the upstream side halfway between the corners of the mesh. The tracer was injected into the water stream through these holes. For tracers, he used NaCl solutions ($\nu/D_m = 700$) and heated water ($\nu/D_t = 7$).

Gibson, in his measurement of the rate of scalar decay attempted to substantiate Hinze's equation, Equation (46). His curve had a slope which was very close to - 3/2 but later work by Keeler and the present study tend to indicate that this was merely a coincidence. Gibson also made measurements of scalar spectra. They followed a universal form and fit the curves given in Figure 5 fairly well.

Keeler's work was done after Corrsin's relation, Equation (54), had been derived. He used three grids with the same M/d ratios but different values of M. This was done in order to determine whether changing the scale of turbulence would affect the scalar decay rate as predicted. Keeler indicated that such a result was found although inspection of his raw data seems to show that the difference is fairly small if not negligible.

In order to insure homogeneity of the scalar field downstream from the grid, Keeler used a "hairbrush" injection system which fed the tracer into the water stream through many hypodermic needles connected to a manifold. For a 4-in. pipe, 156 needles were used; for a 2-in. pipe, 37. The "hairbrush" injection device was placed upstream from the grid and produced a scalar field which was homogeneous at the grid. A drawback to this method was that the injection system introduced turbulence which may have affected the turbulence field downstream from the grid.

Keeler used two tracers, $NaNO_3$ ($\nu/D_m = 500$) and $ZnSO_4$ ($\nu/D_m = 1000$) in an attempt to show the effect of N_{Sc} on scalar decay rate as predicted by Equation (54). His results do indicate a slight difference in decay rate for the two tracers. This appears to be a consequence of the low Reynolds number. Corrsin [17] showed that for $N_{Re_\lambda} = 100$, this difference in N_{Sc} should have essentially no effect on decay rate. The fact that a difference does occur may be significant in regard to the present work for the reason previously noted.

Further reference will be made to the results of Keeler and Gibson as they relate to the present work in Section VI.

REVIEW OF COAGULATION-FLOCCULATION THEORY

Although alum coagulation-flocculation has long been one of the most widely used water treatment processes, the actual mechanism of destabilization of clay particles is still somewhat uncertain. The process is simple in execution. Aluminum or ferric salts are added more or less rapidly to the turbid water and after slow stirring, small "flocs" are formed which are removed by sedimentation and filtration. The result is a clear water free of the colloidal clay particles which are principally responsible for the turbidity.

Despite this apparent simplicity, uncertainty has arisen over the years concerning the mechanisms involved in coagulation-flocculation. In part, this concern is due to the fact that the mechanisms seem to vary with pH, type and concentration of the material producing the turbidity, and the coagulating agent used. Before proceeding with a review of these theories, it is necessary to make a distinction between coagulation and flocculation. For the purposes of this investigation, the term coagulation will refer to the destabilization of the colloidal particles through the addition of coagulant to the water. Flocculation will refer to the collision and aggregation of the destabilized particles into relatively large aggregates known as flocs [31]. These definitions are different from those given by LaMer [32] who defined coagulation as processes which bring about the reduction of the repulsive potential of the electrical double layer of the colloidal particles and flocculation as being the bridging action of high molecular weight polyelectrolytes which brings about a loose three-dimensional floc structure. LaMer's definitions consider coagulation and flocculation as two different mechanisms of colloid destabilization and aggregation. The definitions used in this paper consider coagulation as the process of destabilization of colloidal particles without reference to the particular causative mechanism. The term flocculation is applied to the hydrodynamics of aggregation and floc formation.

The phenomena which cause colloidal clay particles to remain suspended in water are quite well known from colloid chemistry and have long been described in sanitary engineering texts and papers [31–35] and need not be reiterated in detail in this report. It is sufficient to note that much of the theory concerning the mechanism of coagulation centers on the reduction of the zeta potential to a level where the repulsive forces are sufficiently low so that collision can occur and the Van der Waal and other forces can be operative. The colloidal particles can then collide, aggregate, and form large settleable or filterable flocs.

Coagulation Theories

In 1949 Langelier and Ludwig [34] made a systematic study of various clays suspended in water. Their main finding was a correlation between the cation exchange capacity (CEC) of the colloidal material and the coagulant dose necessary to achieve a particular level of removal of turbidity. Although this study has been criticized [36, 37] because of lack of pH control, it is important for two reasons. It demonstrated that alkalinity is important in determining the coagulant dose necessary to achieve satisfactory clarification. Also, it was noted that in many instances efficient clarification requires a binder material of hydrolysis products of aluminum or iron. They concluded that the addition of highly charged cations – Al^{+++} or Fe^{++} – reduced the zeta potential of the colloidal particle to a level where aggregation could take place. Then the hydrous oxide would act to bind the destabilized particles and form large flocs which could then be removed.

In 1965 Kim, Ludwig, and Bishop [36] extended the work of Langelier and Ludwig. Coagulation jar tests were made with the final pH a controlled parameter. They found that at low kaolinite concentrations (< 100 mg/ℓ) there was an inverse relationship between the clay concentrations and the amount of alum necessary to produce clarification. At high concentrations of kaolin, and with bentonite, they found a direct relationship between clay concentrations and the coagulant dose. This implies that at different kaolin concentrations, different coagulation mechanisms may be dominant. At low kaolin concentrations, they found that the optimum pH for best coagulation was the same as the isoelectric pH of the aluminum-hydroxo complex formed by the alum and the alkalinity in the water. That is, turbidity removal was greatest – for a given kaolin concentration and alum dosage – at the pH of least solubility of aluminum hydroxide. At high concentrations of kaolin and with bentonite they found that a slight positive charge on the aluminum-hydroxo compounds which were formed resulted in best turbidity removal. They concluded that for suspensions with high particle concentrations, a reduction in zeta potential to the point where aggregation of destabilized particles may take place provided the most efficient clarification.

Packham [38] reported similar findings. Conditions for the most rapid coagulation of dilute concentrations of kaolin were those leading to the most rapid precipitation of aluminum hydrolysis products. He noted that the turbidity in samples of river water from Britain behaved similarly to dilute kaolin suspension. He also used bentonite and more concentrated suspensions of kaolin and, as did Kim, Ludwig, and Bishop, obtained results different from those obtained using dilute kaolin suspensions.

Many authors [37–41] have pointed out that when alum is added to water, the Al^{+++} ion undergoes hydrolysis, the extent and character of which depends on the pH and aluminum concentration. Figure 6 shows the concentrations of various aluminum species at different pH values in equilibrium with freshly precipitated $Al(OH)_3$. However, it should be recognized that equilibrium may not be reached quickly and that the transition from Al^{+++} to $Al(OH)_3$ occurs through successive substitutive reactions. Stumm and Morgan [41] noted that the net charge on

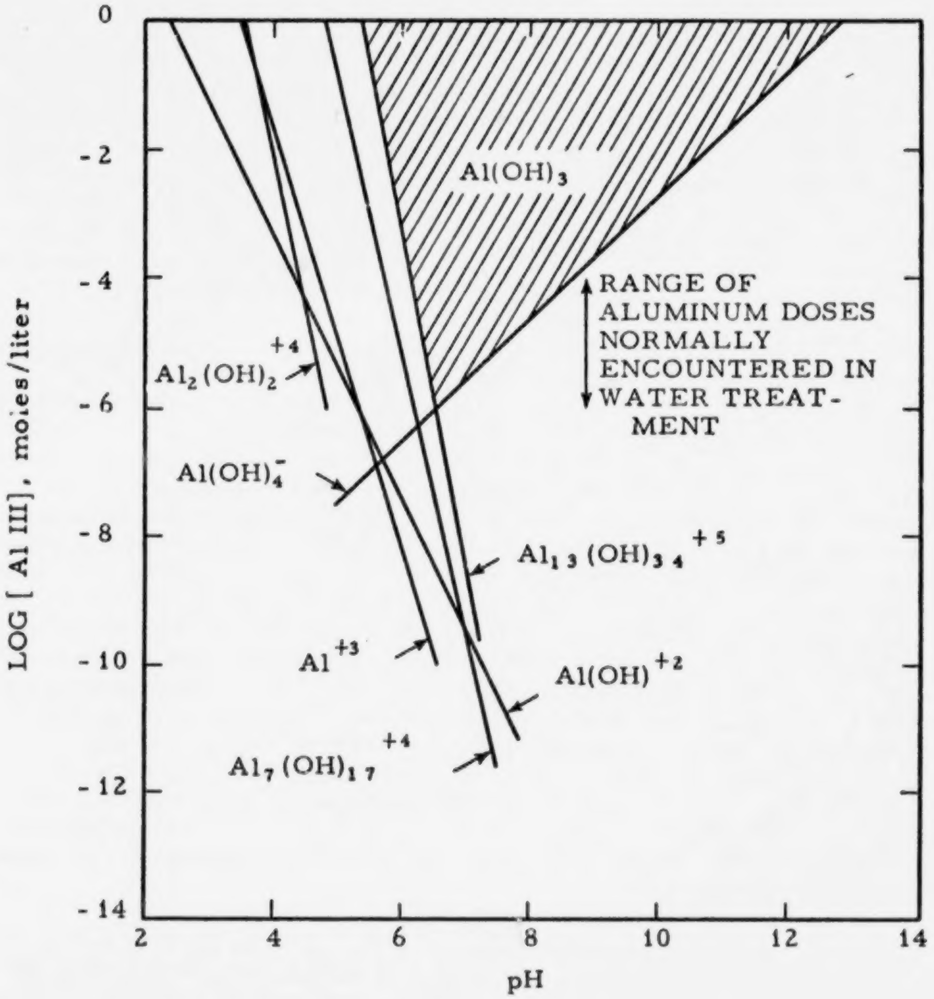

FIGURE 6. CONCENTRATION OF VARIOUS ALUMINUM SPECIES IN EQUILIBRIUM WITH FRESHLY PRECIPITATED $Al(OH)_3$ (FROM BLACK AND CHEN [39])

any aluminum-hydroxo compound is probably an average value, with different charges being associated with different aluminum atoms or groups of atoms. Moreover, the forms present are probably not restricted to those shown in Figure 6 [38, 41]. Polymers can be formed by hydroxyl groups acting as a bridge between two or more metal atoms. These are termed "olation" reactions.

Table 1 [38] shows the various types of reactions which are involved in aluminum hydroxide precipitation. Listed first are the ligand exchange reactions. These reactions occur in sequence when Al(III) is added to water. Also listed are examples of olation reactions which result in polynuclear polyhydroxo species. The important point is that at a particular pH and concentration of aluminum in water, not just one, but many aluminum-hydroxo compounds will be formed. However, one species — insoluble aluminum hydroxide for example — may predominate, especially if sufficient time is allowed.

Black and Chen [39] made studies of coagulation of clay by alum using microelectrophoretic techniques to help determine the mechanism of coagulation. They noted that in most instances in water treatment, the aluminum ion concentration falls between 10^{-6} and 10^{-4} M (see Figure 6). For this range in aluminum ion concentration, the predominant aluminum species in each of three pH ranges are as follows: Below pH 4 the hydrated trivalent aluminum ion is the most active species. In the region between pH 4 and pH 6, one or more of the hydrolyzed aluminum polynuclear cations, such as $Al_6(OH)_{15}^{+++}$ or $Al_8(OH)_{20}^{+4}$, may predominate. From pH 6 to pH 8, insoluble aluminum hydroxide may be considered most important.

They concluded that different mechanisms were responsible for coagulation in each of the three pH ranges. Below pH 4 the trivalent aluminum ion acts to reduce the zeta potential of the colloidal particles and produce destabilization and agglomeration of particles. In the range where the multivalent polymeric aluminum-hydroxo species exist, specific adsorption of these ions onto the surface of the clay particle was concluded to be effective in producing destabilization by reduction of zeta potential. Between pH 6 and 8, physical enmeshment (or sweep flocculation or sweep coagulation) by aluminum hydroxide or mutual coagulation between positively charged aluminum hydroxide colloids and negatively charged clay particles were concluded to be the mechanisms involved.

The concept of specific adsorption of multivalent aluminum-hydroxo compounds onto the clay particles leads to consideration of a different concept of coagulation as discussed by LaMer [42], Stumm and Morgan [41], Stumm and O'Melia [37], and Hahn and Stumm [40]. This may be termed the "chemical approach" as opposed to concern with reduction of zeta potential by electro-kinetic attraction of counter-ions. Although this division is convenient, it can be — as with all simplifications — misleading. For example, while chemical forces may act to cause adsorption of positively charged aluminum species, the effect of this adsorption is the reduction of zeta potential, allowing coagulation to occur [39, 40]. Thus, both chemical and electrokinetic phenomena are involved. Perhaps one of the best examples of the chemical approach to colloid destabilization is the coagulation of a negatively charged clay colloid by a negatively charged long chain polymer. Since the two constituents are both negatively charged, chemical forces must be acting in the process [42].

TABLE 1

TYPES OF REACTIONS INVOLVED IN HYDROLYSIS OF Al(III)
(FROM PACKHAM [38])

Ligand Exchange Reactions

1 a. $[\,Al(H_2O)_6\,]^{+++} + H_2O \rightleftarrows [\,Al(H_2O)_5\,OH]^{++} + H_3O^+$

b. $[\,Al(H_2O)_5\,OH]^{++} + H_2O \rightleftarrows [\,Al(H_2O)_4\,(OH)_2\,]^{+} + H_3O^+$

c. $[\,Al(H_2O)_4(OH)_2\,]^{+} + H_2O \rightleftarrows [\,Al(H_2O)_3\,(OH)_3\,] + H_3O^+$

2 $[\,Al(H_2O)_3\,(OH)_3\,] + X^{=} \rightleftarrows [\,Al(H_2O)_4\,X]^{+} + 2H_2O$

3 $[\,Al(H_2O)_4(OH)_2\,]^{+} + X^{=} \rightleftarrows [\,Al(H_2O)_4\,X]^{+} + 2OH^-$

(X Represents a Divalent Ion)

Olation Reactions

4 a. $2[\,Al(H_2O)_5\,OH]^{++} \rightleftarrows$

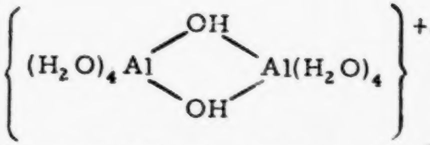

$+ 2H_2O$

b. $[\,(H_2O)_4\,Al(OH)_2\,Al(H_2O)_4\,]^{+4} \rightleftarrows [\,(H_2O)_4\,Al(OH)_2\,Al(H_2O)_3\,OH]^{+3} + H_3O^+$

c. $[\,(H_2O)_4\,Al(OH)_2\,Al(H_2O)_3OH]^{+3} + [\,Al(H_2O)_5\,OH]^{+2} \rightleftarrows$

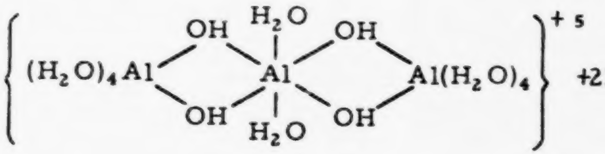

$+2H_2O$

There has been considerable disagreement among investigators over whether a "chemical" or "physical" approach should be taken in attempting to understand the coagulation process. It has now become apparent, however, that both chemical and physical phenomena need to be considered.

In 1967 Stumm and O'Melia [37] published a paper in which they attempted to describe the mechanism of coagulation at various pH's and colloid concentrations. They drew upon the work of others as well as their own. They concluded that at high surface concentrations (square meters of colloidal surface per liter), coagulation takes place by adsorption of multinuclear hydrolysis products of Al(III). At low concentrations of colloidal material — particularly kaolin concentrations less than 100 mg/ℓ — sweep flocculation, or enmeshment by insoluble aluminum hydroxide, is responsible for removal of colloidal material from suspension. For sweep flocculation to occur, the pH must be such that there is a tendency to precipitate insoluble aluminum hydroxide.

Figure 7 summarizes Stumm and O'Melia's conclusions. At low surface concentrations, coagulation takes place through nonstoichiometric sweep flocculation (zone 4). At higher surface concentrations, adsorption of soluble Al(III) hydrolysis products is responsible for destabilization of the clay particles (zone 2). Stumm and O'Melia also term this stoichiometric coagulation.

It should be pointed out that mere physical enmeshment is not an adequate description of Stumm and O'Melia's sweep flocculation (zone 4). This would imply that the presence of the clay particles does not affect the hydrolysis reactions of the Al(III), i. e., that the clay is merely a passive component. This is probably not entirely correct. The studies of Kim, Ludwig, and Bishop [36] and Packham [38] show that for low concentrations of kaolin at constant pH, the concentration of alum necessary to produce coagulation is inversely related to the kaolin concentration. (Furthermore, in the present study, it has been found that addition of alum to clear water resulted in floc of poorer quality being formed much more slowly than when alum was added to the same water containing 25 mg/ℓ of kaolin.)

Stumm and O'Melia point out two possible reasons for the inverse relationship between colloid concentration and coagulant dose. With colloidal particles providing interfaces for localized over-saturation, the critical supersaturation necessary for rapid precipitation could decrease with increasing clay concentration. The alternative explanation considers mutual coagulation of the negatively charged colloids with small particles of aluminum hydroxide precipitates or aluminum hydroxo compounds. It can be postulated that at low colloid concentrations, an insufficient number of particles is present to provide the necessary contact opportunities in a reasonable time and the presence of $Al(OH)_3$ particles can produce efficient aggregation. Thus, increasing the clay particle concentration can reduce the necessary coagulant dosage.

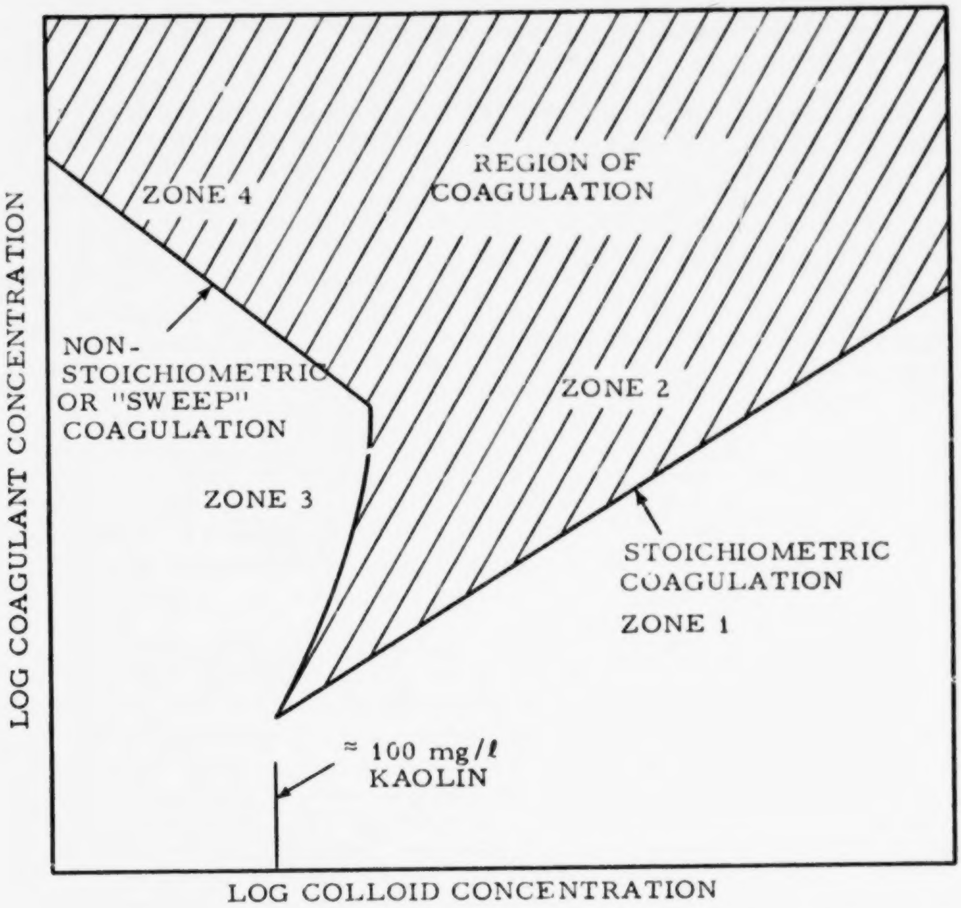
LOG COAGULANT CONCENTRATION
REGION OF COAGULATION
ZONE 4
NON-STOICHIOMETRIC OR "SWEEP" COAGULATION
ZONE 2
ZONE 3
STOICHIOMETRIC COAGULATION
ZONE 1
≈ 100 mg/ℓ KAOLIN
LOG COLLOID CONCENTRATION

FIGURE 7. EFFECT OF COLLOID CONCENTRATION ON COAGULANT REQUIRED FOR DESTABILIZATION (AT CONSTANT pH) (FROM STUMM AND O'MELIA [37])

In summary, while there is still confusion and disagreement over the exact mechanism of coagulation which may be effective under particular circumstances, some general statements may be made. Neither the chemical or double layer models can adequately describe the phenomena observed in the coagulation of various colloidal materials at all concentrations or pH values.

At low concentrations of kaolin — less than 100 mg/ℓ — and at pH values near 7, it appears that rapid precipitation of uncharged insoluble aluminum hydroxide is associated with efficient coagulation. This implies a "sweep flocculation" model. At higher concentrations of kaolin, and with other colloidal suspensions such as silica and bentonite at moderate concentrations, some other mechanism is operative — most likely the adsorption of multivalent polynuclear aluminum-hydroxo compounds onto the surface of the colloid leading to reduction of the negative charge and destabilization.

Review of Flocculation Kinetics

Smoluchowski [43, 44] first developed expressions for the frequency of collisions of particles suspended in a fluid. Where the fluid is at rest, collisions can take place due to Brownian motion. This is called perikinetic flocculation. The frequency of such collisions is given by Equation (55):

$$I_{ij} = 4 \pi D_{ij} R_{ij} n_i n_j \qquad (55)$$

where I_{ij} is the number of contacts made per unit time and unit volume; D_{ij} is the combined diffusion coefficient, $D_i + D_j$; R_{ij} is the collision radius which equals the sum of the particle radii, $R_i + R_j$; and n_i and n_j are the number concentrations of particles of radius R_i and R_j.

In addition to perikinetic flocculation, particles can collide as a result of their motion with the fluid. This is termed orthokinetic flocculation and is perhaps of greater importance in water treatment. Smoluchowski showed that for laminar flow, the collision frequency is given by

$$J_{ij} = \frac{4}{3} n_i n_j R_{ij}^3 \frac{dU}{dZ} \qquad (56)$$

where J_{ij} is the collision frequency due to laminar motion; dU/dZ is the laminar velocity gradient; and n_i, n_j, and R_{ij} have the same definition as in Equation (55). This equation is not useful because it is restricted to laminar motion. In all instances of orthokinetic flocculation used in water treatment, turbulent motion is present.

In 1943 Camp and Stein [45] used Smoluchowski's basic model to develop a relationship giving the frequency of collision in turbulent motion. Using a theory of Stokes, they related the energy input to the system and the resulting root-mean-square velocity gradient.

$$G = \sqrt{\frac{P/V}{\mu}} \qquad (57)$$

where G is the root-mean-square velocity gradient, P is the power input, V is the volume, and μ is the viscosity.

The resulting collision frequency equation is

$$H_{ij} = \frac{4}{3}\, n_i\, n_j\, R_{ij}^3\, G \tag{58}$$

Several other equations [31, 46–50] have been developed giving the particle collision frequency in turbulent flow. Most bear a very close resemblance to Equation (58), although various assumptions were made in order to provide a more sophisticated treatment of the problem. The above equation can be modified to give, instead of the frequency of collisions, the rate of removal of the smallest, or primary, particles from the system. A simplified form is

$$\frac{dn_1}{dt} = - K_A n_1 G \tag{59}$$

where K_A is an aggregation rate coefficient. Argaman and Kaufman [31, 46] and Parker, Kaufman, and Jenkins [51] have added another term which represents the formation of primary particles due to surface erosion of larger particles. In simplified form this is

$$\frac{dn_1}{dt} = - K_A n_1 G + K_B G^2 \tag{60}$$

where K_B is a breakup rate coefficient. This equation is usually of interest when applied to a CSTR. For one compartment, a materials balance at steady state gives

$$Q n_1^0 - Q n_1^1 - K_A n_1^1 G V_r + K_B G^2 V_r = 0 \tag{61}$$

where Q is the flow rate, V_r is the reactor volume, n_1^0 is the influent concentration of primary particles, and n_1^1 is the effluent concentration of primary particles. Rearrangement of the above equation and replacing V_r/Q by T, the mean residence time, yields

$$\frac{n_1^0}{n_1^1} = \frac{1 + K_A G T}{1 + \frac{K_B G^2 T}{n_1^0}} \tag{62}$$

n_1^0/n_1^1 is termed the "performance parameter" and is often used in plotting results of flocculation studies. For convenience, the ratio of the initial to final turbidity as measured by a light-scattering turbidimeter is often taken to be equal to n_1^0/n_1^1.

PREVIOUS WORK CONCERNING INITIAL MIXING AND TREATMENT PROCESSES

There has been very little work published to indicate that rapid initial mixing may be significant in water and wastewater treatment processes. The reactions which occur when chemicals are added to the water stream are often quite complex, as described earlier, as well as quite rapid. Physical-chemical reactions can occur between the added chemical, the component of the water stream which is the object of treatment (e.g., clay turbidity), and other constituents of the water stream (e.g., alkalinity). Reactions between the chemical and these other constituents may act in such a way as to reduce the effectiveness of the treatment process. For example, in alkaline waters poor mixing may result in complete hydrolysis of the aluminum in only a fraction of the stream being treated.

The relation between mixing and extent of reaction has been of interest in chemical engineering studies. Toor [24] has studied the relation between mixing and extent of reaction for a simple case, a very fast reaction in which two reactants, dissolved in separate streams of water, of equal molecular diffusivity combine to form a product.

$$A + B \rightarrow C \quad . \qquad (63)$$

By the term very fast reaction, it is meant that the rate of reaction is much faster than the rate of mixing. Therefore the extent of the reaction is controlled by the extent of the mixing process. For the case where the reactants are present in stoichiometric amounts, it is found that the fractional completion of reaction, F, is equal to the fractional completion of mixing, η, i.e.,

$$F = \eta = 1 - \frac{a'}{a'_o} \quad . \qquad (64)$$

For the case where one reactant is present in excess, for example, β times the stoichiometric amount, the expression is more complicated.

$$F = 1 + (\beta - ^1 \left\{ 1 + g\left[a'_o (1 - \eta) \right] \right) \qquad (65)$$

where

$$g(x) = \frac{x}{\sqrt{2}} \operatorname{ierfc} \left(\frac{1}{\sqrt{2}\, x} \right) \quad . \qquad (66)$$

Equations (64) and (65) are shown in Figure 8 for various values of β. This graph indicates that when one of the reactants is introduced in excess, the reaction will be completed, i. e. , the limiting reactant will be completely utilized, before mixing is completed.

Keeler [22] and Vassilatos and Toor [52] have experimentally verified Equations (64) and (65), and the concept behind Equation (64) had been known and used previously [53].

In alum coagulation-flocculation of a turbid water, the alkalinity of the water may be considered to be a reactant present in excess of that needed to react completely with the coagulant added to the stream. Reaction of the alkalinity with the alum before the alum has become completely mixed with the turbid water may act to detrimentally affect process performance. Of course, this process is much more complicated than the simple case studied by Toor. First, the reactions are very complex, their rate and extent depending upon alkalinity and pH. Secondly, the rate of reaction does not appear to be so fast that it cannot be overcome by providing much faster mixing. This second point is fundamental to the present study: by providing more rapid mixing, crucial reactions which can occur before the alum has been dispersed evenly throughout the clay particles can be made to occur after this mixing has taken place. Alternatively, these reactions may be prevented in favor of desirable physical-chemical reactions between the alum and the turbidity particles.

In a manner somewhat analogous to the way in which increasing one of the reactants at a given degree of mixing will increase the fractional completion of reaction in Figure 8, increasing the alkalinity may allow completion of certain hydrolysis reactions at a lesser degree of mixing, i. e. , at a time when greater segregation between the alum and the turbidity exists. Thus, at high alkalinities, it may be even more important to attempt to insure that the rate of mixing is faster than the rate of the crucial reactions.

In a study concerned with water and wastewater treatment, Rudolfs and Gehm [54] published a paper in 1936 describing treatment of wastewater with $FeCl_3$. They found that slow mixing allowed undesirable hydrolysis reactions to occur which decreased the efficiency of the process.

More recently, Selleck and coworkers [55–57] reached a preliminary conclusion that rapid initial mixing can be very important in wastewater chlorination efficiency. They concluded that the combined chlorine residuals formed in wastewater undergo rapid reactions in the first milliseconds of contact with the waste stream. These changes result in a decrease in the bactericidal effectiveness of the chlorine. If the mixing of the chlorine with the waste stream is rapid enough, the more bactericidal compounds will come in contact with the bacteria, and process performance will be improved. (Studies of chlorination and initial mixing are presented in Appendices A and B.)

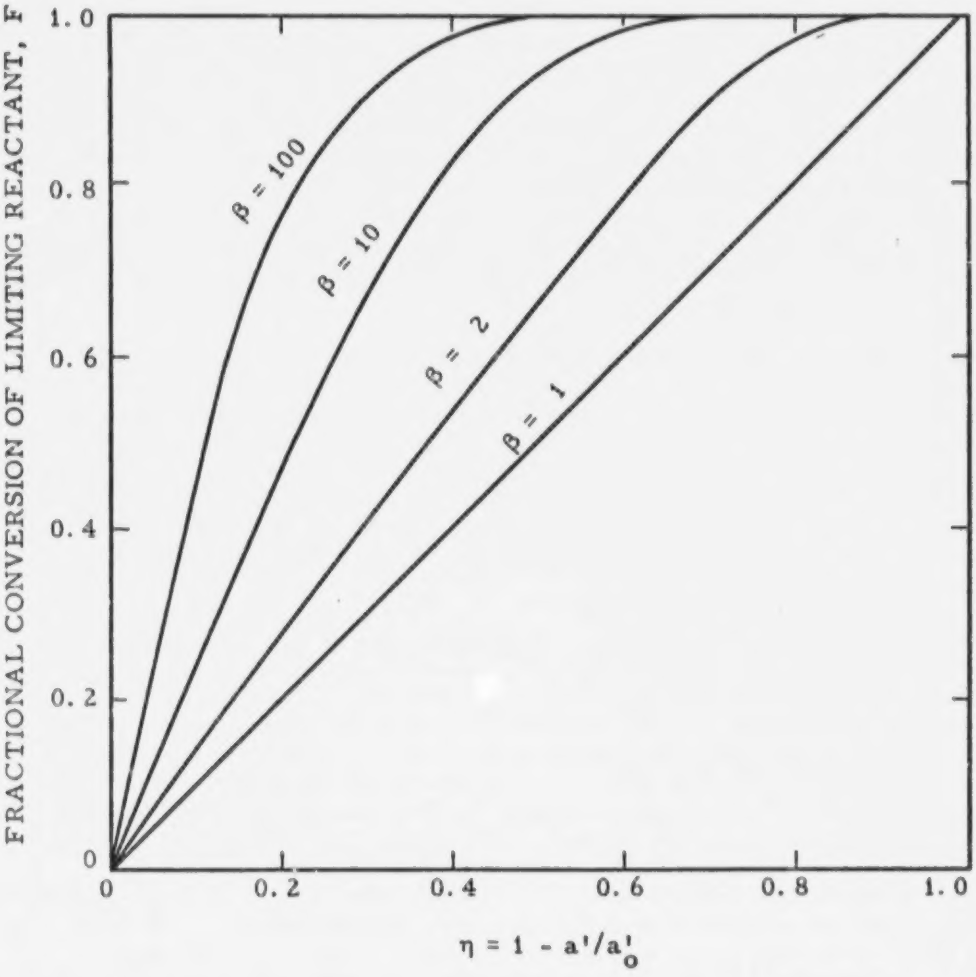

FIGURE 8. FRACTIONAL CONVERSION AS A FUNCTION OF ACCOMPLISHED MIXING (FROM TOOR [24])

The increasing study and use of polyelectrolytes as coagulants and coagulant aids may provide another area in which rapid initial mixing may be important. Riddick [58] notes that a long chain polymer may, if mixing is not accomplished sufficiently rapidly, react with other similar polymers or itself and would be unavailable for reaction with the colloidal material.

Recently, Vrale and Jorden [59] made studies of the relation between rapid mixing and alum coagulation-flocculation, the same process with which this study is concerned. A high-speed backmixed reactor (flash mixer) and several 1-in. I. D. tubular, plug flow reactors were used. After the alum was mixed with the turbid water (tap water with SiO_2 colloid, $NaHCO_3$, and $CaCl_2$ added) in the initial mixing device, jar tests were made to determine if the various initial mixers caused differences in performance. They concluded that more rapid initial mixing resulted in better turbidity removal and that the high-speed backmixed reactor, which is normally regarded as an adequate initial mixing device and which is often used in plant design, actually is much poorer than a plug flow system.

Similar results have been found by Wilson [60] in work done previously at the Sanitary Engineering Research Laboratory at the University of California. In these experiments, kaolin was used to provide the colloidal turbidity. With both jar tests and continuous flow pilot plant flocculation experiments it was found that the tubular reactor initial mixers produced better results than did the backmixed reactor, presumably because segregation between the alum and water streams was eliminated more rapidly when the tubular reactors were used.

In one sense, rather than being a duplication, the two investigations, one by Vrale and Jorden and the other by Wilson, complement each other. Vrale and Jorden used colloidal SiO_2 to provide turbidity. They found a stoichiometric relationship between the colloid concentration and the coagulant dose necessary to produce coagulation (at a constant pH). In Stumm and O'Melia's terminology [37], this corresponds to an adsorption-destabilization mechanism of coagulation. Wilson used a dilute kaolin suspension. As noted previously, this seems to correspond to a sweep flocculation mechanism of coagulation. It has been shown, therefore, that initial mixing seems to be important regardless of the coagulation mechanism. This is important with respect to application of such studies to full-scale water treatment facilities where both types of colloidal material may be present. It is also important in that it may mean that the sweep flocculation mechanism and the adsorption-destabilization mechanism are not so different as they might first appear. As pointed out previously, the term sweep flocculation is somewhat inappropriate in that the clay particles do not act as a passive component. That initial mixing is important with both mechanisms seems to indicate other more basic similarities between them.

SECTION V

MIXING STUDIES: APPARATUS AND METHODS

INTRODUCTION

The experiments described in this and the following section were done in order to determine what characteristics of the grid, the turbulent flow field, and the scalar material affect the intensity of segregation at points downstream from a biplane grid when a tracer is introduced into the flow through numerous orifices in the grid bars. Closely related to this is the question of what design parameters should be used in the construction of such grids for use in water and wastewater treatment facilities.

This second question can be divided into two parts. First, what parameters related to the grid affect the time of mixing — the time required to reach some arbitrarily-defined low value of the intensity of segregation (for example, it could be defined as the time required for I_s to be such that $a'/\overline{A} = 10\%$)? Second, what is the relation between the time of mixing and process performance, i. e., how rapid must the mixing be in order to produce a significant improvement in performance? The latter question will be dealt with later when experiments involving alum coagulation-flocculation of turbid water will be discussed.

The work of Gibson and Keeler [22, 27] was used as a starting point for the present studies [11, 26, 30]. In some instances, their conclusions have been substantiated by these experiments; in other instances, new conclusions have been drawn which conflict with previously held theories.

The present studies tested the theory of Corrsin [17, 28] in that an effort was made to determine what design parameters may determine the scales of turbulence and segregation which in turn should affect the rate of scalar decay in the system being studied.

EXPERIMENTAL APPARATUS

Single Electrode Conductivity Probe

The total resistance of a uniform piece of conducting material is related to its resistivity by the following equation,

$$R = \rho \frac{L}{A} \tag{67}$$

where R is the total resistance, ρ is the specific resistivity in ohm-ft, L is the length of the material, and A is the cross-sectional area. In a standard conductivity cell, two electrodes of equal size are used. They are separated by a distance L, and the conducting solution between the probes has a constant cross-section, A. Equation (67) can be written in terms of a cell constant,

$$R = \rho K_c = \frac{K_c}{\sigma} \qquad (68)$$

where $K_c = L/A$ is the cell constant and $\sigma = \rho^{-1}$ is the specific conductivity of the fluid. Conductivity probes are usually calibrated in terms of the cell constant. Knowing the resistance measured by the cell in a given fluid, the conductivity can be calculated.

Consider a conductivity cell with two electrodes, A and B which vary greatly in size. Assume that the conducting solution occupies only the space between the electrodes. Equation (67) can be written in integral form,

$$R = \int_A^B \frac{\rho}{A(\ell)}\, d\ell \quad . \qquad (69)$$

The greatest contribution to the total resistance will come from the parts of the system where $A(\ell)$ is very small, i. e., near the small electrode. Suppose now that ρ varies from point to point within the system. If this variation is not so great that it dominates the effect of the changing area, then R will tend to be a function of the resistivity near the small electrode.

With a probe of this type, a conducting tracer such as NaCl solution is used. At low concentrations, the conductivity of the solution is proportional to concentration. A change in conductivity will be detected by the probe and, through the associated electronic apparatus, a voltage can be measured which is proportional to the concentration at a "point" defined by the effective volume of the probe.

This is the principle upon which the single electrode conductivity probe operates. The end of a small diameter wire protruding from the tip of a probe acts as the small electrode. The ground of the system acts as the other electrode. The single electrode probe was developed simultaneously by Gibson [11, 30] and Keeler [22, 27] and was an improvement over the probe develcped by Lamb, Manning, and Wilhelm [61]. Their probe consisted of a large and small electrode which allowed current to leak to grounds in the system. Using the system ground as the large electrode eliminated this problem.

It is possible to develop some estimate of the volume over which this type of probe effectively measures resistivity by considering a spherical electrode of radius r_o immersed in an infinite body of electrolyte [11]. For this geometry, Equation (69) may be written

$$R_\infty = \int_{r_o}^{\infty} \frac{\rho}{4\pi r^2}\, dr \tag{70}$$

$$R_\infty = \frac{\rho}{4\pi r_o} \quad . \tag{71}$$

From Equation (68) the cell constant is

$$K_c = \frac{1}{4\pi r_o} \quad . \tag{72}$$

If the effective cell volume is taken to be that volume closest to the sphere which contributes 90% of R_∞, this volume can be easily found from

$$0.9\, R_\infty = \int_{r_o}^{B} \frac{\rho}{4\pi r^2}\, dr \tag{73}$$

which leads to

$$0.9\, B = 10\, r_o \quad . \tag{74}$$

Therefore, the effective probe radius can be considered to be approximately 10 times the radius of the sphere. This gives some indication of how close to a "point" the probe is measuring.

Keeler concluded that the shape of the probe tip was very important in determining the spatial resolution of the probe because a blunt tip disturbed the flow field in the vicinity of the tip. He noted that when Gibson replaced a 50-micron blunt probe by one 20 microns in diameter, there was no apparent increase in the ability to resolve high frequency components of the scalar spectrum. Gibson also concluded that the blunt shape of the tip may have been the limiting factor in spatial resolution.

The major contribution to the rms concentration fluctuation is from the lower wave number portion of the scalar spectrum. Therefore, when rms values are measured, spatial resolution is not so important, and larger, more blunt probes can be tolerated, which simplifies construction problems.

The probe used in this study had a tip 3 mils (75 microns) in diameter. This is larger than those used by Gibson (10—51 μ) and Keeler (1—25 μ) and is the same size as the small electrode of the probe developed by Lamb, Manning, and Wilhelm. Attempts were made to build smaller probes in order to compare the results obtained from using different sized probes. However, difficulties were encountered and no reliable results were obtained. While no photographs of the probes actually used by Gibson are available, it is believed from his description of their construction that the probes used in the present study may have been of superior shape. He used a cast epoxy tip and attempted to make the tip as sharp as possible using needle files and a microscope.

Keeler's probes were designed specifically to avoid the problems which a blunt tip might incur. The method of construction was very tedious and difficult [22]. All of his probes were small enough so that the rms fluctuations measured with them were only weakly dependent on the probe diameter beyond a distance of 10 mesh lengths from the grid.

Noting that the purpose of the present study was to determine the parameters which affect the rate of mixing downstream from a grid, "true" values of rms concentration fluctuations were not essential in the sense that what was sought was a comparison of the mixing obtained from various grids. Nevertheless, the present work may be criticized on the grounds that smaller probes, with better tip shapes, might have resulted in higher observed rms values. All experiments of the present study were made with probes of the same size so that the results would be consistent. Furthermore, based on the results and conclusions of Gibson and Keeler, the rms values obtained should be reasonably close to the "true" rms concentration fluctuations. Moreover, comparison of results with those of Gibson (see Appendix C) showed good agreement.

Probe Construction

A drawing of the single electrode conductivity probe used in the mixing experiments is shown in Figure 9. Photographs are shown in Figures 10 and 11. It was constructed from 5/16-in. O. D. thin-walled glass tubing. The tube was heated and drawn out to form a tapered tip, having a hole only slightly larger than the 3-mil platinum wire used for the electrode. It was found that tubing with reasonably thin walls produced the best tips. A short section of 3-mil platinum wire was then put through the tip and held in place at both ends, and a casting resin was poured into the large end of the tip. The viscosity of this resin was such that, before setting, a small ball of resin was formed outside the small end of the tip. The platinum wire protruding from this ball of resin was cut off, and the ball of resin was carefully filed down to a sharp point with the platinum electrode protruding from the end. A binocular microscope was used to aid this process.

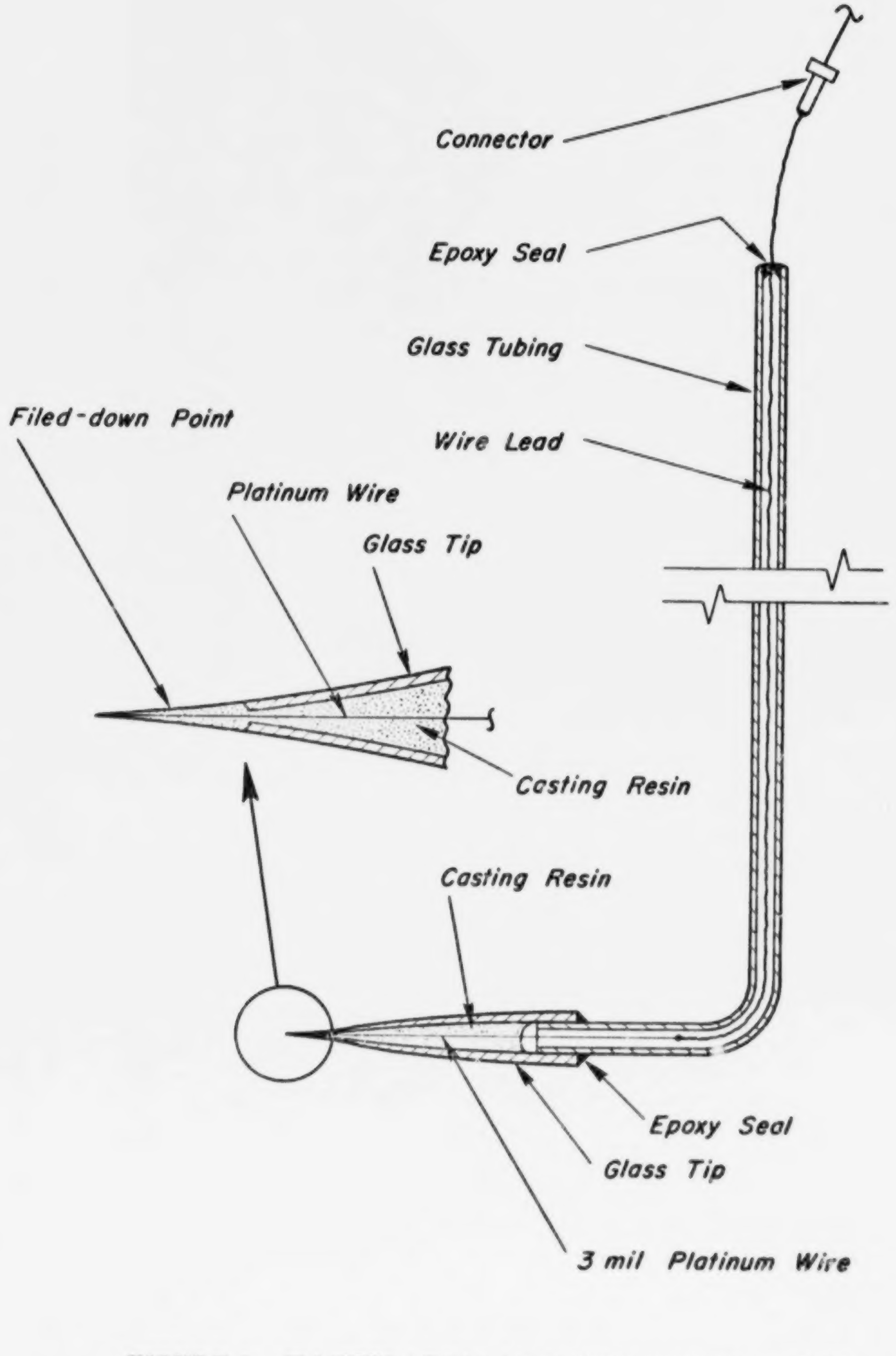
Connector
Epoxy Seal
Glass Tubing
Wire Lead
Filed-down Point
Platinum Wire
Glass Tip
Casting Resin
Casting Resin
Epoxy Seal
Glass Tip
3 mil Platinum Wire

FIGURE 9. ILLUSTRATION OF CONDUCTIVITY PROBE

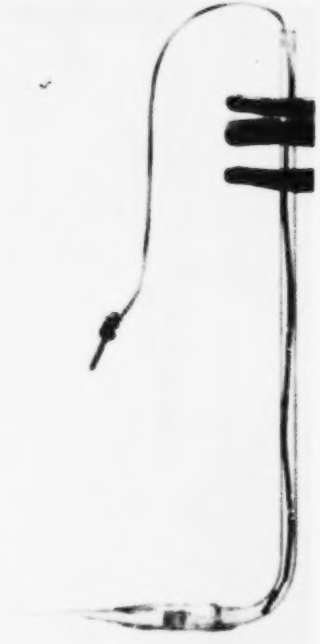

FIGURE 10. SINGLE ELECTRODE
CONDUCTIVITY PROBE

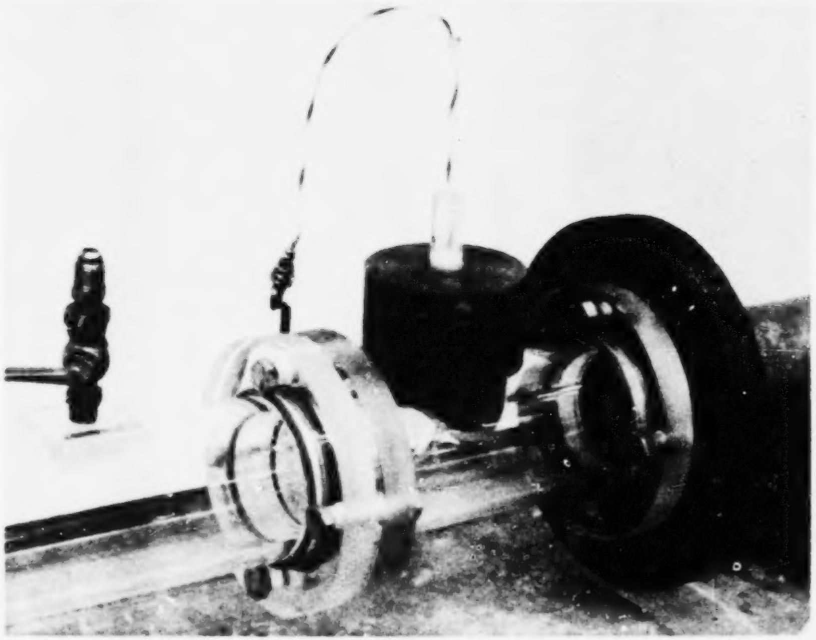

FIGURE 11. PROBE IN PLACE IN
TUBULAR REACTOR

No doubt some errors due to probe interference with the flow field did occur, but the difficulty of making probes in a manner similar to Keeler and the insensitivity of rms values to probe shape and size made more sophisticated probes unnecessary.

After the probe tip was constructed, a wire lead was soldered to the platinum wire and a glass tube with a 90° bend was cemented to the probe tip with epoxy resin.

After the probe was constructed, the platinum electrode was coated with platinum black (finely divided platinum). When current flows across the surface of the electrode, hydrogen and oxygen gases are formed. These gases add resistance to the system in addition to that caused by the solution resistivity. A capacitive reactance is also produced. An alternating current will allow some of the hydrogen and oxygen to recombine and reduce the additional impedance. For this reason, high frequency AC current is used in conductivity measurements. It has also been found that adding a coat of platinum black by electrolysis reduces the surface impedance.

For these experiments, the probes were platinized in a solution of chloroplatinic acid and lead acetate according to the method proposed by Standard Methods [62] with the exception that a Hewlitt-Packard 6215A DC power supply was used to supply the voltage. This allowed control of the voltage to obtain best results. Approximately 2 volts with a platinizing time of 30 to 40 seconds was used.

Electronic Equipment

A Tektronix 3C66 carrier amplifier was used to transform the resistivity (and hence concentration) near the tip of the probe into a voltage which could then be analyzed for rms and mean values. The 3C66 amplifier is a plug-in unit for the Tektronix 560 series oscilloscopes. A model 564B storage oscilloscope was used.

The oscilloscope permitted the trace (representing concentration vs. time for the present work) to be "stored" on the oscilloscope screen as the trace was normally on the screen for only a few milliseconds. Storing a trace allows better visualization of the concentration-time signal. Although the storing apparatus was not used directly in this work, it proved to be useful for demonstrating the use of the single electrode conductivity probe.

A block diagram of the 3C66 carrier amplifier is shown in Figure 12. [63]. It has the advantage of being a completely prepackaged unit. Although it was designed for use with strain gauges, it was used for the present work without any modifications. The 3C66 unit operates on the principle of the AC bridge. A sketch of such a bridge is shown in Figure 13. When the bridge is balanced, $\xi = 0$. The condition for this is,

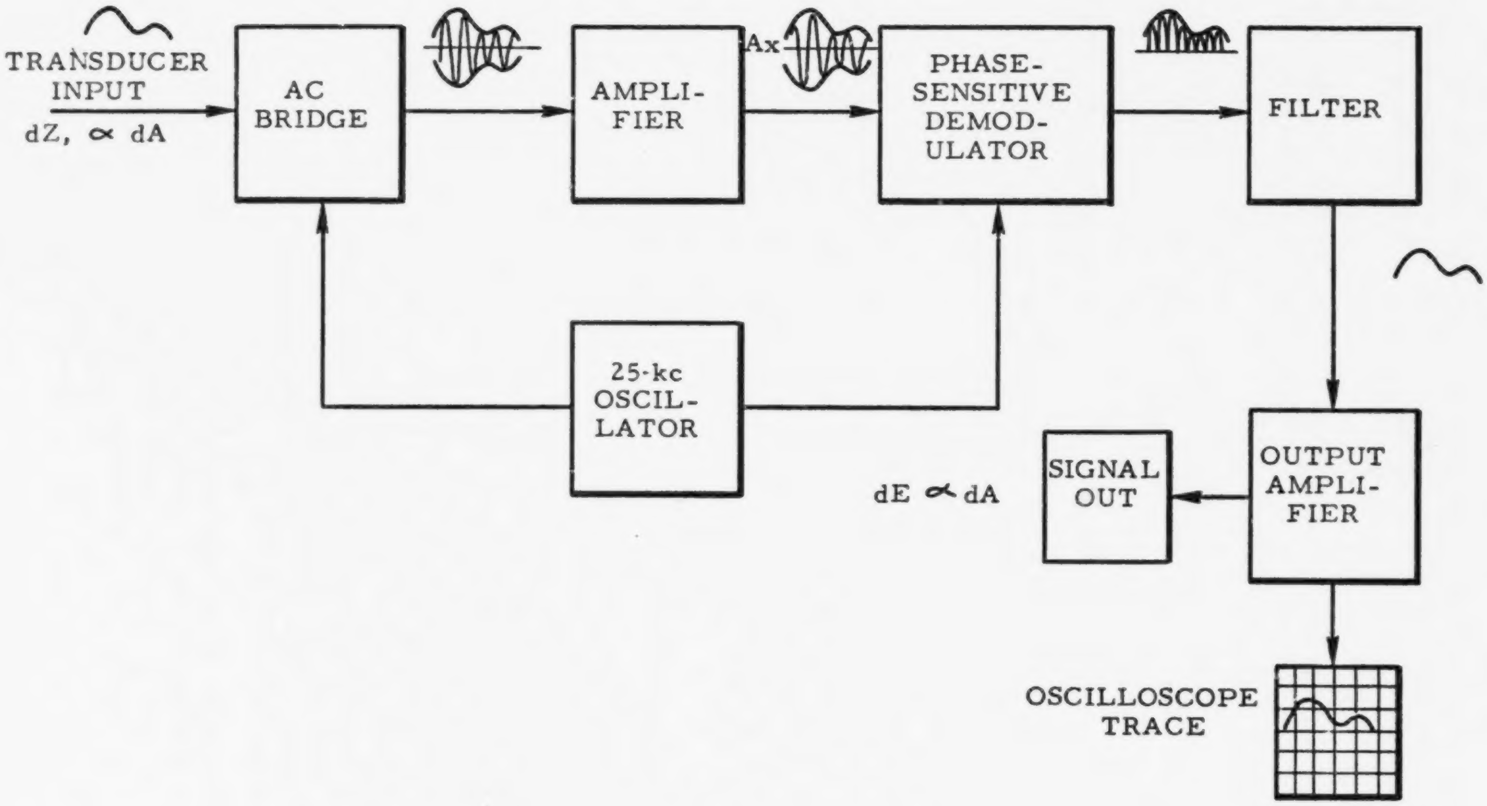
TRANSDUCER INPUT
dZ, ∝ dA
AC BRIDGE
AMPLI-FIER
Ax
PHASE-SENSITIVE DEMOD-ULATOR
FILTER
25-kc OSCIL-LATOR
dE ∝ dA
SIGNAL OUT
OUTPUT AMPLI-FIER
OSCILLOSCOPE TRACE

FIGURE 12. BLOCK DIAGRAM FOR TEKTRONIX TYPE 3C66 CARRIER AMPLIFIER

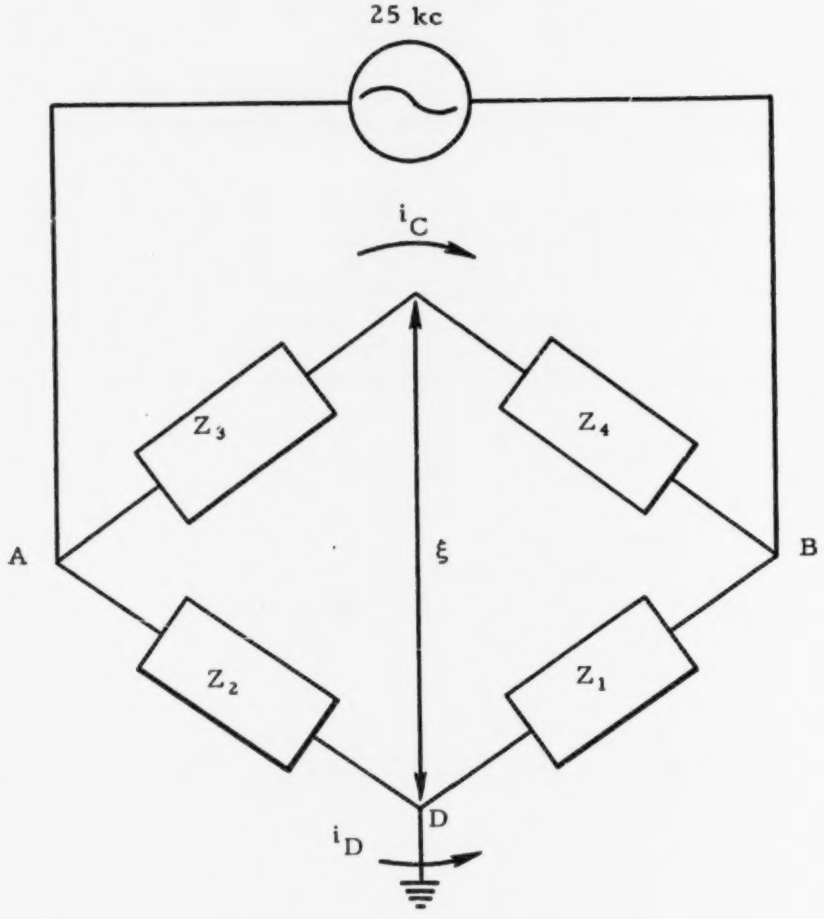

FIGURE 13. AC BRIDGE CIRCUIT

$$\frac{Z_1}{Z_2} = \frac{Z_4}{Z_3} \tag{75}$$

where Z_1, Z_2, Z_3, Z_4 are the impedance in each of the arms. It is found that the maximum sensitivity occurs when $Z_1 = Z_2$ and $Z_3 = Z_4$. Under these circumstances a change in Z_1 will be reflected by a change in ξ as follows:

$$\frac{d\xi}{E} = \frac{1}{4}\,\frac{dZ_1}{Z_1} \qquad (76)$$

where E is the voltage drop accross the branches from A to B. This relation holds as long as $\xi << E$; otherwise the response becomes nonlinear.

The probe was connected to the AC bridge in a manner which required the use of only one external arm. A 120-ohm resistor was placed parallel to the probe across arm No. 1 of the bridge as is shown in Figure 14. Under such circumstances, the conditions for balance are $Z_1 = Z_2 = Z_3 = Z_4$, and the resistance in each arm is approximately 120 ohms. Ignoring the reactive portion of the impedances across arm No. 1, it is possible to determine the change in ξ produced by a change in R_p.

$$R_T = \frac{R_p R'}{R_p + R'}\ ,\quad R' << R_p \qquad (77)$$

$$\frac{dR_T}{dR_p} = \frac{(R_p + R')R' - R_p R'}{(R_p + R')^2} = \frac{R'^2}{(R_p + R')^2} \qquad (78)$$

$$\frac{dR_T}{R_T} = \frac{R'^2}{(R_p + R')^2}\,\frac{R_p + R'}{R_p R'}\,dR_p = \frac{R'}{(R_p + R')R_p}\,dR_p\ . \qquad (79)$$

Since $R' << R_p$,

$$\frac{dR_T}{R_T} = \frac{R'}{R_p^2}\,dR_p\ . \qquad (80)$$

Ignoring the reactive impedance, Equation (80) can be substituted into Equation (76)

$$\frac{d\xi}{E} = \frac{1}{4}\,\frac{R'}{R_p^2}\,dR_p\ . \qquad (81)$$

The change in probe impedance is represented by dZ_1 in Equation (76) and by dR_p in Equation (81). In Equation (76), dZ_1 represents the change in probe impedance while in Equation (81), it is represented by dR_p. Using an arrangement which required only one external arm made it necessary to sacrifice sensitivity, since $R' << R_p$. For measuring rms values with the probes used in this study there was no problem in obtaining a sufficiently strong signal. However, if attempts

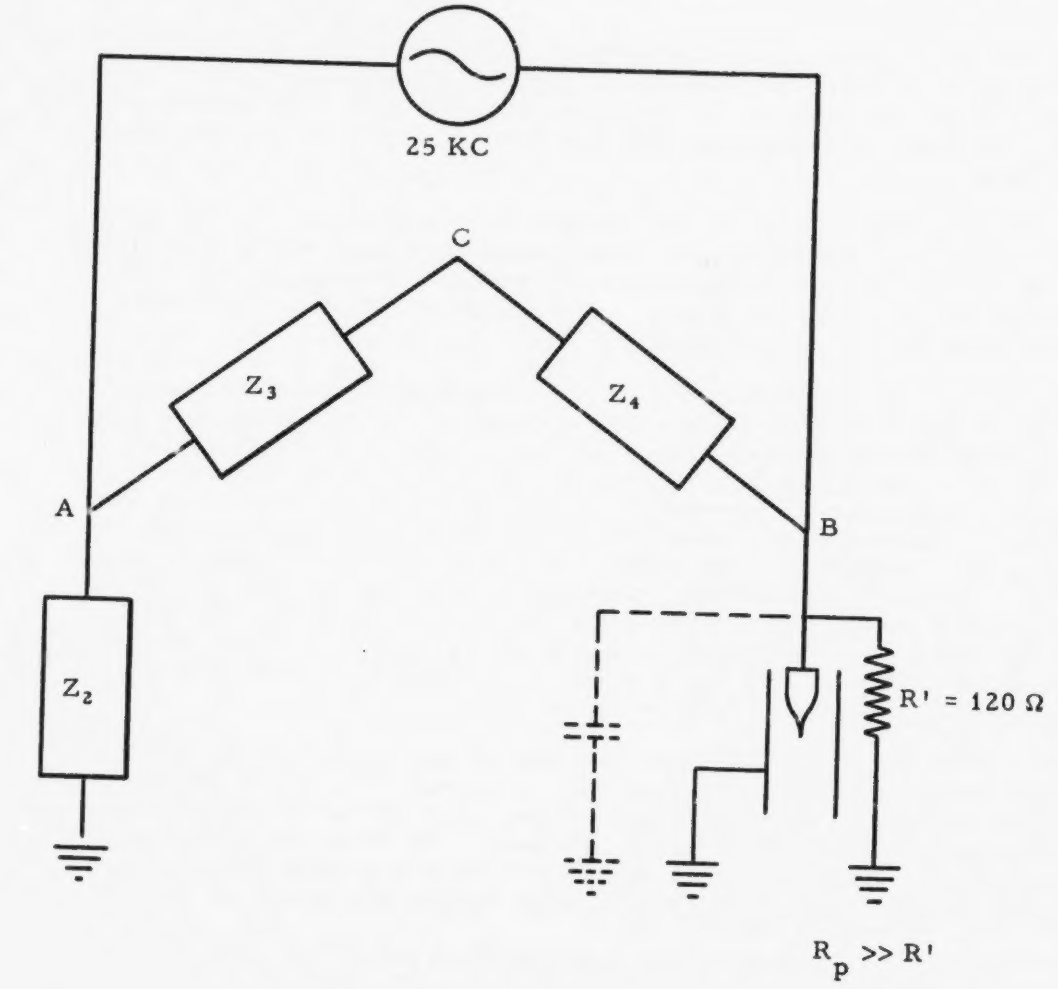

FIGURE 14. PROBE CONNECTED IN PARALLEL WITH 120-ohm RESISTOR

had been made to measure high frequency, low amplitude portions of the spectra, it might have been necessary to use an arrangement utilizing two external arms of the bridge. The probe would be one arm, and a variable capacitor and resistor, representing Z_2 in Figure 14 would be the other arm. A smaller probe might also require a similar arrangement. As $R_p \simeq R_\infty = p/4\pi r_o$, a decrease in r_o would cause in an increase in R_p. From Equation (81) a decrease in $d\xi/E$ would result.

A calibration curve for such a probe is shown in Figure 15. Above 2000 mg/ℓ NaCl the response of the system began to show a nonlinearity due to excessive unbalancing of the bridge. The average concentration in the experiments was about 50 mg/ℓ so this was not a problem.

To obtain the rms value of the concentration fluctuations, a TSI model 1060 rms voltmeter was used. This instrument represents an improvement over the rms voltmeters used in previous studies in that it can average the fluctuations over a longer period of time; the time constant could be varied up to 100 seconds.

The rms voltmeter used by both Gibson and Keeler had a time constant of only 2 seconds. They reported that the output reading of the rms voltmeter fluctuated so greatly that an analog averager had to be built to obtain steady readings. An important drawback to this method of obtaining rms values is that because of the small time constant, the contribution of low frequencies may be underestimated. These may constitute a considerable fraction of the total rms value. Thus, using an rms voltmeter with a greater time constant means more accurate results. For most of the rms made in the present study, a time constant of 10 or 30 seconds was used. These time constants correspond to low frequency cutoffs of approximately 0. 3 and 1 cycle per second, respectively.

In order to be certain that the scalar field was homogeneous at the points of rms measurements, it was necessary to know the mean scalar concentration. This information was also useful in checking probe calibration and the tracer flow rate. To make measurements of mean concentration, a DC voltmeter with a low-pass DC filter was used. The time constant for this meter was 47 seconds.

A disadvantage of using an averaging meter was the low input impedance. When the rms voltmeter and the DC voltmeter were connected to the output of the 3C66 unit simultaneously, the averaging meter tended to affect the reading of the rms voltmeter. For this reason, it was necessary to switch off the averaging meter while rms measurements were being made.

A schematic drawing of the electronic apparatus and probe is shown in Figure 16.

Flow Apparatus

Figure 17 shows a schematic illustration of the flow apparatus for the mixing experiments. It consisted of a multiple-orifice grid and tracer injection system at the head of a 2-in. I. D. tubular reactor. A nonrecirculating system was used to avoid the problem of tracer buildup.

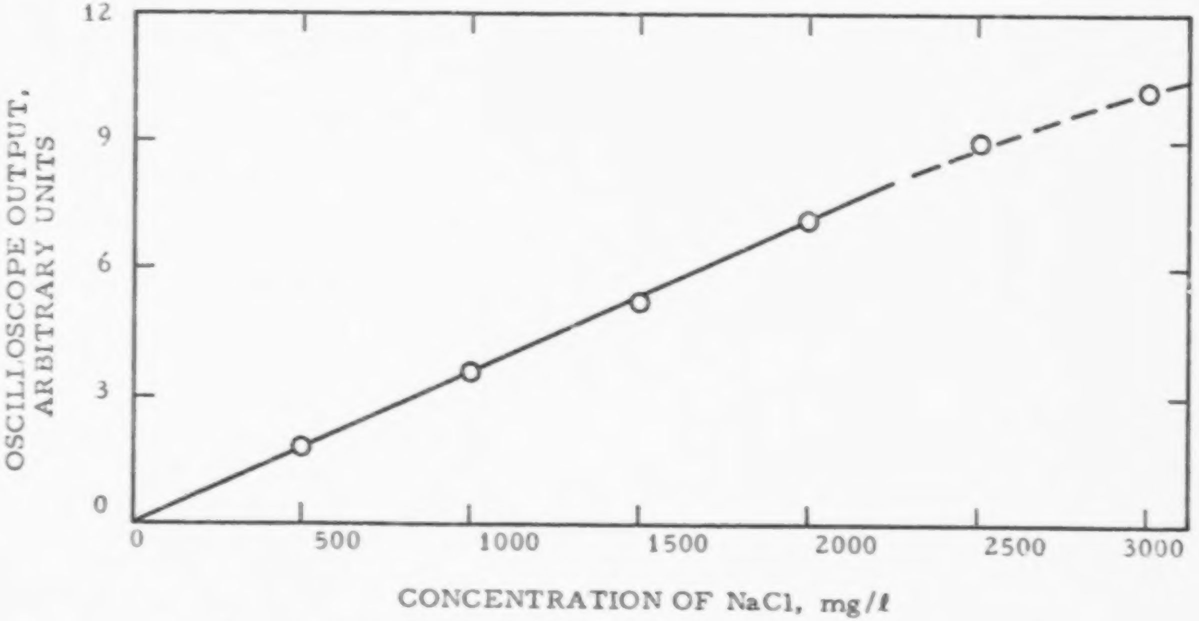

FIGURE 15. TYPICAL CALIBRATION CURVE FOR SINGLE ELECTRODE CONDUCTIVITY PROBE

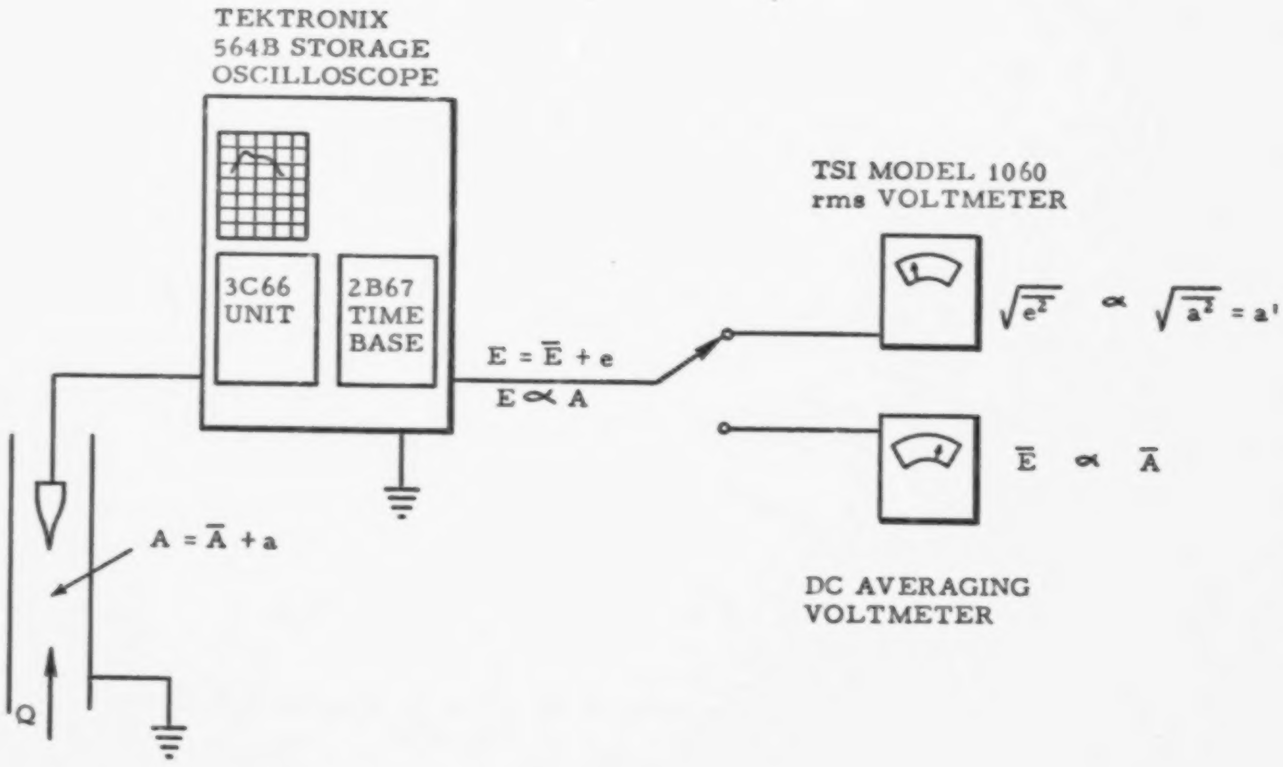
TEKTRONIX
564B STORAGE
OSCILLOSCOPE
3C66
UNIT
2B67
TIME
BASE
$E = \bar{E} + e$
$E \propto A$
TSI MODEL 1060
rms VOLTMETER
$\sqrt{\overline{e^2}} \propto \sqrt{\overline{a^2}} = a'$
$\bar{E} \propto \bar{A}$
DC AVERAGING
VOLTMETER
$A = \bar{A} + a$
Q

FIGURE 16. ELECTRONIC EQUIPMENT FOR MIXING EXPERIMENTS

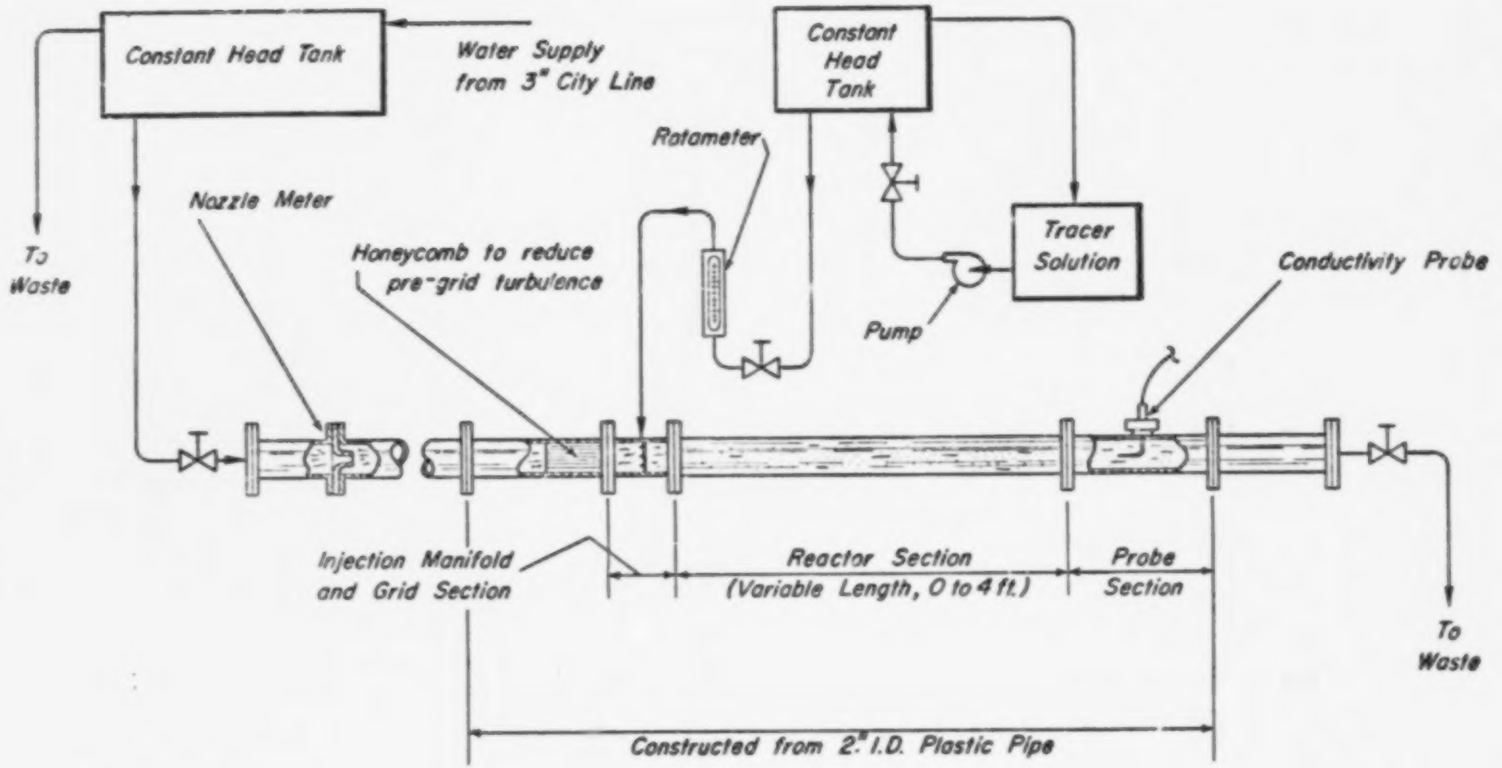
Constant Head Tank
Water Supply from 3" City Line
Constant Head Tank
To Waste
Nozzle Meter
Honeycomb to reduce pre-grid turbulence
Rotameter
Tracer Solution
Pump
Conductivity Probe
Injection Manifold and Grid Section
Reactor Section (Variable Length, 0 to 4 ft.)
Probe Section
To Waste
Constructed from 2" I.D. Plastic Pipe

FIGURE 17. SCHEMATIC ILLUSTRATION OF EXPERIMENTAL SETUP FOR MIXING EXPERIMENTS

The raw water was taken directly from a 3-in. East Bay Municipal Utilities District (EBMUD) line and fed to a constant head tank. This tank was important for two reasons. It eliminated fluctuations in the flow rate, and it helped to eliminate air bubbles from the water by allowing them to escape to the atmosphere. Air bubbles can cause difficulties in that they represent a region of very high resistivity. Any of these passing close to the probe would be detected by the probe and would produce an error in the amplifier output.

From the constant head tank, the water flowed through an I. S. A. nozzle flow meter and into the tubular reactor. A 4-in. section of aluminum "honey-comb" was placed upstream from the grid to help reduce the level of turbulence to avoid affecting the intensity of segregation downstream from the grid.

A drawing of the injection manifold and grid section is shown in Figure 18. It was constructed of clear plastic. The tracer flowed from a constant head tank through a rotameter into the manifold, entered the grid bars through the wall of the 2-in. pipe, and was injected into the flow through the injection orifices drilled in the grid bars.

Downstream from the grid was a variable length tubular reactor (0, 4, 8, 12, 16, 24, or 48 in.) which was also constructed of transparent plastic. Flanges with rubber gasket seals were used to connect the various sections together.

Beyond the tubular reactor section was the probe section as shown in Figure 19. This section was also used to divert part of the flow through the flocculator during the coagulation experiments. Two valves, one upstream and one downstream of the reactor section, were used to control the flow through and the pressure in the tubular reactor.

Multiple-Source Grids

The grids used for this study were constructed from brass tubing, 1/4-in. or 1/8-in. O. D. Metal was chosen in preference to plastic because it was easier to drill holes in metal having the same orifice coefficient. With plastic there is a tendency for the edges of the holes to become chipped. Gibson used plastic grid bars and found that because it was impossible to drill perfect holes, the tracer flow from adjacent sources varied greatly and artificially augmented the concentration fluctuations downstream. The orifices were 0.021-in. or 0.0135-in. in diameter, depending on the number of sources. It was desired that the tracer injection velocity be slightly greater than the main stream velocity. Brass tubing was chosen because it is fairly resistant to corrosion. The bars were held in place with silicone rubber cement.

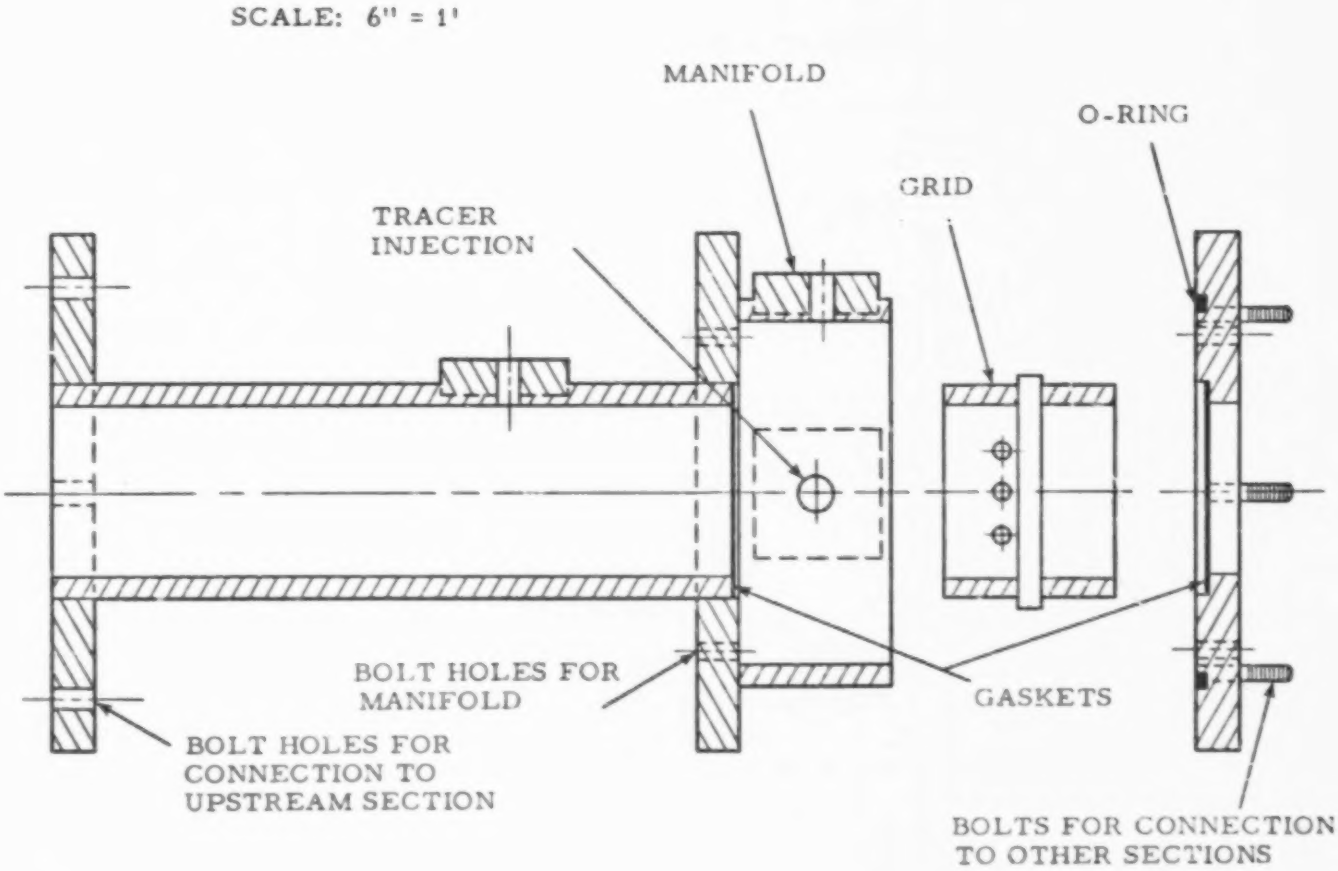
SCALE: 6" = 1'
MANIFOLD
O-RING
GRID
TRACER INJECTION
BOLT HOLES FOR MANIFOLD
GASKETS
BOLT HOLES FOR CONNECTION TO UPSTREAM SECTION
BOLTS FOR CONNECTION TO OTHER SECTIONS

FIGURE 18. CUTAWAY VIEW OF INJECTION MANIFOLD AND GRID SECTION

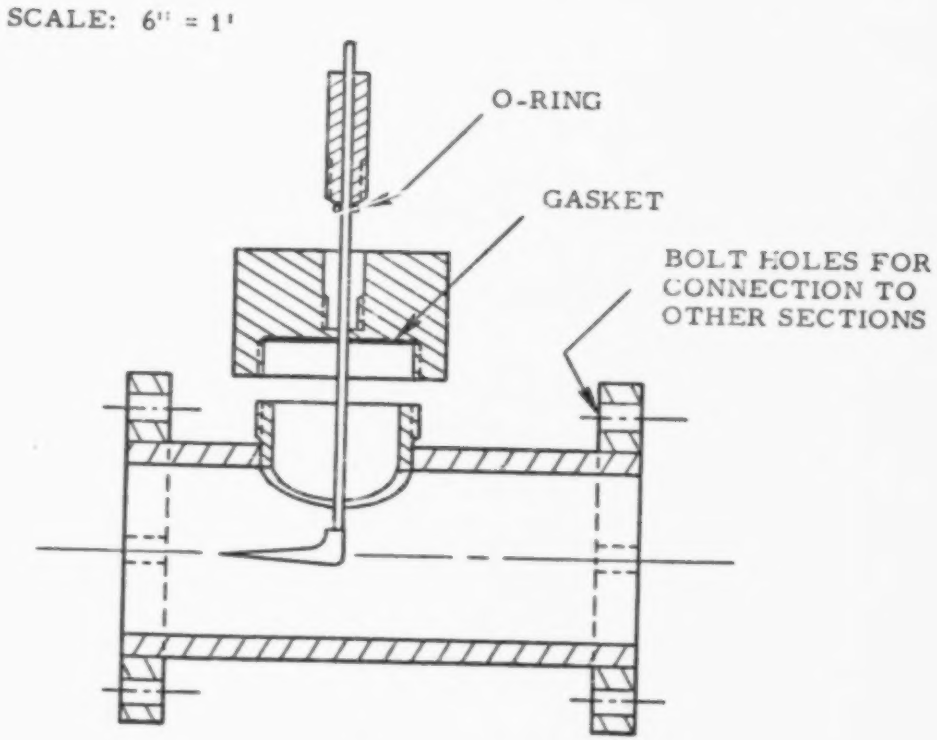
SCALE: 6" = 1'
O-RING
GASKET
BOLT HOLES FOR
CONNECTION TO
OTHER SECTIONS

FIGURE 19. CUTAWAY VIEW OF PROBE SECTION

A photograph of one of the grids is shown in Figure 20. For this grid, d = 1/8 in., $M/d = 4$, and the number of sources is 12. Seven grids were employed and their characteristics are listed in Table 2. Figure 21 shows the injection manifold section.

TABLE 2

GRID CHARACTERISTICS

Grid No.	M(in.)	d(in.)	M/d	No. of Sources	Source Diam (in.)
1	0.5	0.25	2	4	0.021
2	0.5	0.25	2	9	0.021
3	0.5	0.125	4	9	0.021
4	0.5	0.125	4	24	0.0135
5	0.5	0.125	4	12	0.0135
6	0.25	0.125	2	21	0.0135
8	0.5	0.125	4	4	0.021

EXPERIMENTAL PROCEDURE

During each run, measurements of mean concentration and rms concentration fluctuation were made with one grid, at a particular distance downstream from that grid. Measurements were generally made at the centerline, although the variation of mean and rms values across the cross-section was investigated. The parameters which were varied during a run were the ratio of mainstream flow to tracer injection flow, Q_M/Q_T, and the mainstream velocity, V_M. This latter parameter determines the grid Reynolds number, $V_M d/\nu$ or $V_M M/\nu$. Several runs were made in order to determine the decay of rms fluctuations with distance from the grid. Decay curves for different grids could in turn be compared in an attempt to determine what parameters might be appropriate for design. Also, it was desirable to develop a rational model for predicting the scalar decay which can be expected from any given grid.

Usually 20 liters of a 250-g/ℓ salt solution were prepared in advance for several runs. On the day of the run, a portion of this was diluted to a 50-g/ℓ concentration in the tracer solution tank (see Figure 17). This tracer concentration was used for all runs. The tracer pump

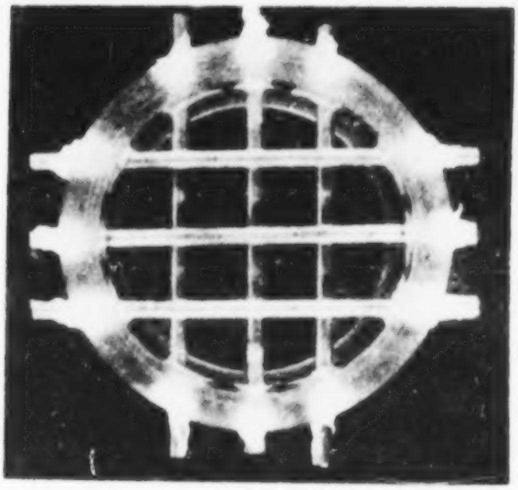

FIGURE 20. MULTIPLE-ORIFICE GRID

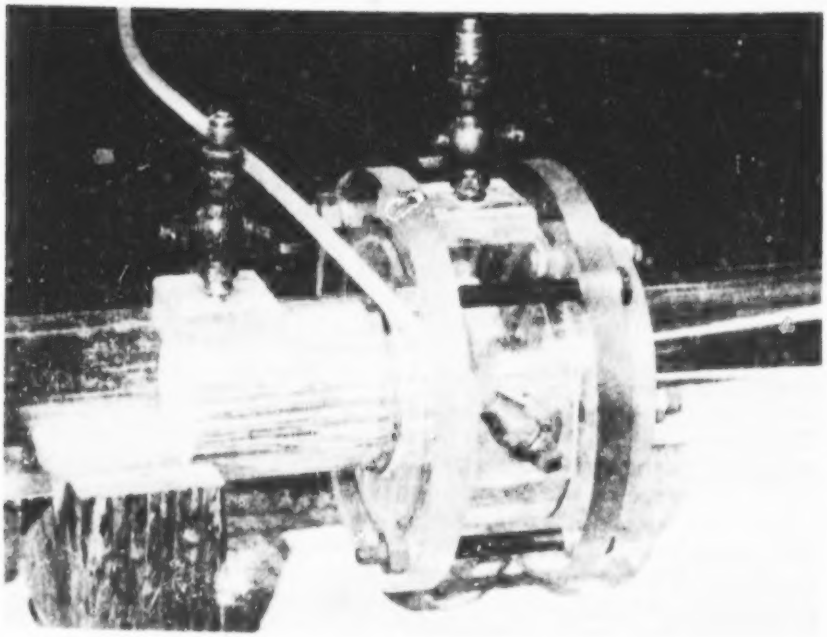

FIGURE 21. INJECTION MANIFOLD AND GRID SECTION

was started and the manifold was filled with tracer solution. Then the mainstream flow was started by passing water through the large constant head tank. When there was flow through the tubular reactor, it was necessary to have a small tracer flow rate into the system in order to prevent backflow of fresh water into the manifold.

Because the water taken from the city line was much colder than the ambient temperature, it was necessary to let the water run for approximately 30 minutes in order to obtain an equilibrium temperature. This was important as changes in conductivity are related to temperature as well as concentration variations. The pressure in the tubular reactor was adjusted to be great enough to prevent air bubble formation due to too low a pressure and low enough to allow the tracer to flow into the reactor. Then the flow was stopped and the conductivity probe put in place. The flow was started and adjusted to the desired value. The tracer flow was shut off and the AC bridge of the 3C66 unit was balanced.

The conductivity measured under these conditions was due essentially to dissolved minerals normally present in the water. However, there was also a slight leakage of tracer from the grid bars which could not be prevented. This meant an error in the mean scalar concentration reading because the balance condition of the bridge did not correspond to conditions of zero tracer injection. In order to eliminate this error from the results, the tracer flow was shut off and a relief valve on the manifold was opened at the end of each run. This caused fresh water to flow from the reactor into the grid bars and out of the manifold through the relief valve. No leakage of tracer into the tubular reactor occurred, and the amount of error previously incurred due to such leakage could be determined. The rms value was not affected by this error.

After the bridge was balanced, the tracer injection flow rate was set to a desired value. The output of the 3C66 unit was connected to the rms voltmeter and the rms voltage was read. The output of the 3C66 unit was then connected to the averaging DC voltmeter, and the mean value of the signal was read. When this was completed, the tracer injection flow rate or the mainstream flow rate was changed and the measurements repeated.

Drift of the bridge balance condition was at times a problem, and it was often necessary to shut off the tracer flow during a run to insure that the bridge was still balanced and, if necessary, to rebalance it.

At the end of the run, the probe was calibrated in a beaker by adding incremental amounts of tracer solution to tap water. During the first few runs, a calibration was made both before and after the run. However, it soon became apparent that the probe calibration was fairly stable and that such checking was not necessary. The fresh water used for the probe calibration was taken from the tubular reactor waste stream at the end of the run to insure that the temperature was the same as that of the water used during the run. After a run the tracer supply apparatus was drained of tracer solution and fresh water was pumped through it in order to inhibit corrosion.

HEAD LOSS THROUGH GRIDS

If grid initial mixers are used in water and wastewater treatment plants, the head loss through the grid may be an important consideration in design. In many cases, allowable head loss may be limited to a few inches. Therefore, loss of head measurements were made for two grids having different M/d ratios, and these were compared with predicted values.

Baines and Peterson [64] have studied the head loss caused by flow through grids. They assumed that all the loss takes place downstream from the grid, in the region where flow expansion takes place. They further assumed that the coefficient of contraction is 1.0; i.e., that the maximum fluid velocity as it passes through a grid is defined by that part of the cross-sectional area which the grid bars do not cover. Using principles of momentum and energy, they found that

$$K_L = \frac{h_L}{V_M^2/2g} = \frac{S^2}{(1-S)^2} \qquad (82)$$

where $S = A_{bars}/A_{total}$.

It can be shown that the drag coefficient,

$$C_D = \frac{K_L}{S} \quad . \qquad (83)$$

Therefore,

$$C_D = \frac{S}{(1-S)^2} \quad . \qquad (84)$$

It can also be shown that, when square-mesh grids are used, this relation is equivalent to Equation (35) used in the linear decay law for turbulence given by Batchelor and Townsend [14].

In a note on the article by Baines and Peterson [64], T. T. Siao noted that as $S \rightarrow 0$, C_D should become asymptotic to 1.2, the value for circular cylinders, instead of zero as Equation (84) predicts. Thus, Equation (82) is in error for low solidity grids (i.e., high M/d).

The modification suggested by Siao is shown in Figure 22. $K_L = h_L/(V_M^2/2g)$ is plotted against M/d. S is related to M/d for square-mesh grids by

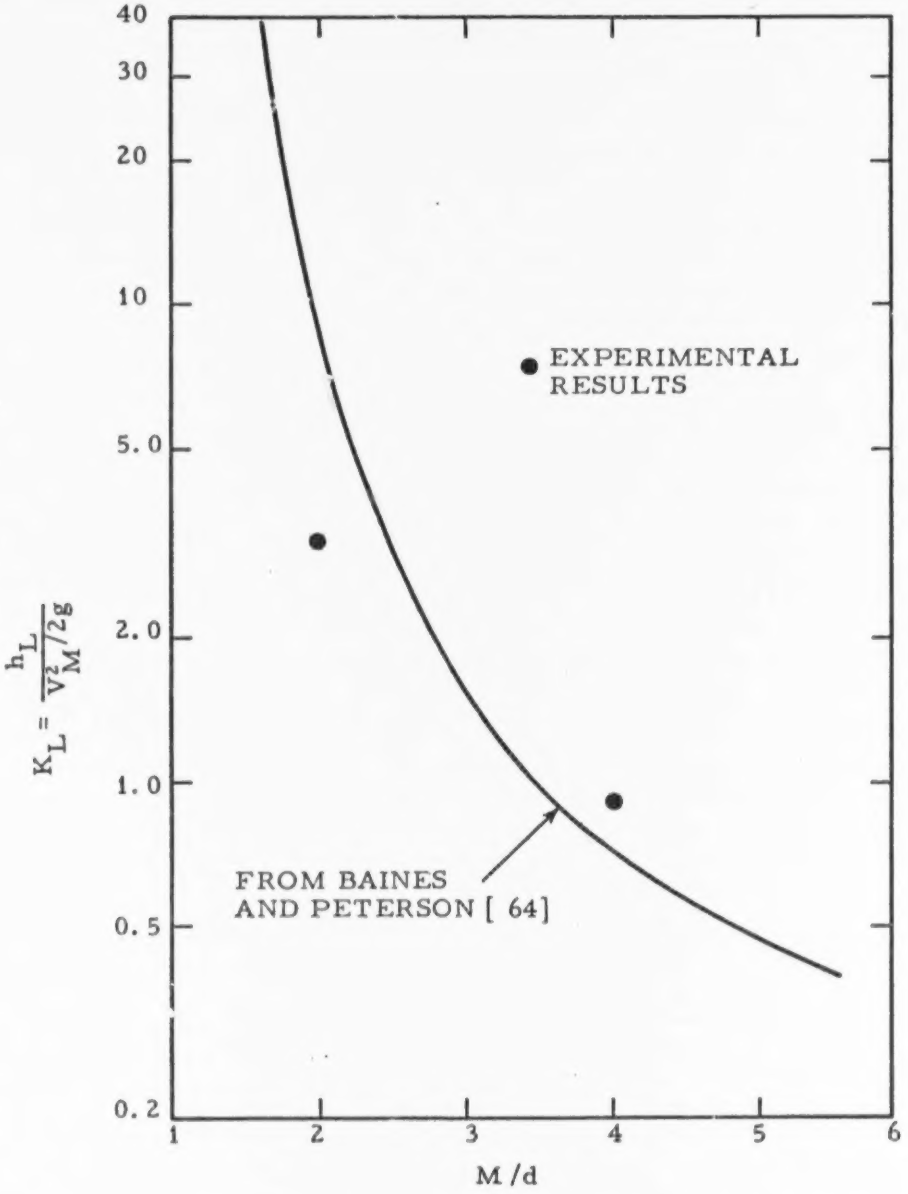

FIGURE 22. HEAD LOSS COEFFICIENTS FOR SQUARE-MESH GRIDS

$$S = 1 - \frac{\left(\frac{M}{d} - 1\right)^2}{\left(\frac{M}{d}\right)^2} \quad . \qquad (85)$$

The head loss coefficients for two grids of the present studies (M/d = 4 and M/d = 2) are also shown in Figure 22. These coefficients were determined by measuring the head a few inches upstream from the grid and 4 ft downstream from the grid. An estimate was made of the head loss due to wall friction by using a friction factor corresponding to a smooth pipe. This estimated loss was subtracted from the total measured head loss to obtain a value for the head loss due to the grid alone. Measurements were made at five velocities in equal increments from 1 to 5 fps, and at 0.8 fps. There was a tendency to have higher values of K_L for some of the measurements at 0.8 and 1.0 fps — 10% to 20% higher. As will be suggested in Section VI, this could be a sign that a change in the character of the turbulent wake occurs at such velocities. This change, if it does occur, also affects the mixing provided by the grid.

For higher velocities, the values of K_L were quite consistent. It is the average of these values which is plotted as experimental results in Figure 22. For the low solidity grid (M/d = 4), the experimental point falls close to the line. For the high solidity grid (M/d = 2), the experimental point falls substantially below the curve. This may be due to the fact that there was a slight space (d/2) between the horizontal and vertical grid bars. Thus, the contraction of the flow was probably not as great as assumed by Equation (82), and the head loss coefficient was lower than predicted. The head loss which would be expected from each grid at different velocities is given in Table 3.

TABLE 3

HEAD LOSS THROUGH GRIDS AT VARIOUS VELOCITIES

V_M, fps	h_L (inches)	
	M/d=4 S=0.45	M/d=2 S=0.75
1.0	0.2	0.6
2.0	0.8	2.5
3.0	1.7	5.7
4.0	3.0	10.0
5.0	4.7	15.7

SECTION VI

MIXING STUDIES: RESULTS AND ANALYSIS

RESULTS

In this section the mixing experiments which were performed are described. These experiments were intended to meet objectives 1) and 2), i. e., to determine the parameters governing the degree of mixing downstream from a grid initial mixer. The experiments were designed in such a manner that as much information as possible was obtained from them. After the various experiments are discussed, a general model incorporating the results of these studies will be developed.

Figure 23 shows a typical curve giving the rms concentration fluctuations, at the pipe centerline, downstream from a particular grid (Grid No. 1: M = 1/2 in., d = 1/4 in., 4 tracer orifices in the cross-section of the 2-in. pipe). a'/a'_o is plotted against x/d. From a study of previous experiments concerning turbulence, in spite of the point made in Section IV and M/d should affect the turbulence level, and the present mixing studies, it appears that d is a more appropriate parameter to use in normalizing the distance from the grid. The decay curve of Figure 23 follows an equation of the form,

$$\frac{a'}{a'_o} = \alpha \left(\frac{x}{d}\right)^{-a} \qquad (86)$$

which is essentially the same as Equation (45a). Two important points can be made regarding this graph.

The first point concerns the effect of mainstream velocity on the mixing at downstream point. The figure shows data for three mainstream velocities, V_M = 1, 2, and 3 fps (some measurements were made at higher velocities during the first few runs). These velocities correspond to grid bar Reynolds numbers ranging from $V_M d/\nu = 1.7 \times 10^3$ to 5.1×10^3. At a particular value of Q_M/Q_T, the ratio of mainstream flow to tracer injection flow, there is no consistent difference between the values of a'/a'_o at different mainstream velocities. That a'/a'_o is not a function of mainstream velocity is consistent with the work of others [11, 22].

In some of the runs, there was a tendency to obtain abnormally high values of a'/a'_o at the lowest mainstream velocity of 1 fps. This

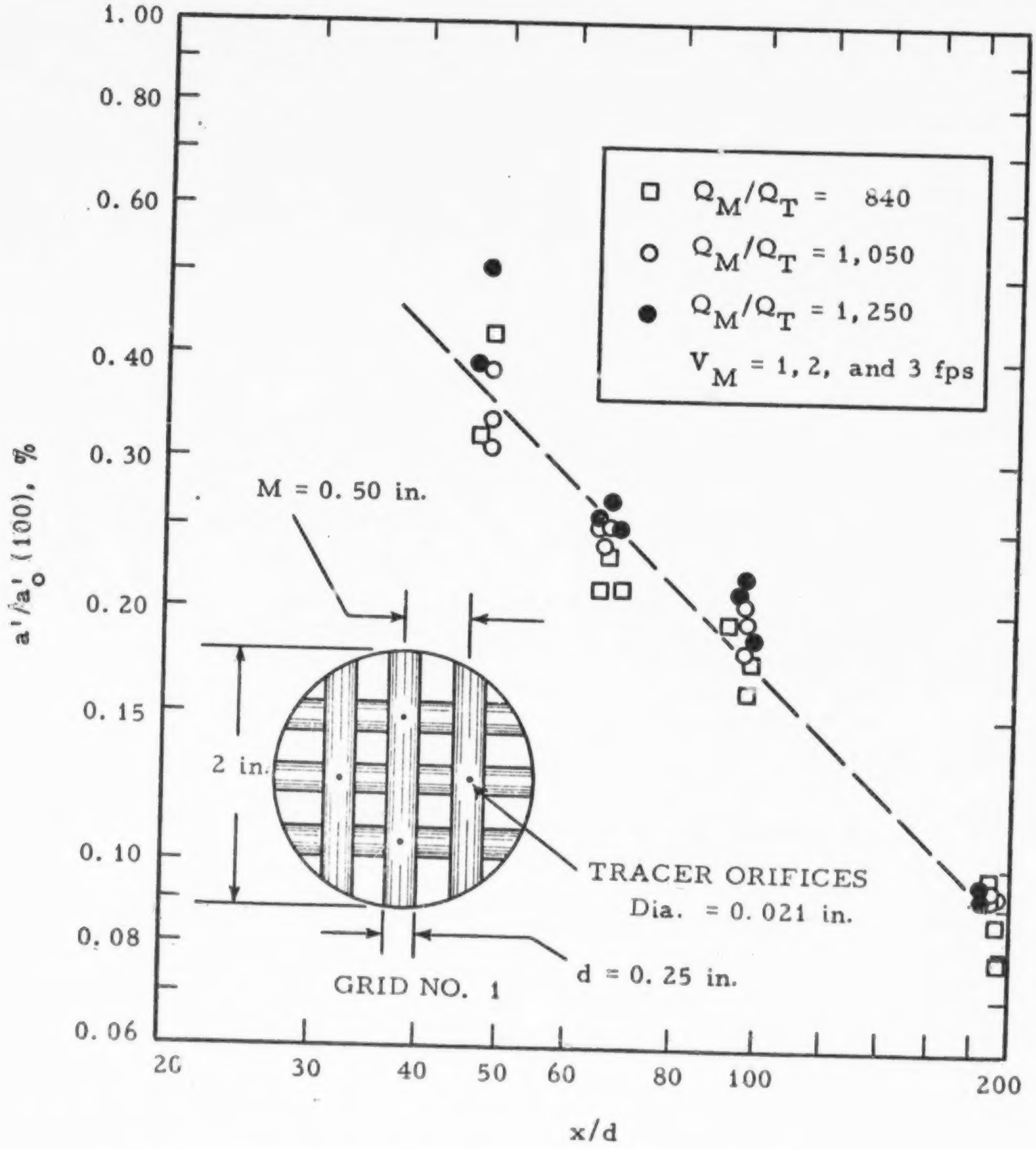

FIGURE 23. DECAY OF CONCENTRATION FLUCTUATIONS DOWNSTREAM FROM A GRID

may be due to some change in character of the turbulent wake behind the grid bars at this velocity. Inspection of curves giving drag coefficient and vortex shedding frequency vs. Reynolds number [18, 65] for circular cylinders showed no change in character at any Reynolds number near those at which the present experiments were done. A grid with a low M/d ratio is not, however, a good approximation of an infinitely long circular cylinder. Also, the measurements of head loss through the grids showed that the head loss coefficient $K_L = h_L/(V_M^2/2g)$ was substantially greater at a velocity of 1 fps than at higher velocities. This is another indication that some change in the turbulent wake did indeed sometimes occur at the lowest mainstream velocity. One of Gibson's graphs [11] showed a similar jump at a low velocity although he did not comment on it.

The second point regarding Figure 23 involves the value of a'_o used to normalize a'. It can be shown [22] that if a tracer of concentration A_T and flow rate Q_T enters a tubular reactor where the mainstream flow rate is Q_M, the spatial root-mean-square concentration fluctuation across the cross-section is,

$$a'_o = A_T\sqrt{Q_T/Q_M} \quad . \tag{87}$$

To use a'_o as the initial rms concentration fluctuation for an isotropic scalar field, the assumption must be made that the tracer is spread out across the cross-section so that the mean concentration at all points of the cross-section is the same while little decay of the concentration fluctuations has taken place. It might then be expected that measurements of time-averaged rms concentration fluctuations near the grid would give results of the same order of magnitude as the calculated value given by Equation (87). However, this is not what occurs. Measurements approximately 1 in. downstream from the grid showed that the rms values were from 1% to 4% of the calculated value (there was considerable variation because of substantial differences in mean concentration across the cross-section).

It appears that two different mixing phenomena are occurring. The first involves mixing in the turbulent wake of the grid bars. This process is effective for only a few grid bar diameters downstream, but it is very important. The vortices shed by the bars act to spread the tracer as it leaves the orifice. This also acts to greatly decrease the concentration fluctuations at a "point." A short distance from the grid, the turbulent wakes from the individual grid bars will coalesce, and isotropic decaying turbulence will develop. The time-averaged tracer concentration is fairly constant across the cross-section, and the decay of the rms concentration fluctuations follows Equation (86).

It should be noted that there may still be considerable segregation beyond the "wake-mixing" zone. For example, if $\bar{A}$, the average concentration of the tracer following complete mixing with the mainstream, is 50 mg/ℓ, a'_o can be computed as approximately 1500 mg/ℓ for the present work. If a' = 15 mg/ℓ at some point downstream, $a'/\bar{A} = 0.30$, which indicates an appreciable variation from the mean. However, $a'/a'_o = 0.01$, a small number which gives the impression of very little segregation.

Both Gibson and Keeler observed similar phenomena, but their interpretations were somewhat different. Keeler used a "hairbrush" injection system upstream from the grid in order to obtain a homogeneous scalar field at the grid. In measurements very close to the grid, he found that the rms values were approximately 10% of the values given by Equation (87). He noted this and assumed that most of the mixing took place between the injection system and the grid. He did not, however, relate this reduction in scalar fluctuations to the spreading which occurred as the tracer left the injection needles.

Gibson did not make any direct comment on the fact that his measured rms values were much lower than the calculated values. He was concerned with the fact that at a given point downstream a' was proportional to Q_T/Q_M instead of $\sqrt{Q_T/Q_M}$ as would be the case if Equation (87) held. He developed a model to explain this phenomenon. This model also — almost inadvertently — gives an explanation of why the measured rms values were so low. Gibson's model will be examined more closely later.

Some of the scatter in Figure 23 is due to the increase of a'/a'_o with increases of Q_T at a fixed value of Q_M. In most of the experiments, Q_M/Q_T did not vary by more than a factor of 6 (for Figure 23, this factor is 1.5) and was set so that the mainstream velocity was of the same order of magnitude as the tracer injection velocity. Furthermore, for the grids with an M/d ratio of 4, the scatter due to variations of Q_M/Q_T was even greater.

Figure 24 shows a' at a given x/d and Q_M plotted against Q_T for such a grid. There is almost a direct proportionality between a' and Q_T. This is the same phenomenon Gibson observed. He concluded that it was probably caused by the tracer injection orifices for his experiment facing upstream. In most of the present experiments, the tracer injection orifices faced downstream. It seems, therefore, that the phenomenon is due to the fact that Equation (87) is inappropriate for describing the initial rms concentration fluctuation of the isotropic scalar field. It is, however, appropriate for describing the initial rms concentration fluctuation for the two unmixed streams before the wake-mixing zone and should be used for this. The effect of Q_M/Q_T in determining the value of a' downstream from a grid will be considered more closely later. Now, other experiments designed to ascertain how other parameters may affect the mixing will be discussed.

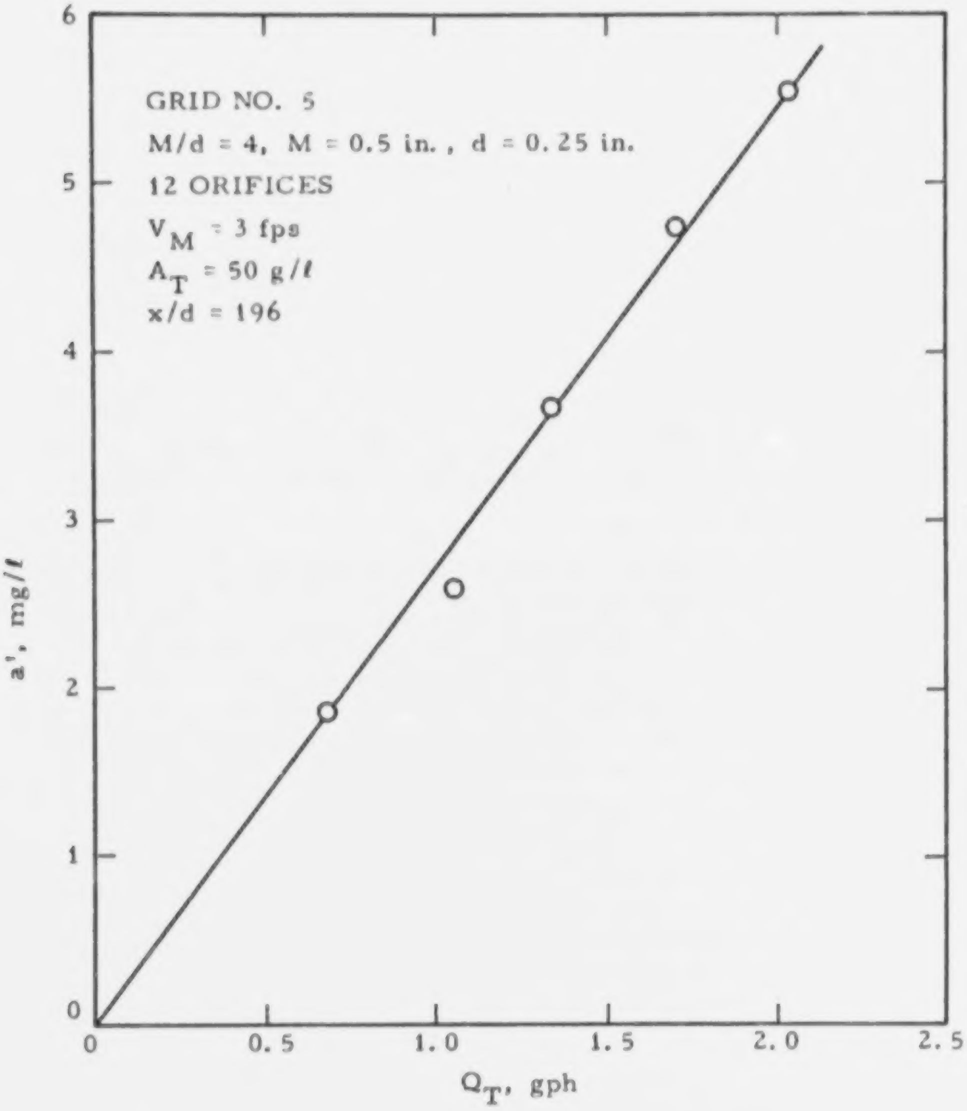

FIGURE 24. a' vs. Q_T FOR GRID WITH M/d = 4

Effect of Scale of Turbulence on Decay Rate

In Section IV, it was noted that the scalar decay rate, a, in Equations (45) and (86) was closely related to the right-hand side of Corrsin's equation,

$$\frac{u_1'}{a'}\ \frac{da'}{du_1'} = \frac{2 + N_{Sc}^{-1}}{3\left(\frac{3}{2}\right)^{2/3}\ \left(\frac{L_s}{L_f}\right)^{2/3} + 2\left(\frac{5}{3}\right)^{3/2}\ \frac{\log N_{Sc}}{N_{Re_\lambda}}} \qquad (54)$$

and is in fact equal to it if the right-hand side of Equation (54) is a constant as decay proceeds.

L_s and L_f are the two most important parameters in this equation as, in any mixing system, they are the parameters which can presumably be varied by changing the physical configuration of the system. It was noted in Section IV that L_f is apparently a function of the grid bar diameter, d.

In order to show the effect of the scale of turbulence on the decay rate, experiments were carried out with two grids. The number of tracer orifices for both grids was nine, and the center-to-center spacing of the bars, M, was 1/2 in. The bar diameters for the two grids, however, were 1/4 and 1/8 in., respectively. The results are shown in Figure 25. For the grid with the smaller value of d, L_s/L_f should be greater, and the decay rate (slope of the scalar decay curve) should be less. This is what was observed.

Keeler also attempted to show qualitatively the effect of L_s/L_f in Equation (54). He used two grids with the same M/d ratios, but with one grid, the values of M and d were twice that for the other. The same hairbrush injector was used for both grids. Through a rather ingenious method of plotting his results, he showed a pronounced difference in scalar decay for the two grids. More conventional plotting of the data (as in Figure 25) shows that there was actually very little difference in the two values of a. The reason for the different results of his experiments and those of the present study is not clear. Perhaps in his study the value of L_s/L_f was low enough so that a change in the value did not affect the complete expression on the right-hand side of Corrsin's equation.

In discussions of this sort, it should always be kept in mind that Corrsin's equation strictly applies only to those conditions of high N_{Re_λ}, unattainable in laboratory experiments. The values of N_{Re_λ} for the present study varied from 30 to 60. Such values were termed "moderate" by Corrsin [17].

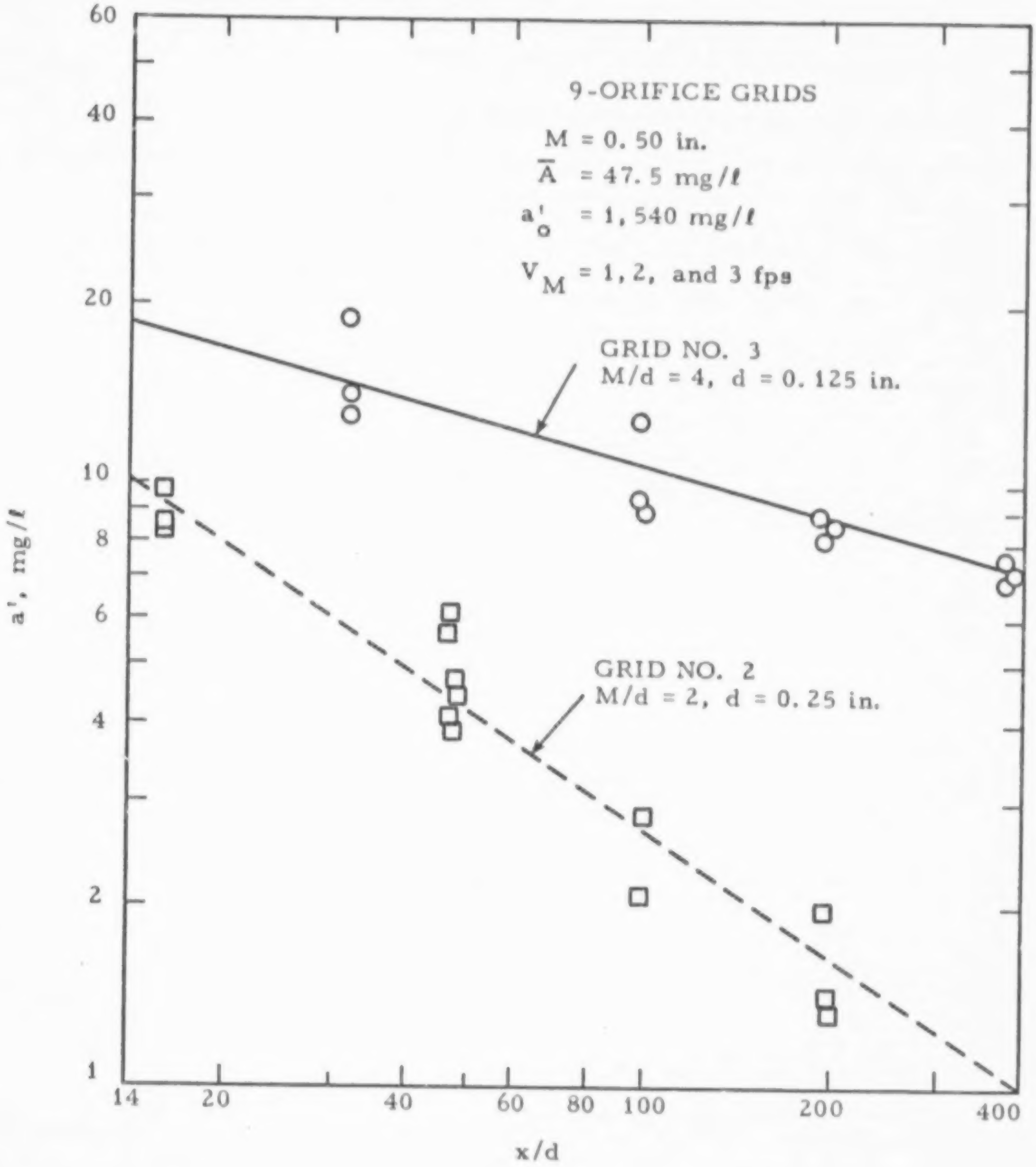

FIGURE 25. EFFECT OF SCALE OF TURBULENCE ON SCALAR DECAY RATE

Gibson estimated that $u'L_f/\nu$ should be greater than 3.3×10^5 for an inertial subrange to occur. For the present work, this parameter is estimated to be approximately 10^3.

Effect of the Number of Tracer Orifices

As was noted in Section IV, it has been assumed by some investigators [22, 29] that the scale of segregation, L_s, is a function of the number of tracer orifices with an increase in the number of orifices presumably decreasing L_s. Further, a decrease in L_s should cause an increase in the scalar decay rate according to Equation (54). To test this, experiments were conducted with two grids, identical except for the number of orifices; one had 4 and the other had 9. The scalar decay curves for the two grids are shown in Figure 26. For the 9-orifice grid, the rate of decay was actually slightly less, instead of greater, as might be expected if the above assumption were true. The conclusion which is drawn from this is that an increase in the number of orifices does not increase the scalar decay rate. As noted previously, there seems to be no rational basis for such an assumption, and these results seem to refute it.

Figure 26 does seem to indicate that the "wake-mixing" is affected by the number of tracer orifices. At low values of x/d, a' is lower for the 9-orifice grid.

Such a conclusion is further substantiated by studies involving grids with M/d ratios of 4. Four such grids were used with 4, 9, 12, and 24 tracer orifices. It was assumed that the scalar decay rate of the 9- and 24-orifice grids applies to the other two grids even though measurements involving the latter were only made at one x/d value for each one. Starting with Equation (86),

$$\frac{a'}{a'_o} = \alpha\left(\frac{x}{d}\right)^{-a} \tag{86}$$

one can solve for α:

$$\alpha = \frac{a'/a'_o}{(x/d)^{-a}} \tag{88}$$

Figure 27 shows a plot of α vs. n, $^{-1}$ the inverse of the number of tracer orifices. Except for the value at $n = 4$, there is a fairly strong correlation between α and n^{-1}. Extrapolation of the curves of Figure 26 to $x/d = 1$ also shows a direct proportionality between n^{-1} and α. Therefore it will be concluded for the purposes of this study that in fact α is proportional to n^{-1}. Of course, it will be evident from a study of the plotted data that a slight shift of the line drawn through the data points will change the value of α tremendously, perhaps by as

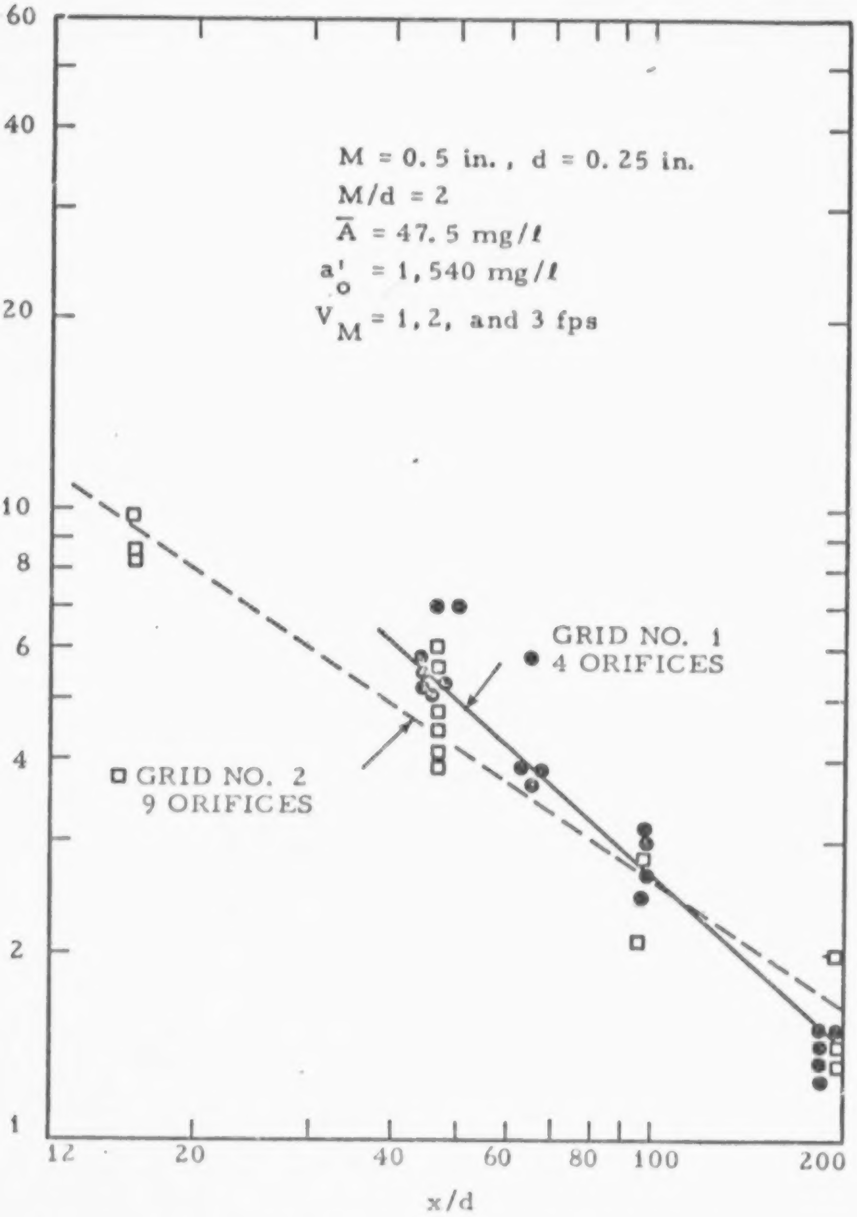

FIGURE 26. EFFECT OF THE NUMBER OF ORIFICES ON SCALAR DECAY RATE, M/d = 2

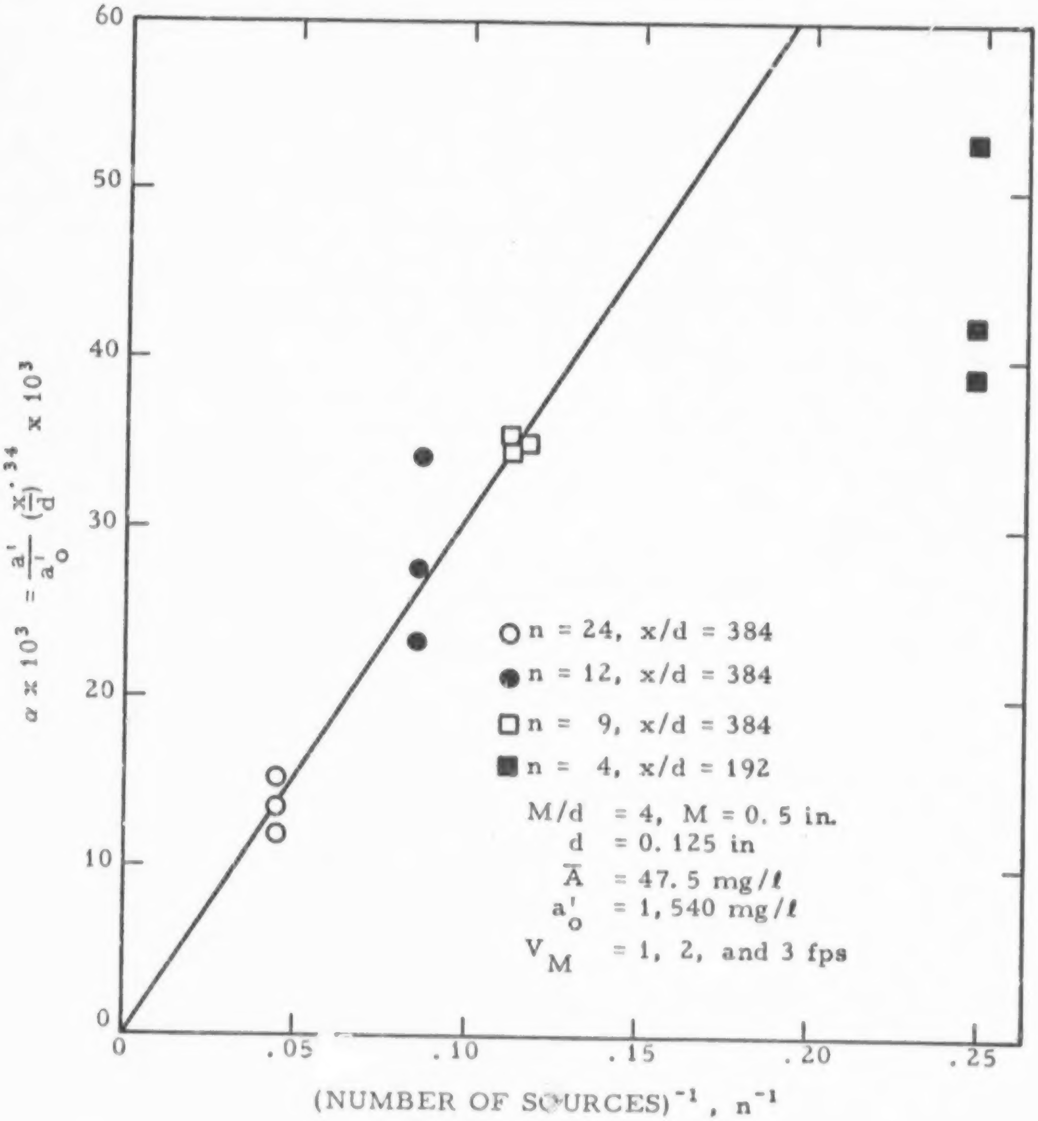

FIGURE 27. INVERSE RELATIONSHIP BETWEEN NUMBER OF SOURCES AND α FOR GRIDS WITH M/d = 4

much as 50%. This sensitivity must be kept in mind when working with log-log plots of this sort. Any value of α obtained from such extrapolation should be recognized to be of low accuracy.

Effect of Injection Sources Facing Upstream

An effort was made to find ways of modifying the injection system in order to increase the scalar decay rate through a change in the scale of segregation. An experiment was carried out in which a grid was turned around such that the tracer injection orifices faced upstream. The scalar decay curve for this condition was compared with one for a grid with normal orientation (tracer injection downstream). The results are shown in Figure 28.

The values of a' close to the grid are higher for the case in which the orifices face upstream, apparently because the "wake-mixing" is not so effective in reducing the scalar fluctuations. The rate of decay, however, is much greater. Whether or not there is a difference in the scale of segregation is not known. However, it has been shown that a difference in the scalar field will affect the scalar decay rate even though the turbulent flow field is essentially the same.

It was originally planned that measurements of L_s would be made by using one probe, making measurements of a Eulerian time correlation, relating this to the Eulerian space correlation discussed in Section IV, and calculating the scale of segregation, L_s. This was to have been done by recording the data digitally on magnetic tape and utilizing a CDC 6400 computer to make the calculations. However, because of time limitations and a desire to proceed with experiments relating process performance (in alum coagulation, wastewater coagulation, and wastewater chlorination) to goodness of mixing, the studies involving measurement of L_s were not carried out. Such an experiment would prove very interesting, particularly in relation to Figure 28, as the scale of segregation has apparently not been measured for any system.

It is interesting to note that when the grid used for the experiment described above was in the upstream injection orientation, the system was very similar to one used by Gibson: upstream injection, d = 1/8 in., and orifices placed halfway between grid bar intersections. M was slightly different for the two studies — 5/8 in. for Gibson's and 1/2 in. for the present work. A comparison of his results and those of this study is presented in Appendix C.

Comparison of Geometrically Similar Grids

As it may be difficult to design grids with bars 1/4 or 1/8 in. in diameter for full-scale treatment plants, it is important to attempt to determine how scaling these grids in size affects the resulting

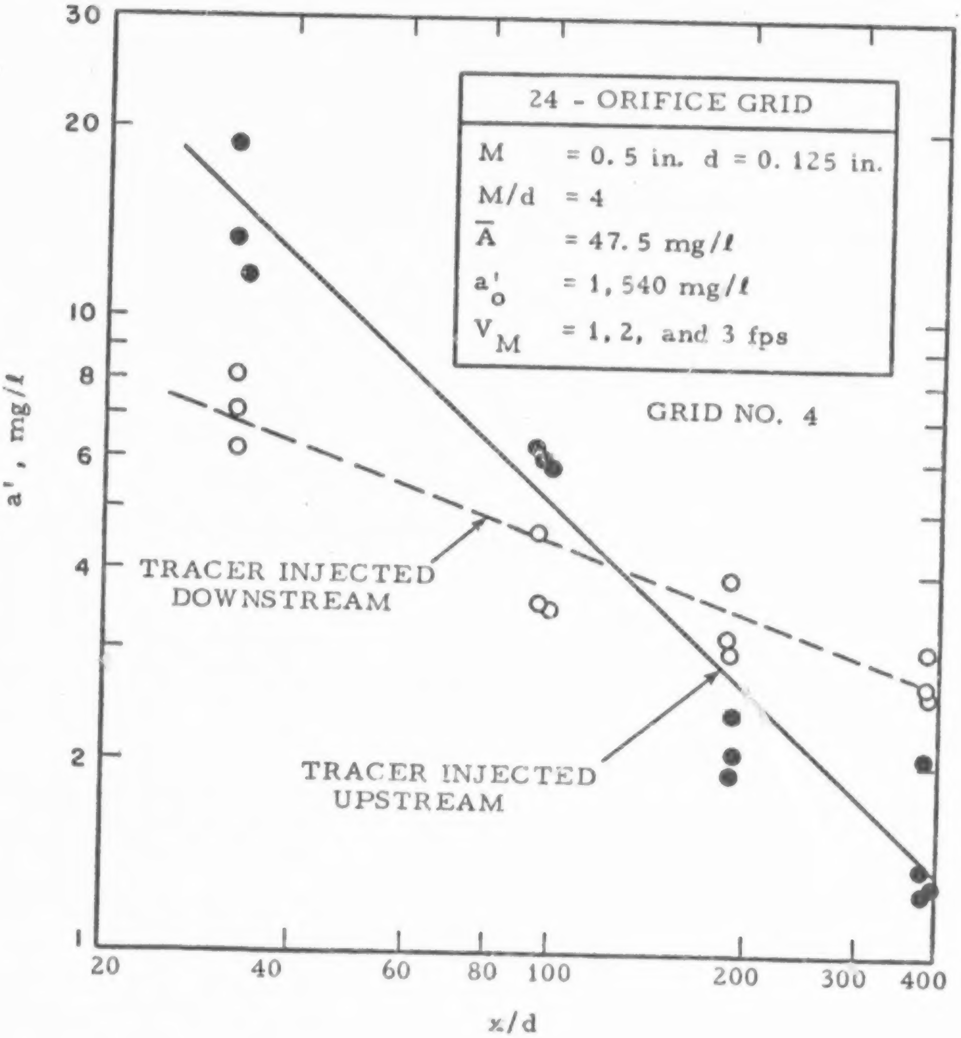

FIGURE 28. EFFECT OF CHANGING ORIENTATION OF TRACER INJECTION SYSTEM ON SCALAR DECAY RATE

scalar decay. In order to make a study of the scaling effect, a grid with M and d values one-half those of grid No. 1 was constructed with 21 orifices and designated as grid No. 6. For perfect similarity it should have had $4^2 = 16$ orifices. However, because of problems with the geometry of the configuration, exact similarity could not be obtained in this respect.

A comparison of results obtained with the two grids is shown in Figure 29. The results for grid No. 6 were very poor, giving a curve which only with great imagination could be considered a straight line on log-log paper. It would be very difficult to define a slope through these points and impossible to estimate a value of α with any accuracy. It is apparent, however, that the smaller grid gives poorer results than does the larger grid. Furthermore, attempting to compare results from these two geometrically similar grids ignores two previous conclusions; the slope of the scalar decay curve (for downstream injection from the grid bars) is a function of the grid bar size, and the displacement of the scalar decay curve, or α, is a function of the number of sources. For that reason, perhaps it is appropriate to compare the results obtained using grid No. 6 with those obtained using grid No. 4 (d = 1/8 in., M = 1/2 in., 24 orifices). These two grids are very similar with the exception that M/d = 4.0 for grid No. 4 and 20 for grid No. 6. The comparison of results is shown in Figure 30. The agreement is quite good, and while it cannot be said to confirm the previous conclusions, it is at least compatible with them.

It should be noted that Keeler concluded, through comparison of his results with Gibson's, that the M/d ratio affects the displacement of the scalar decay curve. Such a conclusion seems intuitively reasonable. However, because of differences in the tracer injection systems for the two studies and differences in their methods of calculating a'_o, it seems that comparison of results obtained in the two studies cannot be made. Keeler measured a' very close to the grid and empirically determined that the initial rms concentration fluctuation in the isotropic scalar field was equal to $\bar{A}$.

Gibson, in developing a model to explain why a' was proportional to Q_M/Q_T for his work, found that the initial rms concentration fluctuation of the isotropic scalar field was proportional to $\bar{A}$, and he therefore apparently used $\bar{A}$ to normalize a'. Therefore, the two curves which Keeler compares are graphs of $(a'/\bar{A})^2$ vs. x/M. As the tracer injection systems are different and the values of Q_M/Q_T are different (approximately 100 for Keeler and 2000 for Gibson), the fact that there is a difference in displacement between the two curves cannot be used to prove that M/d affects the value of α in Equations (86) or (45).

SUMMARY OF MIXING STUDIES RESULTS

It would be desirable to relate the results produced by the various grids and obtain an overall description of the mixing process which

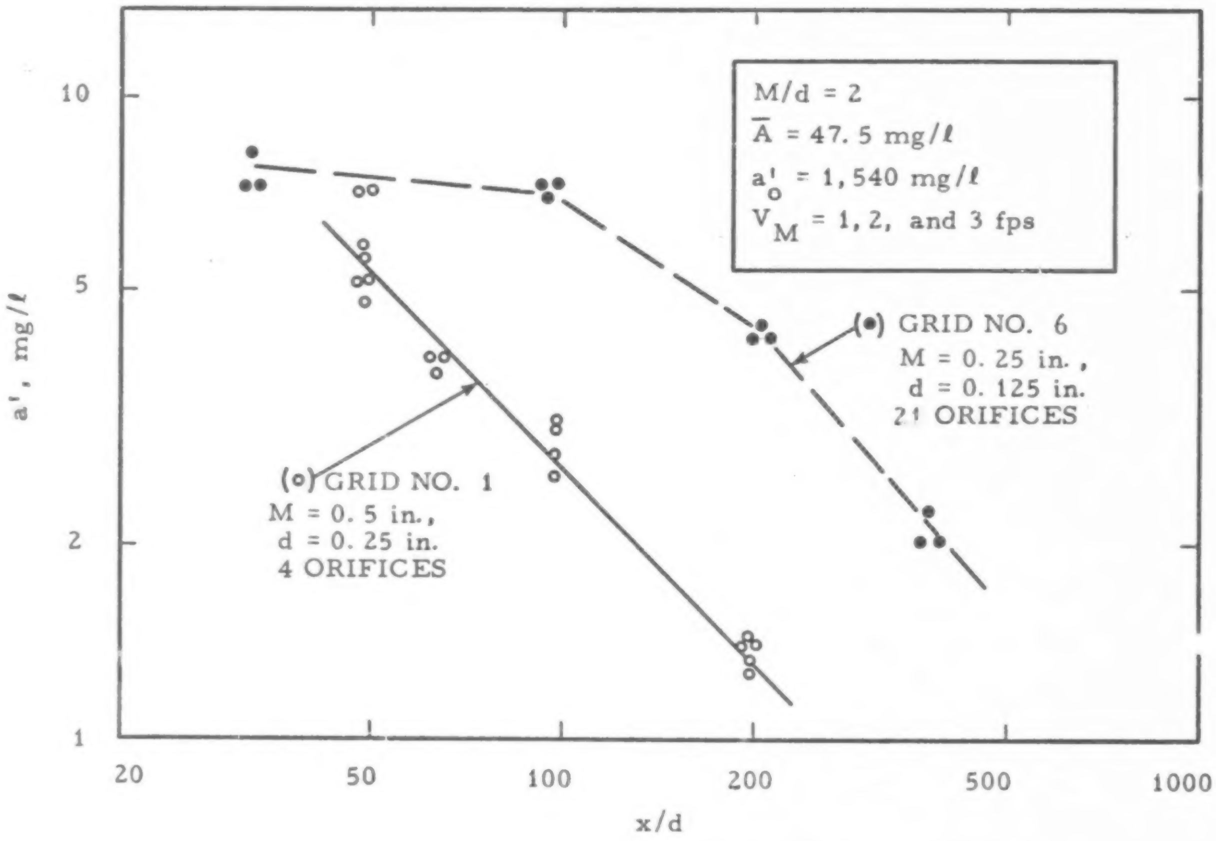

FIGURE 29. RESULTS OBTAINED FROM GEOMETRICALLY SIMILAR GRIDS

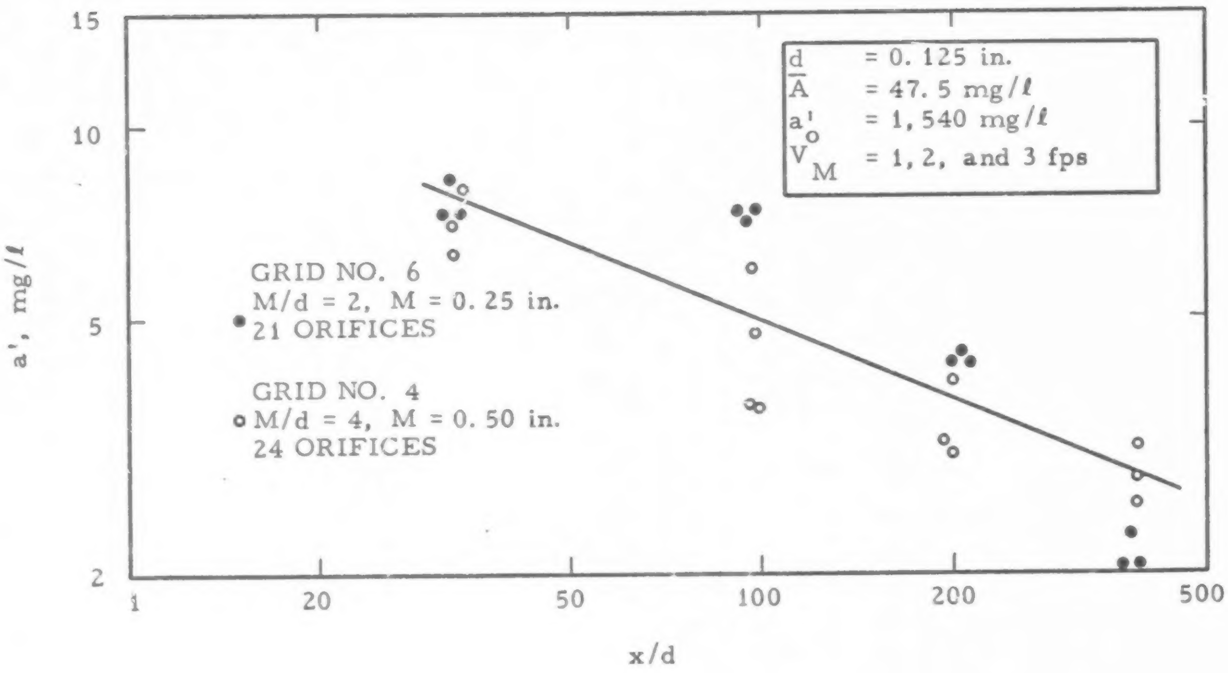

FIGURE 30. EFFECT OF VARYING M

occurs under the conditions found in this study. To that end, the conclusions reached in the previous sections are summarized below.

1. The degree of mixing at a point downstream does not depend on the mainstream velocity. The time necessary to reach a given degree of mixing is inversely proportional to the mainstream velocity.

2. a'_o as calculated by Equation (87) is not a good indication of the initial rms concentration fluctuations in the isotropic scalar field. A great deal of mixing occurs as the tracer spreads upon leaving the orifice in the turbulent wake of the grid bar.

3. At a point downstream, a' can be said to be proportional to Q_M/Q_T rather than $\sqrt{Q_M/Q_T}$ as suggested by Equation (87). This is the same as the phenomenon observed by Gibson and is closely related to the "wake-mixing" described above.

4. Because it determines the integral scale of turbulence, the grid bar size affects the rate of scalar decay as predicted by Corrsin, the rate increasing as the grid bar diameter increases.

5. Within the limits of the present work, the number of tracer orifices does not seem to greatly affect the scalar decay rate. It is therefore concluded that the number of sources does not affect the scale of segregation. Such parameters as method of tracer injection (upstream or downstream, for example) do seem to have a strong effect on the scalar decay rate when the turbulent flow field is essentially unchanged. The conclusion drawn is that Corrsin's prediction concerning the effect of the scalar field, as described by L_s, on the scalar decay rate, has been qualitatively shown.

6. The number of sources as well as the method of injection seems to affect the "wake-mixing." To a reasonable degree, the value of a' measured at a given distance downstream is inversely proportional to the number of tracer orifices in a given cross-sectional area.

7. Within the limits of these studies, the M/d ratio seems to be important only in that more closely spaced bars can provide a greater number of tracer orifices per square inch.

Not all of the data substantiates each of these conclusions. In some cases it has been necessary to allow considerable latitude in incorporating specific results into the general model. However, such interpretation is necessary if any general conclusions are to be drawn. These conclusions have been drawn with the objective of determining the design parameters for use with prototype grids. In particular, it appears that "wake-mixing" may be the most important consideration in designing prototype grids. From results of the process studies described in Section VII, the time necessary for adverse chemical-physical reactions to occur seems to be sufficiently short such that the degree of mixing taking place in the first fraction of a second determines whether process performance will be satisfactory. It may be that the portion of the scalar decay in the isotropic scalar and turbulence fields will be unimportant in this regard.

INTERPRETATION OF RESULTS: MODEL DEVELOPMENT

A model which combines the above summary of results in a quantitative and concise manner can be developed. It is a semi-empirical model in that while the straight-line, log-log form of the decay curve and the dependence on the scales of turbulence and segregation have been derived theoretically, the actual values of the coefficients must be determined from experiment. The general decay equation is written,

$$\sqrt{I_s} = \frac{a'}{a'_o} = \alpha\left(\frac{x}{d}\right)^{-a} \tag{86}$$

where $\alpha = f_1\,(n_s,\ Q_M/Q_T,$ injection system$)$, $a = f_2(d,$ injection system$)$, and n_s = the number of tracer orifices per square inch of reactor cross-section, in.^{-2}.

Let a'_1 be the initial rms concentration fluctuation in the isotropic scalar field

$$\frac{a'}{a'_1} = \alpha'\left(\frac{x}{d}\right)^{-a} \tag{89}$$

where $\alpha' = f_3$ (injection system).

To derive an expression for a'_1, assume that the tracer becomes partially mixed with a portion of the mainstream flow rate which passes close to the injection orifice. This portion will be Q_p and is defined by,

$$Q_p = K_p\, n_s\, Q_M \quad , \quad Q_T << Q_p << Q_M \tag{90}$$

where $K_p = f_4$(injection system). K_p is essentially the cross-sectional area with which the tracer is mixed. This approach is similar to Gibson's but is different in that he arbitrarily set a value for K_p. He also assumed that the tracer was completely mixed with the flow rate Q_p. He called this premixing.

In this wake-mixing region, the average concentration of the tracer mixed with this portion of the flow is,

$$A_p = \frac{A_T Q_T}{Q_p} = \frac{A_T Q_T}{K_p n_s Q_M} \quad . \tag{91}$$

It will be assumed — somewhat arbitrarily — that the rms concentration fluctuation over the cross-section is,

$$a_1' = K_w A_p \tag{92}$$

where $K_w = f_5$ (injection system). Substituting in Equation (91),

$$a_1' = \frac{K_w A_T Q_T}{K_p n_s Q_M} \quad . \tag{93}$$

Eliminating a_1' from Equations (89) and (93),

$$\frac{a' K_p n_s Q_M}{K_w A_T Q_T} = \alpha' \left(\frac{x}{d}\right)^{-a} \quad . \tag{94}$$

Combining coefficients,

$$\frac{a' n_s Q_M}{A_T Q_T} = \alpha'' \left(\frac{x}{d}\right)^{-a} \quad . \tag{95}$$

This equation describes the rms concentration fluctuation, a', which can be expected at a normalized distance downstream, x/d, in terms of the known parameters n_s, Q_M, Q_T, and A_T, and the experimentally determined scalar decay rate, a, and wake-mixing coefficient, α''. a is determined by the grid bar diameter and the type of tracer injection system (for example, upstream injection or downstream injection from the grid bars). α'' is determined by the type of tracer injection system used. α'' has the units L^{-2} because it includes K_p, the cross-sectional area near each source which defines the flow rate involved in the wake-mixing, or premixing as Gibson terms it.

Since,

$$\overline{A} = \frac{A_T Q_T}{Q_M} \quad , \tag{96}$$

then Equation (95) can be modified to

$$\frac{a'n_s}{\bar{A}} = \alpha'' \left(\frac{x}{d}\right)^{-a} \quad . \qquad (97)$$

This can be transformed to a relation involving a'_o, the initial rms concentration fluctuation of the two unmixed streams, by use of Equations (87) and (96).

$$\frac{a'}{a'_o} n_s \sqrt{\frac{Q_M}{Q_T}} = \alpha'' \left(\frac{x}{d}\right)^{-a} \quad . \qquad (98)$$

In order to illustrate that the results of this study can be described reasonably well by this model, the data from seven different grids are shown in Figure 31 $a'n_s/\bar{A}\ \alpha''$ is plotted against x/d. All the data points represent injection from the downstream side of the grid bars. n_s varies from 1.3 to 7.6 orifices per square inch. $\bar{A}$ varies from 19 to 57 mg/ℓ. To reduce the total number of points plotted, only the data for V_M = 2 fps are shown.

There is, as might be expected, considerable scatter, but it does not seem excessive. For the grids with d = 1/4 in., taking the tracer source density into account actually increases the difference in results between the 4-orifice and 9-orifice grids (see Figure 26 for comparison). The wake-mixing, as manifested by the value of α'' which fits the data best, does, however, seem to be described quite well by this model. As mentioned previously, it could well be that the wake-mixing is the crucial step in the mixing process.

The value of α'' which seems to fit these data is 5 in.$^{-2}$. The decay rate, -a, is approximately -0.4 for the 1/8-in. grid bars and -0.8 for the 1/4-in. bars. The use of this model to compare results of the present study with those of Gibson in the case of the tracer being injected upstream is given in Appendix C. The agreement seems to be quite good.

The question which naturally arises concerns the extrapolation of these results to grids with larger bars. The results of the alum coagulation tests suggest that the grid bars in prototype mixers will probably be held to 1/2 in. or less. The decay rate for such a grid will probably be somewhat greater than the -0.8 for the 1/4-in. bars used in the present work. How much greater cannot be determined. Presumably, though, the value of α'' which is controlled by the wake-mixing would be the same. In Appendix D are estimates of the scalar decay curves for grids with larger bar diameters.

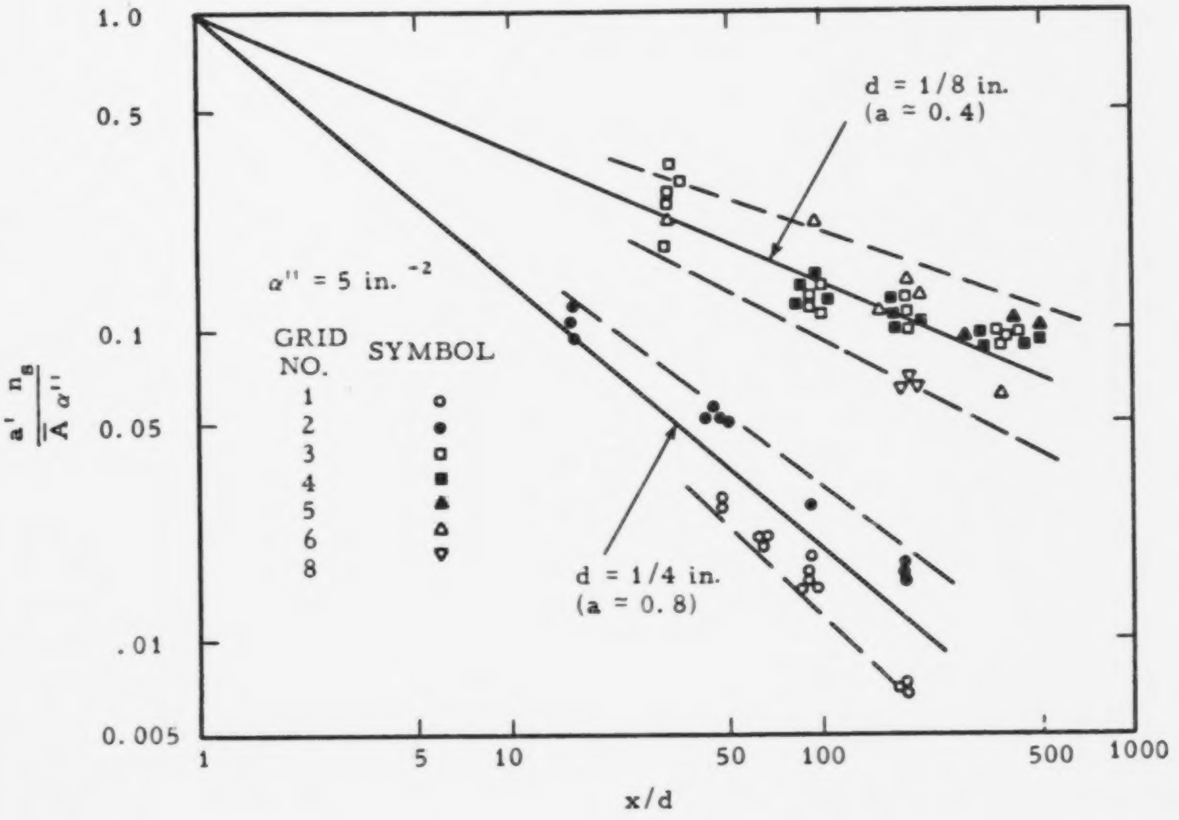

FIGURE 31. GENERAL MIXING MODEL: RESULTS FOR SEVEN GRIDS

SECTION VII

INITIAL MIXING AND ALUM COAGULATION -- FLOCCULATION

The purpose of the experiments described in this section was to demonstrate that rapid initial mixing is important in certain water and wastewater treatment processes, specifically alum coagulation-flocculation of a turbid water. Another purpose was to show that grid-type initial mixers, the mixing characteristics of which were described in Section VI, can be used to effect the rapid mixing. As stated previously, very rapid mixing of the chemical with the water stream before certain reactions can occur or be completed might result in improved process performance.

Alum added to a turbid water with sufficient alkalinity undergoes very complex, rapid, and irreversible reactions. This study and previous work have shown that if the Al(III) can come in contact with all the turbidity particles before these reactions have proceeded too far, then the alum can be more effective in performing its task of aiding clarification. It will be shown that the effect of initial mixing is dependent upon the alkalinity of the water. If the alkalinity is sufficiently low, slow initial mixing will not detrimentally affect the process performance. However, increasing the alkalinity results in an increasing sensitivity to the adequacy of the initial mixing.

Because of the prohibitive cost and difficulty of performing field experiments, the work described herein involves pilot-plant studies. This allowed close control of all parameters involved, but from the point of view of demonstrating the applicability of this concept to full-scale water and wastewater treatment plants, there is one difficulty. While it is not difficult to develop a device producing very rapid mixing in a 2-in. diameter pipe, it is a more difficult task to design and construct a device producing mixing of equal rapidity in a large pipe.

It is possible, through the use of mixing theory and experiments to predict the intensity of segregation (or degree of mixing) at a particular distance downstream from a given grid. However, it is not possible to predict precisely at the present time how rapid the mixing of the chemical stream with the water stream must be in order to avoid poor performance. The rates of the crucial reactions or phenomena are not known. Evidence will be presented which shows that for alum coagulation-flocculation of a turbid water, the time of mixing, the time required to reach some low, arbitrarily defined value of the intensity of segregation, must be very short if performance is to be improved.

This point is important because increasing the rapidity of initial mixing only slightly, such as by improving the flash mixer, may not lead to improved performance. It is believed that a grid-type initial mixing device will help overcome this problem. The mixing provided by a grid in a pipe depends not on the diameter of the pipe but on the physical configuration of the grid: the bar diameter, the bar spacing, and the number of tracer injection orifices per square inch of cross-sectional area. Thus, if grids which are fairly fine with a high injection orifice density can be constructed and placed in large pipes, it may be possible to utilize rapid initial mixing to provide an improvement in water treatment processes or to decrease the amount of chemicals needed for the processes.

SEGREGATION JAR TESTS

In order to show the effect of prolonged segregation in the mixing of alum with a turbid water, a jar test which simulated the difference between slow and rapid initial mixing was devised. Two 500-mℓ samples of turbid water were used. In most instances the turbidity consisted of a 25-mg/ℓ suspension of kaolin, although a 50-mg/ℓ suspension of bentonite was used in a few experiments because of the differences in coagulation characteristics between the two types of clays [36, 38]. An "optimum" alum dose was determined for the turbidity and alkalinity of the sample by using jar tests. Various concentrations of alum were added to samples of turbid water, and the samples stirred in a jar test apparatus. The lowest alum dose which resulted in the most rapid formation of visible floc was chosen as optimum [33].

The experiment representing rapid initial mixing was essentially an ordinary jar test. The previously selected alum dose was added directly to one of the 500-mℓ samples. This was vigorously stirred with a glass stirring rod for a few seconds in order to effect complete mixing. Then the sample was put in a jar test apparatus and stirred — usually for 6 minutes at 70 rpm. The floc formed was allowed to settle for 15 minutes. A pipette was used to remove a sample of supernatant from approximately one-half inch below the surface of the sample in order to avoid entrapping floating floc particles in the supernatant. This supernatant was then analyzed for residual turbidity using a light-scattering turbidimeter (the turbidimeter and chemicals are described in the section on continuous flow coagulation-flocculation experiments).

The experiment was repeated with a second 500-mℓ sample of turbid water with the following modification. This sample was divided into two portions, 100 mℓ and 400 mℓ, for example. The alum was then added to the 100-mℓ portion and was vigorously stirred for 3 to 5 seconds. Then this 100-mℓ portion was added to the remaining 400 mℓ. The two portions were thoroughly mixed with a stirring rod, and the jar test was repeated. This experiment represented poor initial mixing, i.e., prolonged segregation between the alum and a portion of the turbid water.

Generally, the jar test representing poor initial mixing resulted in a higher residual turbidity than the jar test with rapid initial mixing. This difference in results can be presented as the ratio of two aggregation rate coefficients, K_{A_m}, the coefficient for the case of rapid initial mixing, and K_{A_s}, the coefficient for the case of prolonged segregation. The values of rms velocity gradient, G, and time of flocculation, T, were low enough to allow deletion of the breakup term in the equation describing the rate of change of the concentration of primary particles.

$$\frac{dn_1}{dt} = - K_A n_1 G \qquad (70)$$

This equation can be easily solved for a batch system,

$$\ln (n_1 / n_1^o) = - K_A GT \quad .$$

In the segregation jar tests, the values of G and T were the same for the experiments involving rapid and slow initial mixing and can be eliminated from the equation giving the ratio of the two aggregation rate coefficients.

$$\frac{\ln (n_{1\,m} / n_1^o)}{\ln (n_{1\,s} / n_1^o)} = \frac{K_{A_m}}{K_{A_s}} \qquad (99)$$

where $n_{1\,m}$ and $n_{1\,s}$ are the concentration of primary particles remaining for the case of good mixing and poor mixing, respectively. As noted in Section IV, n_1 / n_1^o can be taken as the fraction of turbidity remaining after treatment as measured by a light scattering turbidimeter.

Effect of Bicarbonate Alkalinity on Jar Test Results

The water which is normally delivered to the University of California by the East Bay Municipal Utility District is taken from the Mokelumne River in the Sierra Nevada Mountains. The concentration of dissolved matter in this water is unusually low, the TDS concentration being approximately 32 mg/ℓ. The alkalinity, as $CaCO_3$, is 20 mg/ℓ. It was found that with a 25-mg/ℓ suspension of kaolin in this water, no effect of initial mixing, as measured by the segregation jar test, was apparent. Even with segregation times of up to 30 sec, the results of the jar test representing poor initial mixing produced results which were as good as those produced by the test representing rapid initial mixing.

In order to determine whether increasing the alkalinity might have an effect on the jar test results, sodium bicarbonate was added to the tap water before the kaolin. The jar test described above was repeated at various alkalinities and alum doses. The results are shown in Figure 32 where K_{A_m}/K_{A_s} is plotted against alkalinity. The figure shows the results of initially adding the alum to 100 mℓ and 250 mℓ of the 500-mℓ sample. It can be seen that increasing the alkalinity causes the effect of segregation to be increased. Also, initially adding the alum to a smaller portion of the total sample causes the effect to be greater. The range of alum doses in Figure 32 is 23 to 40 mg/ℓ, depending on the alkalinity. Not shown are the results of segregation jar tests performed with a 50-mg/ℓ bentonite suspension. The data involving bentonite are rather limited, but the increase in the effect of segregation with an increase in alkalinity is also found there. Vrale and Jorden [59] discuss the importance of rapid initial mixing in conjunction with silica suspensions which, as noted in Section IV, have coagulation characteristics similar to bentonite suspensions.

It appears that the alkalinity of the water affects the process by controlling the rate and extent of the hydrolysis and polymerization (or olation) reactions of Al(III) which occur in the presence of the clay particles in the segregated portion of the sample. This may be due, in part at least, to the buffer effect that alkalinity has on the pH as alum is added. Stumm and O'Melia [37] have shown that the reaction rates of Fe(III) and presumably Al(III) are strongly affected by pH. They found that the rate of removal of Fe^{+++} from the system increases 100 times for every unit increase in pH. It is also known that the polymerization reactions are considerably slower than the initial hydrolysis reactions [66], but how they vary with pH is unclear. As alum is added to a portion of the turbid water sample, the pH will be depressed to an extent depending upon the buffer capacity of the water — the lower the alkalinity, the greater the reduction in pH. And as the pH is lowered, the rate of removal of Al^{+++} from the system decreases. Thus, at low alkalinities, the reactions which can be detrimental to process performance might occur more slowly.

Figure 33 shows the final pH vs. the alkalinity for the optimum alum dose in the segregation jar tests. The alum doses in mg/ℓ are shown next to the data points. The final pH increases with increasing alkalinity. This adds to the effect of buffer capacity discussed above since, at higher alkalinities, not only will the extent of depression below the final pH in the segregated portion be less, but the final pH

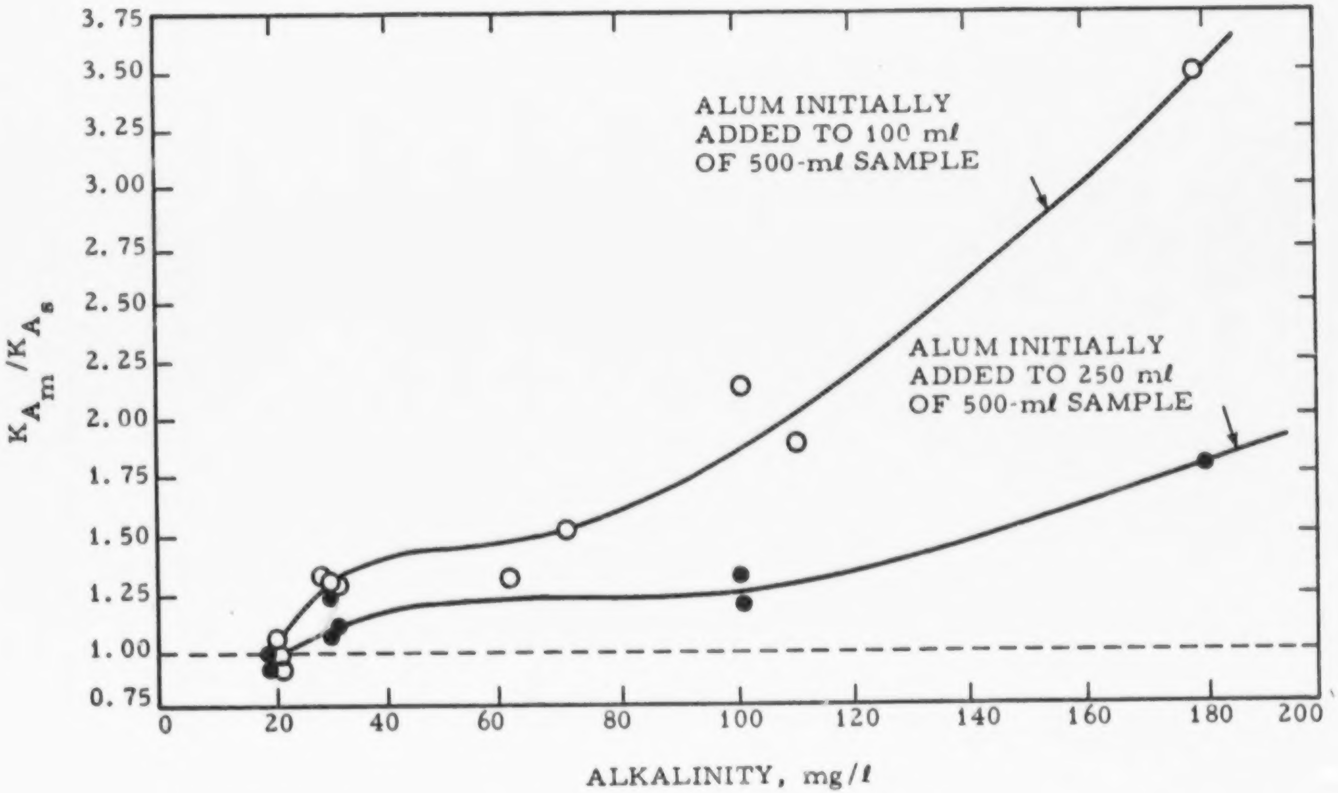

FIGURE 32. EFFECT OF SEGREGATION ON COAGULATION-FLOCCULATION: JAR TESTS

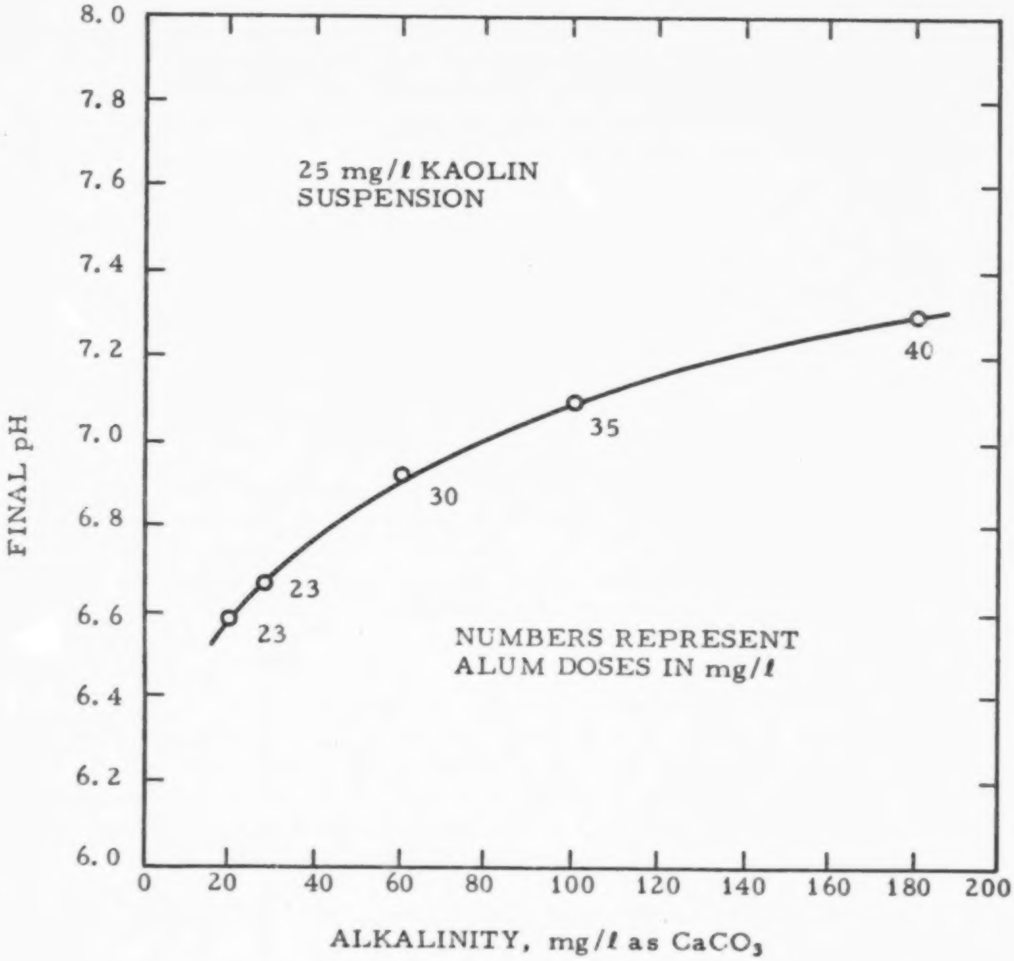

FIGURE 33. RELATION OF pH AND ALKALINITY AT "OPTIMUM" ALUM DOSAGES

itself will be higher. Thus, it is to be expected that at higher alkalinities, the pH in the portion to which the alum is first added will be higher, and the rate of the hydrolysis and polymerizations reactions will be faster.

Buffer capacity may affect the process in another way. At low alkalinities the pH in the portion to which the alum is initially added may be driven low enough to prevent the formation of the insoluble hydroxide (see Figure 1). Not until the mixing is almost complete will the $Al(OH)_{3\,s}$ tend to be formed, and this may be the crucial reaction which it is necessary to avoid. At higher alkalinities the pH in the portion to which the alum is added will not be driven so low, and $Al(OH)_{3\,s}$ can form before mixing is completed. More rapid mixing may overcome this.

It is possible that alkalinity has an even more direct effect upon the hydrolysis reactions. Kim, Ludwig, and Bishop [36] found that the isoelectric pH of the aluminum-hydroxo compounds was dependent upon the alkalinity of the water and postulated that the bicarbonate anion may have a stronger coordination tendency with the aluminum ion than does a hydroxide ion, causing a decrease in isoelectric pH with an increase in anion concentration. It can be concluded from this that the character of the reactions which occur are directly related to the alkalinity.

It should be noted that Kim, Ludwig, and Bishop found that the isoelectric pH decreased with increasing alkalinity. In the present study, the final pH at optimum alum dose increased with increasing alkalinity. Although the optimum pH decreases with increasing alkalinity, the pH range for "good" coagulation becomes wider. Thus, "optimum performance" in the present sense does not necessarily correspond to isoelectric pH.

It is also possible that the hydrolysis and polymerization reactions which occur when Al(III) is added to water are so rapid that their degree of completion depends only on the degree of mixing (see Figure 8). It might then be postulated that the diffusion of the aluminum-hydroxo compounds to the clay particles and the resulting destabilization may take a relatively long time (still less than one second). Very rapid mixing could allow the destabilization to occur in the presence of more clay particles, and better performance would result. It is unclear how varying the alkalinity (or pH) would affect this. It might be that at lower alkalinities, a greater degree of mixing would be necessary to reach a given degree of completion of the hydrolysis and polymerization reactions. Thus, more clay particles would be mixed with the destabilizing compounds, and initial mixing would not be as crucial as at high alkalinities.

Adding the alum to a smaller portion of the turbid water sample results in an increased effect of segregation because the alum is segregated from a greater amount of the kaolin during the period that the crucial reactions are taking place. If less kaolin is present during the occurrence of these reactions, then the residual turbidity after completion of the jar test will be greater.

It should be noted that there is a slight, although reconcilable, conflict between this result and the conclusion regarding the effect of buffer capacity on the phenomena. When the alum was initially added to 250 $m\ell$ rather than 100 $m\ell$ of the turbid water sample, the alum concentration was twice instead of five times the final dose in the total 500 mℓ. Therefore, the pH was not driven as low, and the reactions could occur at a much faster rate, or, alternatively, $Al(OH)_3$ could be formed. It might be expected, therefore, that adding alum to a larger portion of the 500 mℓ would result in an increased effect of segregation. That such a result does not occur means either that buffer capacity is of little importance in the alkalinity-segregation effect relation or that the number of clay particles present during the crucial hydrolysis and polymerization reactions is more important. The latter conclusion seems more likely.

CONTINUOUS FLOW COAGULATION – FLOCCULATION EXPERIMENTS

In order to determine the effect of rapid initial mixing in a continuous flow coagulation-flocculation system, two of the multiple-orifice grids used in the mixing studies described in Section V were utilized as initial mixing devices in conjunction with a tubular reactor. Results obtained using these devices were compared with results obtained using a flash mixer — a backmixed reactor utilizing a high-speed propeller to mix the fluid streams. The flash mixer provided mixing which would be considered sufficiently rapid by contemporary standards. The purpose of these experiments was to determine the advantage, if any, in using a multiple-source grid mixer at the head of a tubular reactor.

EXPERIMENTAL APPARATUS

A diagram of the experimental arrangement utilizing the grid initial mixers and, alternatively, the flash mixer is shown in Figure 34. It is a modification of the apparatus used for the mixing studies. At a point 2 ft downstream from the grid a tube was used to divert part of the flow into the multi-compartment flocculation chamber. The diversion tube was necessary because the flocculator could accommodate only a portion of the flow which the tubular reactor and grid mixer were designed to handle. A flow of 20 gpm was used in the tubular reactor, but only 0.73 gpm was passed through the flocculator. In order to minimize additional mixing caused by the diversion tube, the tube was centered in the tubular reactor. The diameter of the tube was such that the flow velocity in the tubular reactor was equal to that in the diversion tube. There were no valves in the tube to create turbulence. Despite these steps, the tube connecting the tubular reactor to the flocculation chamber did, of course, provide additional mixing of the alum with the turbid water. It was believed, however, that the crucial period would occur upstream from this point in the region very close to the grid, and the experimental results seem to substantiate this.

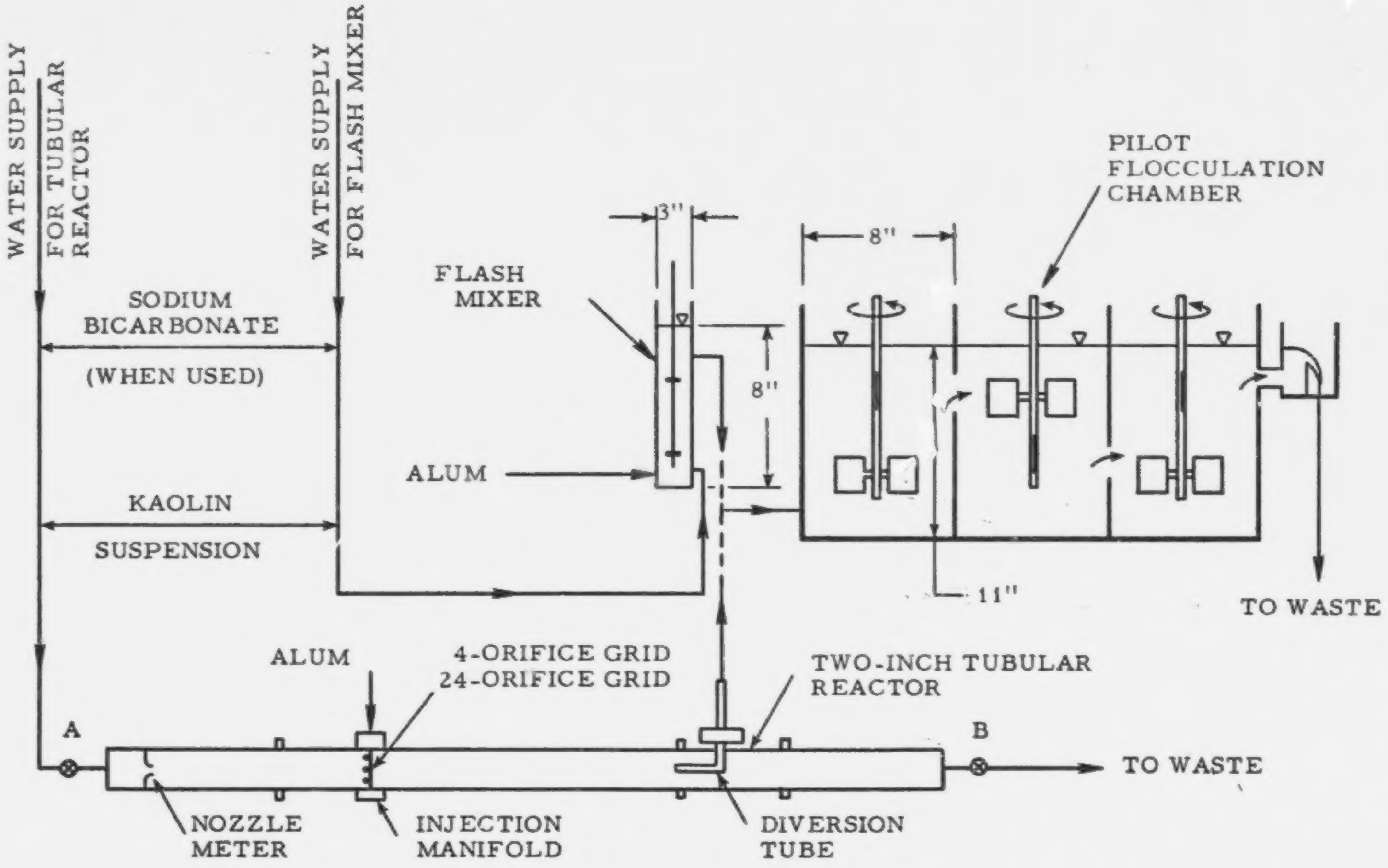
WATER SUPPLY
FOR TUBULAR
REACTOR
WATER SUPPLY
FOR FLASH MIXER
SODIUM
BICARBONATE
(WHEN USED)
KAOLIN
SUSPENSION
FLASH
MIXER
ALUM
3"
8"
8"
11"
PILOT
FLOCCULATION
CHAMBER
TO WASTE
ALUM
4-ORIFICE GRID
24-ORIFICE GRID
TWO-INCH TUBULAR
REACTOR
A
B
TO WASTE
NOZZLE
METER
INJECTION
MANIFOLD
DIVERSION
TUBE

FIGURE 34. INITIAL MIXING APPARATUS FOR CONTINUOUS FLOW COAGULATION-FLOCCULATION STUDIES

The flow from the tubular reactor to the flocculation chamber was controlled by varying the pressure in the tubular reactor section. This was accomplished by adjusting two valves, one downstream and one upstream from the reactor section (Points A and B, Figure 34). The flow was measured directly at the effluent end of the flocculator.

To add the kaolin suspension and the bicarbonate alkalinity to the raw water, a Sigmamotor model T65 positive displacement pump, powered by a Bodine NSH 54 RL motor and a Minarik SH-53 speed controller, was used. This type of pump can provide several streams of fluid simultaneously. The kaolin was added to the 2-in. line at a point approximately 10 ft upstream from the grid. A nozzle meter, a valve, and a 90° elbow between the two points insured that the kaolin was completely mixed with the raw water at the alum injection grid. Sodium bicarbonate was added at a point several feet upstream from the kaolin addition point. Alum was supplied from the same constant head tank employed in the mixing experiments for the salt tracer.

When the alternative setup for using a flash mixer as the initial mixing device was used, the raw water was put through the small constant head tank previously used for the salt tracer and alum solutions. A rotameter was used to measure and control the flow. The Sigmamotor pump described above was used to add the alum to the flash mixer in addition to being used to add the kaolin and sodium bicarbonate to the raw water line. It should not matter, from a hydrodynamic standpoint, that with the tubular reactor there was a much greater flow in the initial mixing unit. At the point of diversion in the tubular reactor, the intensity of segregation and the mean concentration of alum at all points of the cross-section were the same. What was done was merely to divert a portion of this flow to the flocculator. The actual flow through the tubular reactor is not relevant in the sense that a comparison of the efficiency of the two types of initial mixing systems can be made.

The pilot-plant flocculation chamber consisted of eight compartments, each 8-3/4 in. x 8-3/4 in. with a water depth of approximately 11 in. For these experiments, only three compartments were used. All paddles were driven at the same speed by a Bodine NSH 54 RL electric motor and a Minarik SH-53 speed controller.

As noted in Section IV the energy per unit fluid mass and per unit time dissipated in the system by the paddles is an important parameter in flocculation kinetics. It, together with fluid viscosity, determines the rms velocity gradient, G. Others have discussed in some detail the relation between G and the speed of rotation of the paddles [31, 51]. For the paddles used in this experiment, this relation has been determined to be (67)

$$G = 0.15\, N^{1.55} \qquad (100)$$

where N is the paddle speed in rpm and G is in sec^{-1}.

Initial Mixing Units

Two grid mixing devices in tubular reactors and one flash mixer were used in these experiments. The grids were two of those used in the mixing studies described in Section V (Grids 4 and 8, Table 2). The M/d ratio for both grids was 4, and the bar diameters were 1/8 in. The only difference between them was that one had 4 alum injection orifices, and the other had 24. This corresponds to orifice densities of 1.27 and 7.60 in.$^{-1}$, respectively. From the mixing studies, it seemed that the latter grid would provide better mixing than the former because of the relation between wake-mixing phenomenon and the tracer injection orifice density.

The velocity through the tubular reactor was 2 fps. This value was used in order to eliminate some of the problems which seemed to occur at the lower velocities as described in Section VI. For a 2-ft tubular reactor, the residence time was 1 sec. The tube connecting the tubular reactor to the flocculator was about 1 ft long and resulted in a total residence time before the flow entered the flocculation chamber of approximately 1.5 sec. The flash mixer was a 3-in. diameter plastic tube sealed at one end. The turbid water entered on one side at the bottom, and the alum solution entered on the other side. The propeller mixer rotated at 1600 rpm, and the water left the flash mixer near the top. The mean residence time was 23 sec.

Turbidimeter and Chemicals

A Hach laboratory turbidimeter, model 1860, was used to determine the relative number concentration of suspended particles in the coagulation experiments by measuring the turbidity of samples. It operated on the principle that light, passing through a substance before and after treatment, is reflected by particulate matter suspended in the substance. The turbidimeter was standardized with a polyacrylic plastic rod into which a special turbidity material had been cast. Before each reading was taken, the turbidimeter was checked with the standardized rod as the meter reading tended to drift slightly. It was found in the course of doing the experiments that there was a nonlinear relation between the concentration of kaolin suspended in the water and the reading of the turbidimeter. Since the parameter of interest was particle concentration (specifically, relative particle concentration) rather than turbidity per se, it was necessary to relate the two parameters by means of a calibration curve.

The turbidity producing material used in these experiments was kaolin N. F. colloidal, produced by Matheson, Coleman, and Bell. Bentonite and silica are two other types of colloids which could have been used. As noted in Section IV, the coagulation mechanism associated with these types of suspensions appears to be somewhat different from the mechanism associated with dilute kaolin suspensio Packham [38] took samples from several streams in England and found the suspension behaved similar to kaolinite. Both bentonitic an kaolinitic type clays are found in natural waters, but the proportion is seldom reported. While the differences between the two types should be remembered, indications are, from the segregation jar tes and the work of Vrale and Jorden [59], that the effect of rapid initial mixing seems to be independent of the type of colloidal material used.

The alum used was of technical grade. A problem associated with this was the fact that there was a considerable amount of insoluble impurities present. In order to deal with this problem, the alum was dissolved in deionized water in a 20-liter bottle at a concentration of about 25 g/ℓ 24 hr prior to a run. This allowed most of the insoluble material to settle out overnight. Then before the run was made, the supernatant was transferred to another 20-ℓ bottle from which the alu solution was fed to the system during the run. Reagent grade powder $NaHCO_3$, manufactured by Mallinckrodt Chemical Works, was used to provide the additional alkalinity during those runs where it was needed.

The kaolin suspension to be fed to the system was usually prepared the day of the run. The feed suspension concentration was usually 20 to 30 g/ℓ and was prepared with deionized water. The suspension was stirred for several hours prior to the run in order to insure that the clay was broken up into the smallest particles possible. Because the kaolin would not remain in suspension without stirring, the propeller mixer was kept operating during the run. Tests showed that at all times during the run, the kaolin feed concentration remained the same, demonstrating that the propeller mixer was effective in maintaining uniform concentration throughout the bottle. When sodium bicarbonate was required to increase the alkalinity of the water, it also was prepared with distilled water at a concentration of approximately 6 g/ℓ. These concentrations apply to the use of the grid-type initial mixers for which 20 gpm of water were passed through the initial mixing unit. When the flash mixer was used, only 0.73 gpm of water was passed through the initial mixing unit and the feed concentrations were approximately 1/20 the concentrations for the tubular reactor.

It was realized that, while using the same feed concentrations for both the grid and flash mixers, especially for the alum, might be desirable from the standpoint of consistency, there is no apparent reason why such a discrepancy might invalidate the experiment. The concentration of alum was quite high in both cases, and the pH was low enough to insure that the predominant species in both cases was probably the same. It should be noted that changing the alum feed concentration will change the value of a'_o as discussed in Section VI. It will be decreased in value with a decrease in the feed concentration. By lowering the value of a'_o, a' at a given time will also be decreased, and the rate of mixing can be considered to be improved by decreasing the alum feed concentration. In this way, any error caused by using the lower feed concentration for the flash mixer can be considered to be conservative because the rms concentration fluctuations are lower than they would have been if the higher feed concentrations had been used. Even with this advantage, the flash mixer provided the poorest results.

EXPERIMENTAL PROCEDURE

The raw water from the city line was fed to the appropriate constant head tank. The flow was adjusted to the desired value, and if the tubular reactor was being employed, the flow diverted from the tubular reactor was adjusted to the desired value using the valves upstream and downstream from the reactor section. As mentioned previously, this adjustment was very sensitive. When the flow was adjusted to the desired value, the chemicals were fed into the system, and the paddle speed was set to obtain the desired value of G. After the flow from the final compartment had reached steady state, 45 min — three times the mean residence time of 15 min — was allowed for the flocculation process to reach steady state. Then 100 mℓ samples were taken from each of the three flocculation compartments. During the first runs, three replicate samples were taken from each compartment. It was soon found that the results were fairly consistent, and subsequently, only one sample was taken from each compartment. The floc in the samples was allowed to settle for 30 min, and a pipette was used to remove a sample of supernatant for analysis in the turbidimeter. The supernatant was shaken vigorously to disperse any floc remaining and the turbidity measured using the Hach turbidimeter.

The initial turbidity was measured by taking a sample from the outlet of the final compartment to avoid floating material. It was found that at low values of G this method resulted in measured values of turbidity which were too low, due to settling of large flocs in the last compartment. Normally, the average value from several runs, disregarding the low values, was used to determine the initial turbidity.

After the run at the first value of G was completed, the paddle speed was changed in order to obtain another value of G. Then 30 min was allowed — two times the mean residence time — for the process to reach steady state. The sampling procedure was repeated, and another value of G was then selected. It was usually possible to complete runs with four different values of G in one day.

RESULTS

Continuous flow coagulation-flocculation experiments were carried out at two alkalinities, that present in the tap water at the time, 25-28 mg/ℓ, and tap water with sodium bicarbonate added to bring the alkalinity up to 70 mg/ℓ. For the lower alkalinity the alum dose was 23 mg/ℓ for the 25 mg/ℓ kaolin suspension. For the higher alkalinity, the alum dose was 30 mg/ℓ. As noted in the discussion of the segregation jar tests, it is not possible to change the alkalinity of the water and keep all other parameters constant.

Results of continuous flow experiments made at the two alkalinities are shown in Figures 35, 36, and 37. n_1^o/n_1^m, where m is the number of compartments, is plotted against G, the rms velocity gradient in the flocculation chamber. Figure 35 shows the results for one compartment with a mean residence time of 5 min; Figure 36, two compartments and 10 min; and Figure 37, three compartments and 15 min. Also shown are results obtained with three different initial mixing devices — the 24-orifice grid, the 4-orifice grid, and the flash mixer. There was a pronounced tendency for the 24-orifice grid to provide the best results and for the flash mixer to provide the poorest results. The dependency on initial mixing increases with compartmentalization and with alkalinity.

It would be instructive to consider the values of both the aggregation and breakup rate coefficients for the data presented in Figures 35–37. However, because in the range of high G values where breakup would be important, the data are somewhat inconsistent, only the values of K_A, the aggregation rate coefficient, are presented here. For an m-compartment flocculator, the resulting relation is

$$\frac{n_1^o}{n_1^m} = (1 + K_A G T_m)^m \qquad (101)$$

where T_m is the residence time per compartment. From these equations, the value of K_A can be found from the low G part of the performance curves in Figures 35–37. These values are listed in Table 4 for one, two, and three compartments at low and high alkalinity using the flash mixer, 4-orifice grid, and the 24-orifice grid. Also shown are the average values of K_A for each initial mixer at each alkalinity.

Figure 38 shows the average values of K_A normalized with respect to K_A for the flash mixer. The effect of alkalinity can be easily discerned.

The dependence on alkalinity has been discussed in relation to the results of the segregation jar tests. Segregation of the alum with a portion of the clay particles under conditions promoting rapid hydrolysis and polymerization results in a higher residual turbidity after completion of the flocculation process. The alkalinity, through its buffering capacity, or by more direct action of the HCO_3^- ion, influences the rate and extent of these reactions. Thus, with higher alkalinity, it becomes more important to quickly reduce the intensity of segregation in the mixing process.

Perhaps the formation of insoluble aluminum hydroxide is the crucial reaction which results in poor coagulation. It has been noted that the best coagulation of low concentrations of kaolin occurs under conditions of least solubility of Al(III). It may be that the species responsible for the destabilization of the clay particles are some of the positively charged hydrolysis and polymerization products of Al(III) which are adsorbed on the colloidal surface. The insoluble hydroxide would then form at the clay particle surfaces and act as a binder material in the sense first proposed by Langelier and Ludwig [34].

Alternatively, it may be that some of the charged hydrolysis and polymerization products formed early may be better coagulating agents than those formed later. Rapid mixing can bring these initial compounds in contact with more of the clay particles and thus increase their effectiveness.

Whatever the particular species responsible for the critical "reaction" of the alum and the clay, very rapid mixing can result in avoiding the premature formation of those species with poorer coagulating ability in cases of high alkalinity. At lower alkalinities the problem of premature formation of critical species does not occur.

Figure 39 shows a comparison of results obtained when the flash mixer was used and when the alum was added directly to the first compartment of the flocculation chamber. The latter is a very poor initial mixing device, especially at lower values of G. The measurements were made at the higher alkalinity, 70 mg/ℓ. There was no apparent difference in performance between the two systems. The conclusion drawn from this experiment is that a difference in the time of mixing will not necessarily result in a difference in process performance. The time of mixing must be short enough to prevent the critical physical-chemical reactions from occurring to any great degree before the mixing is completed. For example, from Figure 19 it can be found that for the 24-orifice grid it only took 0.36 sec for $a'/\overline{A} = 10\%$ to be reached. A similar situation occurred in the segregation jar tests where the results seemed to be more or less independent of the time of segregation. This will be especially important in field applications where the required short times of mixing will be more difficult to obtain.

TeKippe and Ham [68] recently reported on experiments similar to the one described above in which a flash mixer at the head of a flocculator was used to mix the alum with the turbid water in a pilot-scale study. A silica suspension was used to produce the turbidity. The value of G in the initial mixing unit was varied from 50 to 200 sec^{-1}, and the value of $G\bar{t}$ for the initial mixer was maintained at 48,000. Subsequent to the initial mixing step, the mean residence time and the rms velocity gradient in the flocculator were 15 min and 50 sec^{-1}, respectively. Samples of water were taken from the effluent end of the flocculator and allowed to settle for 5 and 30 min. The residual turbidity in the supernatant for a given settling time was taken as the measure of

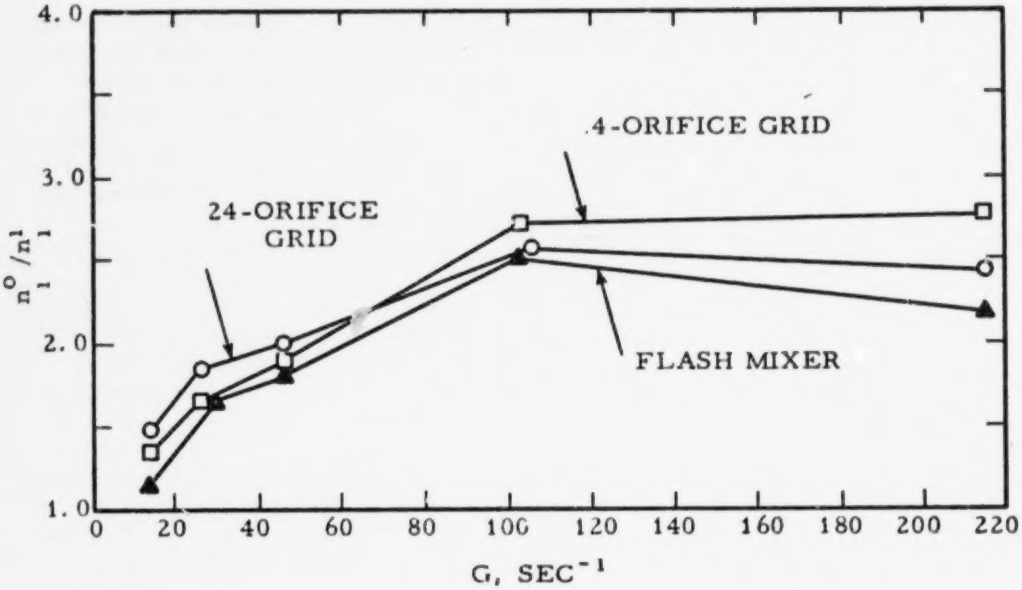

a) ALKALINITY = 28 mg/l

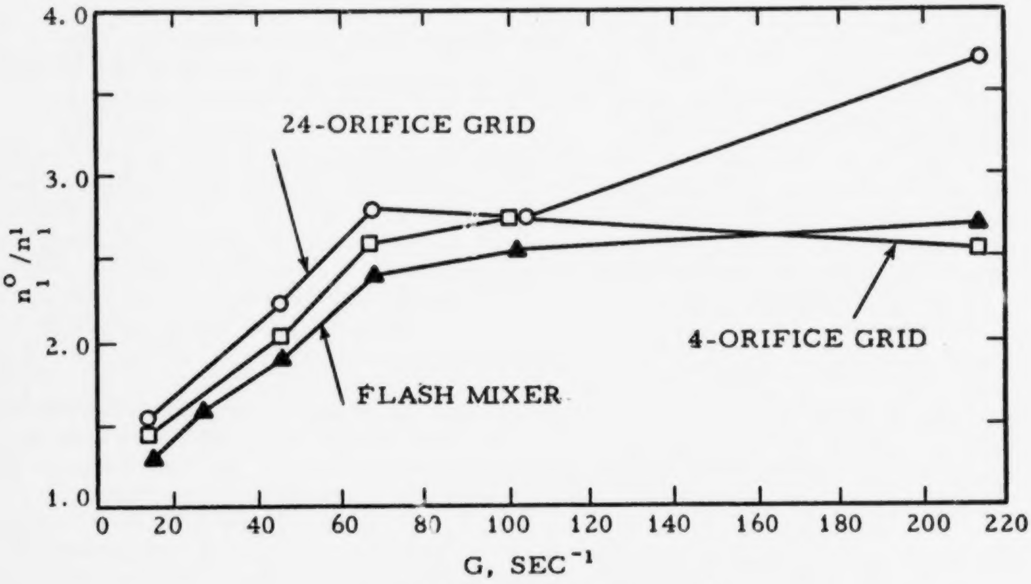

b) ALKALINITY = 70 mg/l

FIGURE 35. EFFECT OF INITIAL MIXING DEVICE ON FLOCCULATION PERFORMANCE: SINGLE COMPARTMENT, T = 5 MIN.

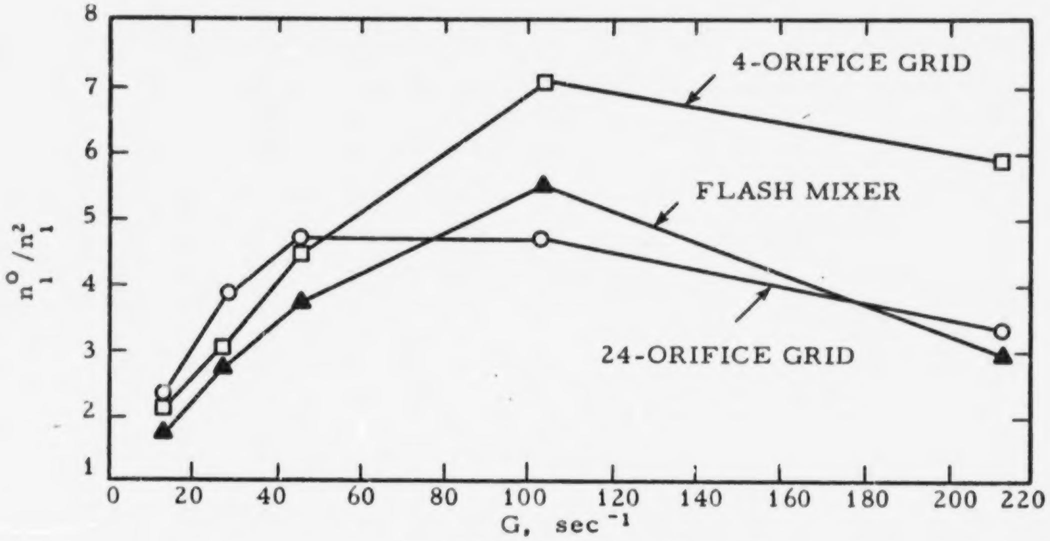

a) ALKALINITY = 28 mg/ℓ

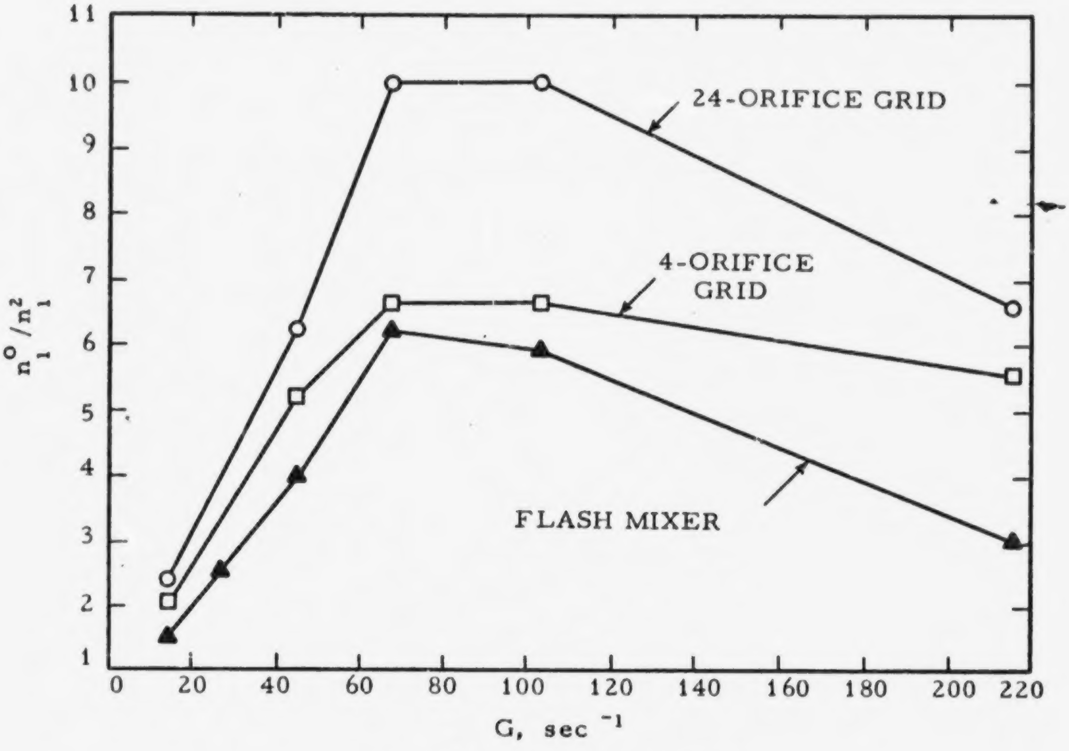

b) ALKALINITY = 70 mg/ℓ

FIGURE 36. EFFECT OF INITIAL MIXING DEVICE ON FLOCCULATION PERFORMANCE: TWO COMPARTMENTS, T = 10 MIN.

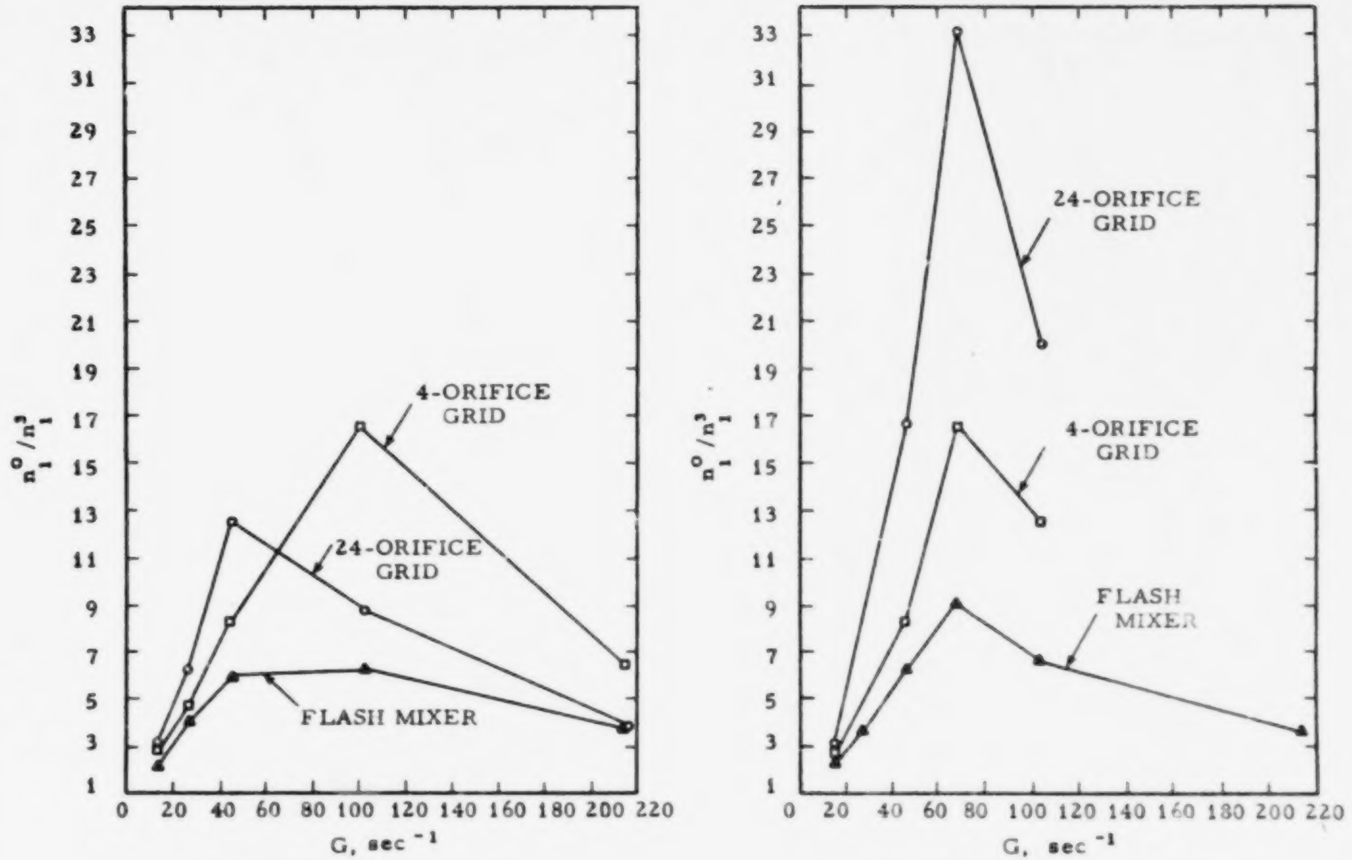

a) ALKALINITY = 28 mg/ℓ

b) ALKALINITY = 70 mg/ℓ

FIGURE 37. EFFECT OF INITIAL MIXING DEVICE ON FLOCCULATION PERFORMANCE: THREE COMPARTMENTS, T = 15 MIN.

TABLE 4

AGGREGATION RATE COEFFICIENTS FOR CONTINUOUS FLOW EXPERIMENTS

Alkalinity mg/l as $CaCO_3$	No. of Compartments	Flash Mixer	4-Orifice Grid	24-Orifice Grid
28 mg/l	1 2 3	0.0040 0.0041 0.0037	0.0043 0.0050 0.0047	0.0054 0.0059 0.0057
	Avg	0.0039	0.0047	0.0057
70 mg/l	1 2 3	0.0040 0.0045 0.0039	0.0050 0.0059 0.0047	0.0061 0.0073 0.0071
	Avg	0.0041	0.0052	0.0068

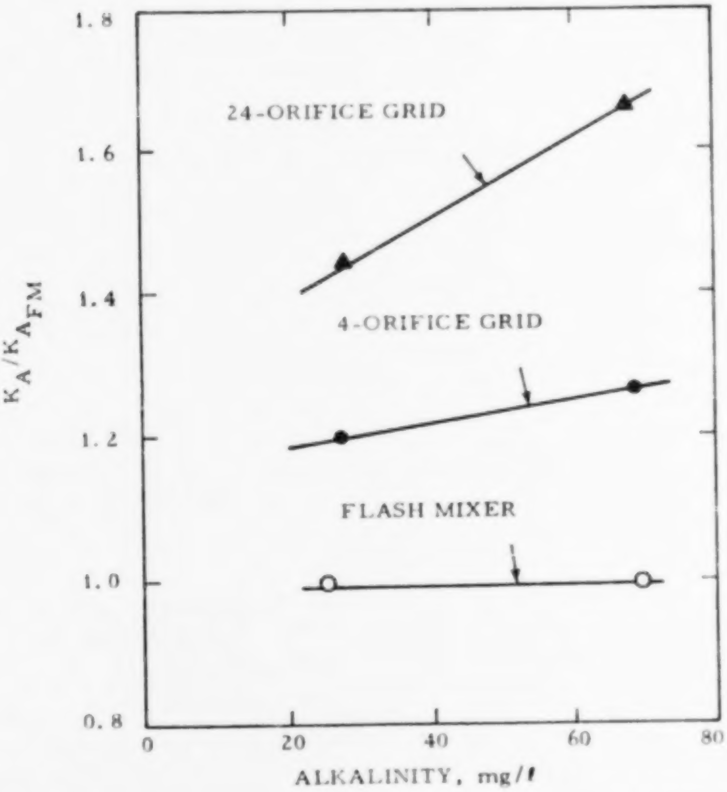

FIGURE 38. EFFECT OF SEGREGATION ON COAGULATION-FLOCCULATION: CONTINUOUS FLOW TESTS

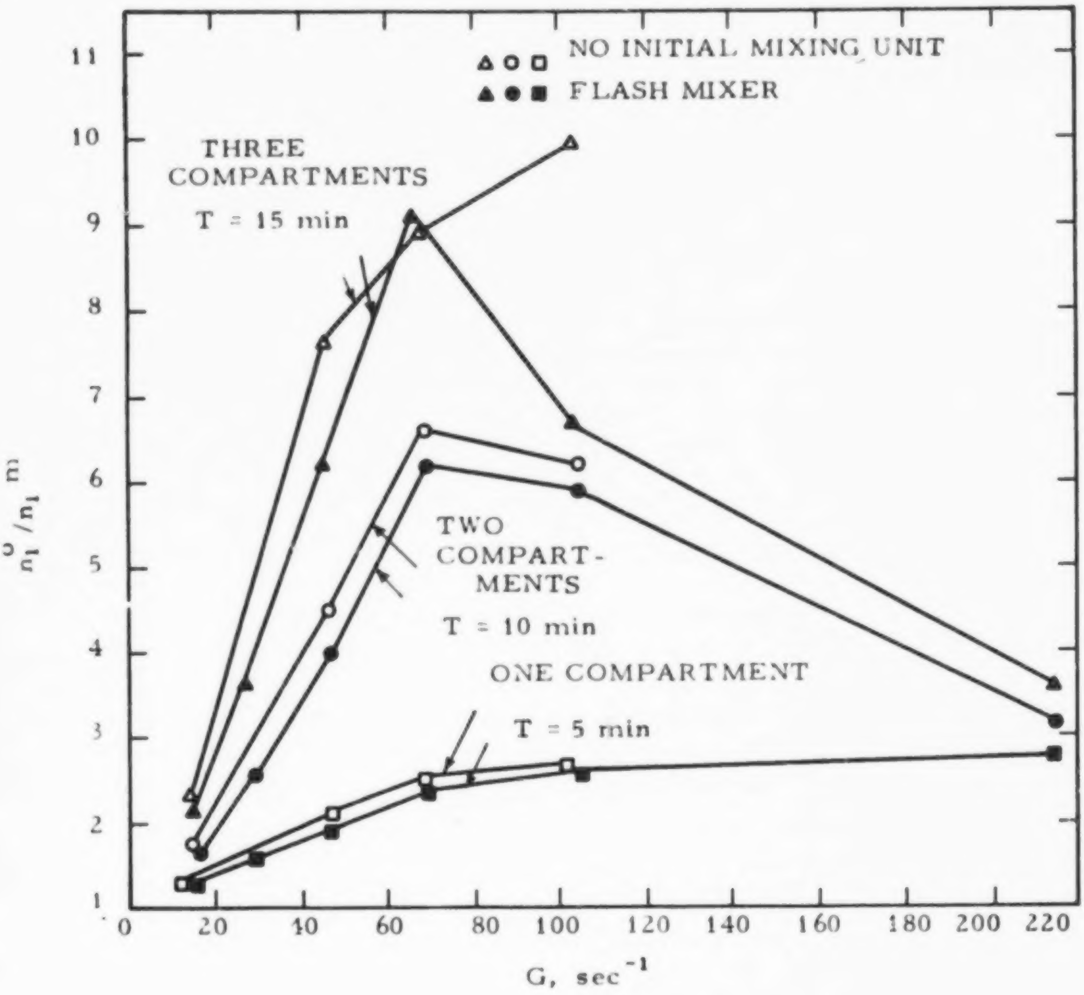

FIGURE 39. EFFECT OF INITIAL MIXING ON FLOCCULATION PERFORMANCE: COMPARISON BETWEEN FLASH MIXER AND NO INITIAL MIXING UNIT, ALKALINITY = 70 mg/ℓ

performance. They reported that the various values of G produced no significant differences in results. This is consistent with the conclusions drawn from the present study.

In considering Figures 35–37, it is necessary to consider that with the flash mixer being used as the initial mixing device (and with the alum being added to the first compartment) backmixing is occurring. In Section IV it was noted that backmixing may be inherently detrimental to coagulation because of reaction of incoming Al(III) species with products of the completed reactions. For example, Vrale and Jorden [25] point out that $Al(OH)_{3\,s}$ particles may act as nuclei to enhance the precipitation of Al^{+++}. The present study produced no conclusive evidence as to whether backmixing is inherently inferior to plug-flow mixing for alum coagulation-flocculation. While the mixing provided by the flash mixer was quite rapid, it is believed that the time of mixing was probably lower than that provided by the grid mixers. No attempt was made to measure the concentration fluctuations at the outlet of the flash mixer. It was assumed that with a mean residence time of 23 sec, the concentration fluctuations at the outlet were probably quite low. That the flash mixer gave the poorest results cannot be taken to mean that backmixing necessarily results in poorer performance. It may only mean that it is difficult to obtain very rapid mixing with such a device.

In terms of a full-scale treatment plant, the argument becomes irrelevant. While it is conceivable that fairly fine grids might be constructed, it would be impossible to construct a flash mixer which would provide mixing times of a fraction of a second, and it seems that mixing times this low are necessary to effect an improvement in performance.

COAGULATION OF WASTEWATER

In order to ascertain whether the initial mixing step is critical in alum coagulation of wastewater, a series of segregation jar tests were conducted at the Sanitary Engineering Research Laboratory of the University of California. As with the kaolin suspensions, a 500-mℓ sample of raw domestic wastewater was divided into two portions, 100 mℓ and 400 mℓ. The optimum alum dose (found from ordinary jar tests) was added to the 100-mℓ portion and stirred vigorously for a specified period of time (5 to 50 sec). Then this portion was added to the remaining 400-mℓ portion. The 500-mℓ sample was then stirred in a jar test apparatus for 6 min, and the resulting floc was allowed to settle for 15 min. A sample of supernatant was taken and analyzed for residual turbidity using a Rossum Model 600 turbidimeter.

For comparison, an ordinary jar test was made with the alum dose being added to the total 500-mℓ sample. The relation giving the ratio of the aggregation rate coefficients for the two experiments is

$$\frac{K_{A_m}}{K_{A_s}} = \frac{\ln (n_{1\,m}/n_1^0)}{\ln (n_{1\,s}/n_1^0)} \quad . \tag{99}$$

The results of these tests at various segregation times are shown in Figure 40. It is significant that K_{A_m}/K_{A_s} continues to increase at the higher segregation times (10 – 50 sec). This is in contrast to the results from the kaolin suspension studies in which there seemed to be little change in performance when the segregation time was increased beyond 3 to 5 sec, the shortest segregation time practicable by the test procedure. The same conclusion was reached by comparing performance obtained from the flash mixer with that obtained by adding the alum to the first compartment of the flocculator. The results with wastewater indicated that it is possible to obtain a very significant improvement in performance (over that of a poor initial mixing device) without the extremely rapid initial mixing required for improvement in a kaolin-water system. Consequently, such fine grid meshes would not be needed and the grid construction problem would be simplified.

It is instructive to make a calculation concerning the grid parameters required to produce a given level of performance. It will be assumed that a value of $a'/\overline{A} = 10\%$ is the level of mixing required. This assumption is strictly arbitrary. From Figure 40 it will be assumed that this level is to be attained in 10 sec. From Appendix D the scalar decay equation for 1/2-in. grid bars is estimated to be

$$\frac{a' n_s}{\overline{A}} = 5.0(x/d)^{-1.13} \quad . \tag{102}$$

If the flow velocity is 2 fps,

$$x = vt = 20 \text{ ft} = 240 \text{ in.}$$

equation 102 can now be solved for n_s

$$n_s = 50\,(480)^{-1.13} = 0.0465 \text{ in.}^{-2} = 6.7 \text{ ft}^{-2} \quad .$$

This means that 6.7 orifices per square foot of reactor cross-section are required to give $a'/\overline{A} = 10\%$ at $x = 20$ ft when the mainstream velocity is 2 fps. A grid with the necessary parameters would be relatively easy to construct.

A calculation similar to the one above was not made for the kaolin system because of the difficulty of estimating the segregation time required to produce an improvement in performance. This is in addition to the problem of estimating what the level of mixing should be at that time.

The results of these tests can probably be assumed to hold if ferric chloride is the coagulant. Lee [69] has found that in lime coagulation of wastewater the rapidity of the initial mixing has only a slight effect on performance.

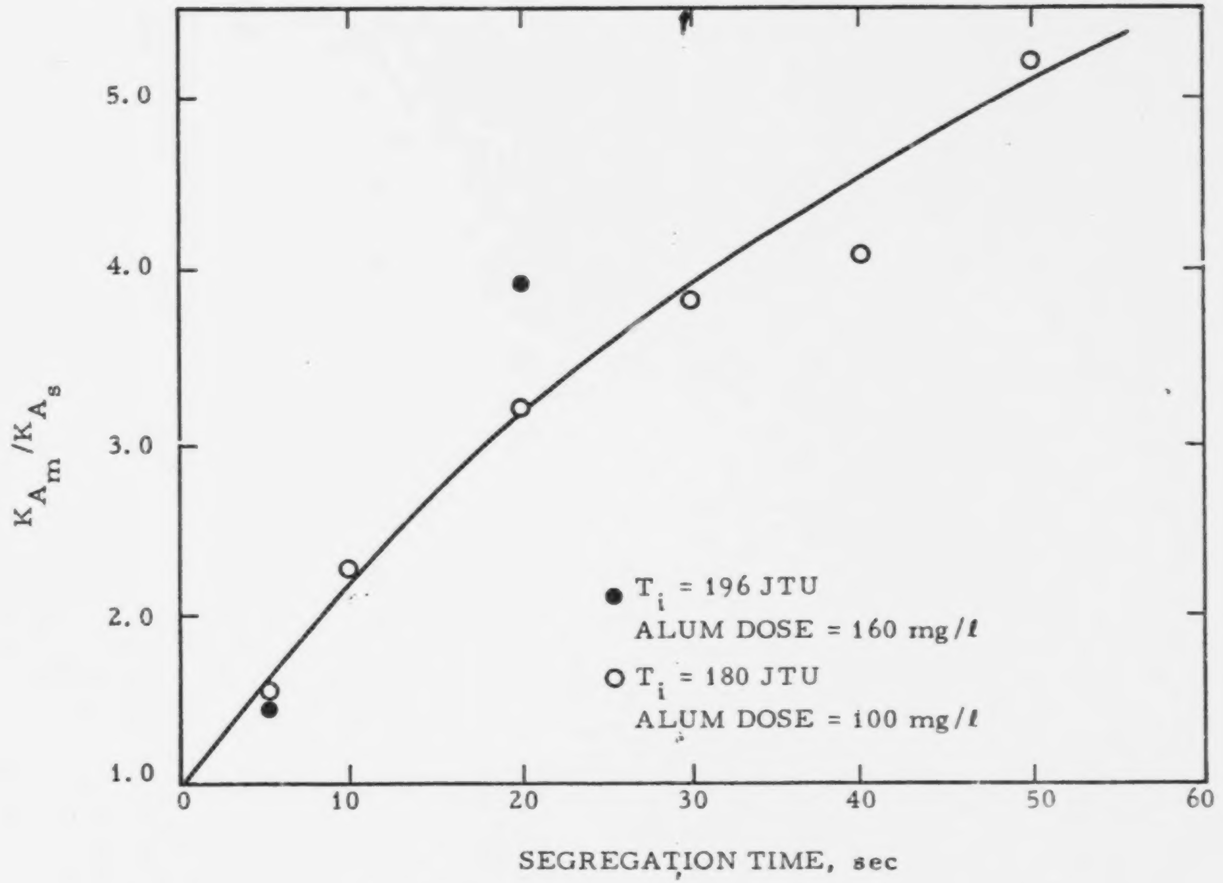

FIGURE 40. SEGREGATION JAR TESTS FOR VARIOUS SEGREGATION TIMES – ALUM COAGULATION OF RAW SEWAGE

SECTION VIII

ACKNOWLEDGMENTS

The research reported herein was supported in part by Research Grant No. 17030 DLX from the Environmental Protection Agency. Ray Campbell provided invaluable assistance in designing and constructing the experimental apparatus. Harvey Collins and the California Department of Public Health aided in conducting the chlorination experiments, and Fang Maw Lee assisted in performing the wastewater coagulation experiments. Useful discussions concerning water chemistry were held with R. Rhodes Trussell. The support of this project by the EPA Project Officer, Dr. Sidney A. Hannah, is also acknowledged.

Preceding page blank

SECTION IX

APPENDICES

Page No.

A. Initial Mixing and Wastewater Chlorination 119

Table 1: Effect of Method of Applying Chlorine on Reduction of Coliform Organisms . . . 121

Figure 1: Schematic Drawing of Experimental Apparatus for Pilot-Scale Chlorination Study 123

Table 2: Physical and Chemical Analyses of Unchlorinated Effluent 125

Table 3: Effect of Initial Mixing on Disinfection of a Primary Effluent in a Tubular Reactor 125

Figure 2: Performance of Various Non-Backmixed Chlorination Units 127

B. Plant-Scale Study of the Effect of Initial Mixing in Wastewater Chlorination 129

Figure 1: PVC Chlorination Grid 133

Figure 2: Multiple-Orifice Grid used as Initial Mixing Device 134

Figure 3: Schematic Drawing of Rancho Cordova Chlorination System 136

Table 1: Analyses of Unchlorinated Secondary Effluent 137

Table 2: Operating Parameters and Bacterial Survival Ratios 138

Figure 4: Coliform Survival Ratio in an Activated Sludge Effluent — Effect of Initial Mixing . 139

Preceding page blank

Page No.

Figure 5: Fecal Coliform Survival Ratio in a Chlorinated Activated Sludge Effluent — Effect of Initial Mixing 140

C. Comparison of Results With Those of Gibson 143

Table 1: Parameters for Mixing Experiments . . . 145

Figure 1: Scalar Decay Downstream from a Grid: Comparison of Results From Present Study with those from Gibson's Study . . . 146

D. Prediction of Mixing for Larger Grids 147

Figure 1: Prediction of Scalar Decay Curves from Experimental Data for d = 1/4 in. 149

APPENDIX A

INITIAL MIXING AND WASTEWATER CHLORINATION

APPENDIX A

INITIAL MIXING AND WASTEWATER CHLORINATION

Recent studies at the Sanitary Engineering Research Laboratory of the University of California showed that rapid initial mixing may be important in the wastewater chlorination process as well as in alum coagulation-flocculation. Selleck and Collins [55] and Selleck, Collins, and White [56] have discussed the reason which they believe causes prolonged segregation of the chlorine from the bacteria to result in poorer performance. The bactericidal compounds are formed by the reaction of chlorine with nitrogenous and carbonaceous matter to form chlorine complexes. The speed of these reactions varies; some are quite fast while others are relatively slow. Selleck and Collins have concluded that the residuals initially formed are apparently much more bactericidal than the compounds formed later. They concluded that rapid initial mixing allows these "hot" residuals to come in contact with the bacteria and act as killing agents.

Selleck and Collins also concluded that backmixing may contribute to poorer disinfection. They noted that reactions may take place between the more bactericidal residuals initially formed upon entering the reactor and the more complex residuals which form over a longer time. Thus, these simple and more bactericidal compounds may be "destroyed" before they can act.

In one experiment described by Selleck, Collins and White [56], chlorination was effected in two alternative ways. In one arrangement, the chlorine was added directly to a CSTR ($\bar{t}$ = 37. 5 min) near the paddle which rotated at 50 rpm. Under the alternative arrangement, the chlorine was added to a short ($\bar{t}$ = 0. 12 min) tubular reactor placed upstream from the CSTR. The tubular reactor consisted of a 1/4-in. PVC tee acting as a constriction in a 3/4-in. line. The chlorine was added through the stem of the tee. Settled wastewater was the effluent to be treated and an aqueous solution of chlorine gas was the disinfecting agent.

Table 1 summarizes the data they obtained with these two systems. Although the total mean residence time was essentially the same, the kill obtained when the chlorine was added at the head of the tubular reactor was much greater. The coliform survival ratio — the parameter used to indicate bactericidal effectiveness — was about one order of magnitude lower in this case. However, the coliform survival ratio for the CSTR alone was approximately the same regardless of whether the chlorine was added directly to the CSTR or to the tubular reactor. The increase in kill was due solely to the more rapid mixing which occurred in the tubular reactor.

TABLE 1

EFFECT OF METHOD OF APPLYING CHLORINE ON REDUCTION OF COLIFORM ORGANISMS

(From Selleck, Collins, and White [56])

Run No.	Chlorine Residual mg/ℓ	Coliform Survival Ratio
A. CHLORINE APPLIED IN TUBULAR REACTOR ($\bar{t}$ = 0.12 min) Ahead of CSTR ($\bar{t}$ = 37.5 min)		
1	3.2	0.00286
2	5.1	0.00419
3	8.1	0.00049
B. CHLORINE APPLIED DIRECTLY TO CSTR		
1	4.2	0.0378
2	6.1	0.052
3	8.8	0.012

Another result is that for each run, the chlorine residual in the CSTR was slightly lower when the chlorine was applied to the tubular reactor. It was concluded that the various reactions involved were driven to a greater degree of completion because of the more rapid mixing.

PILOT-PLANT STUDY

Based on the evidence presented above that the rapidity of the initial mixing is an important parameter in wastewater chlorination, a pilot-scale study was undertaken in cooperation with the California State Department of Public Health. The purpose of the study was to determine if any difference in performance could be effected by using two different initial mixing devices in a tubular reactor, one which produced very rapid mixing, and one which produced relatively slow mixing. If more rapid mixing resulted in better performance, then it would indicate the desirability of carrying out studies at a full-scale treatment plant.

Equipment

A schematic diagram of the apparatus is shown in Figure 1. The wastewater was pumped from a large storage tank through the tubular reactor, a 2-in. I. D. PVC pipe. The distance from the point of chlorine injection to the last of three sampling points was 38 ft. There was a section of straight pipe approximately 8 ft long upstream from the point of chlorine injection to help insure that the flow and turbulence characteristics at the initial mixing device were not affected by the bend.

Sketches of the two initial mixing devices are also shown in Figure 1. The first device was a 3/8-in. I. D. tube which introduced the chlorine feed solution at a point in the center of the tubular reactor. The diameter of the tube was such that the velocity of the chlorine solution entering the reactor was approximately the same as the wastewater velocity, reducing the shear between the two streams. Only the turbulence generated by wall friction and the variation in temporal mean velocity across the pipe cross-section, also produced by the wall friction, acted to mix the chlorine with the waste stream. Studies by Gibson [11], Keeler [22], and Lee [3] and the present mixing experiments have shown that this produces relatively slow mixing in comparison with the other device.

The second initial mixing device was a biplane grid of 1/4-in. bars spaced 1/2 in. center-to-center, similar to those studied in Section VI. In order to obtain maximum benefit from the wake-mixing phenomenon, thirteen 1/16-in. orifices were used as chlorine injection sources. This was a much more efficient mixing device which, it was believed, would produce greater bacterial kills.

Procedures

The experiments were run in the following manner. Effluent from the primary waste treatment plant was collected over a period of several hours in two large storage tanks. Since the two tanks were being filled simultaneously, the composition of the sewage in each was the same. The wastewater in the tanks was stirred slowly to prevent settling of particulate matter in order to further assure constant wastewater composition during the course of the experiment. The chlorine feed line (an aqueous solution of chlorine gas was used) was connected to one of the initial mixing devices. When the single source mixer was used, the section containing the grid and manifold was removed. Wastewater was pumped through the tubular reactor at a velocity of 2 fps (a flow rate of 20 gpm). The chlorine solution was then fed into the reactor.

At each of three points — 10, 24, and 38 ft downstream — a sample was taken and the total chlorine residual determined amperometrically according to the method suggested by Standard Methods [62]. Then three replicate samples for determination of coliform concentrations were taken at each point They were dechlorinated as quickly as possible with a sodium thiosulfate solution. Samples were also taken at a point

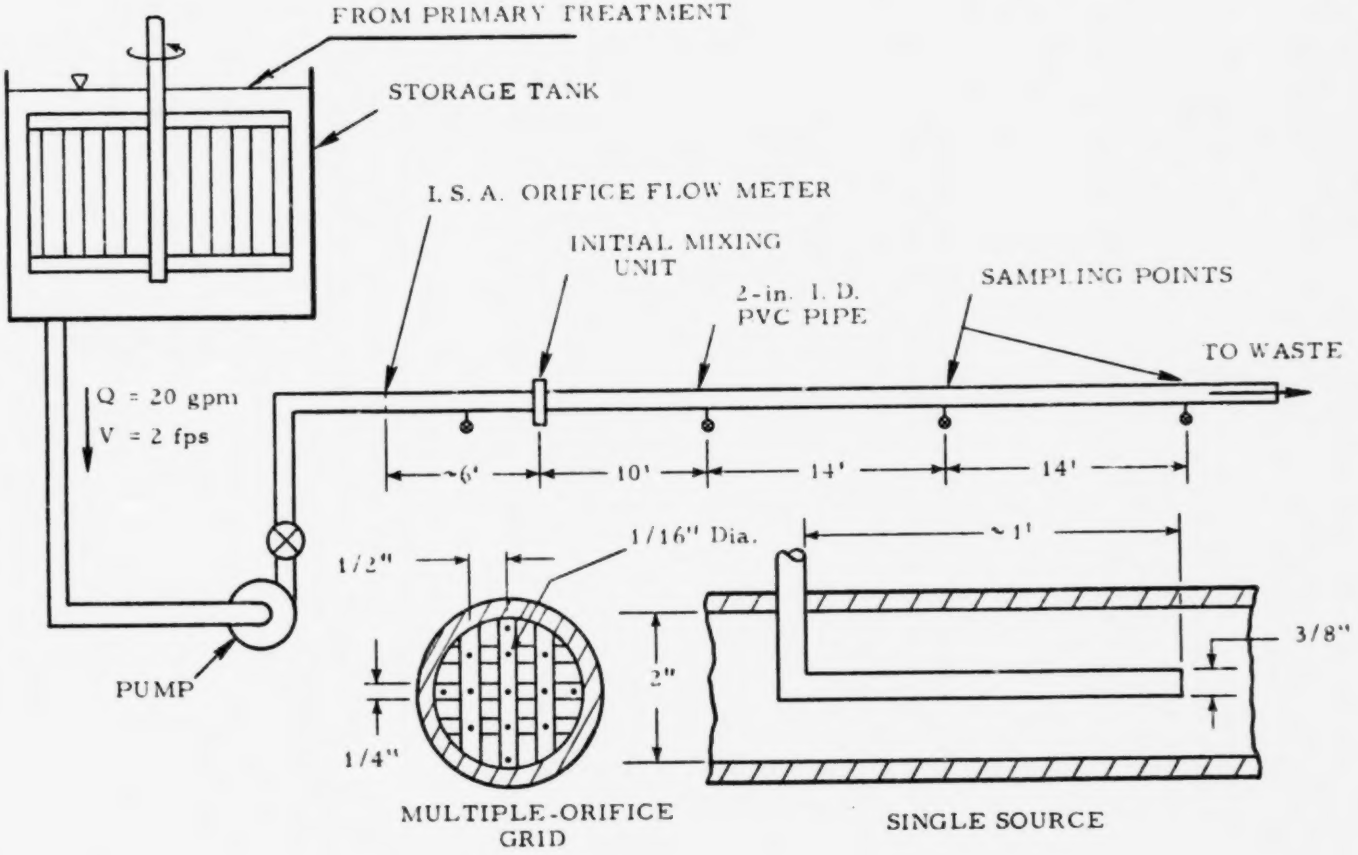
FROM PRIMARY TREATMENT
STORAGE TANK
I. S. A. ORIFICE FLOW METER
INITIAL MIXING UNIT
2-in. I. D. PVC PIPE
SAMPLING POINTS
TO WASTE
Q = 20 gpm
V = 2 fps
PUMP
~6'
10'
14'
14'
1/16" Dia.
~1'
1/2"
1/4"
2"
3/8"
MULTIPLE-ORIFICE GRID
SINGLE SOURCE

FIGURE 1. SCHEMATIC DRAWING OF EXPERIMENTAL APPARATUS FOR PILOT-SCALE CHLORINATION STUDY

upstream from the initial mixing unit to determine the initial coliform concentration. The task of determining the coliform concentrations was performed by the California State Department of Public Health in accordance with Standard Methods.

A sample of wastewater was analyzed at the Sanitary Engineering Research Laboratory at the University of California to determine ammonia nitrogen, organic nitrogen, total suspended solids, volatile suspended solids, and COD concentrations. The techniques were those recommended by Standard Methods. The results of these analyses are shown in Table 2.

Results

The results are shown in Table 3. Two runs were made several weeks apart. During the first run difficulties were encountered which make the results somewhat unreliable, but they have been included for completeness. The main problem centered on uncertainty regarding the wastewater flow rates. This is manifested by the fact that the chlorine residuals were somewhat lower when the grid was used as the initial mixing device. Still, a comparison between the multiple-orifice grid and the single-source chlorine injector can be made. Using the grid resulted in coliform survival ratios about one order of magnitude lower.

During the second run the wastewater flow rate was controlled more closely. Use of the grid resulted in a coliform survival ratio approximately two orders of magnitude lower than did the single source. In fact, the survival ratios for the grid were probably lower than those shown because in the laboratory analysis the MPN's were biased toward higher-than-likely values.

With the single source of chlorine, Table 3 shows that for the first sampling point (contact time = 0.08 min) the chlorine solution was not spread evenly over the cross-section of the tubular reactor at that point. It should be noted that the chlorine contact time will not be the same for all the fluid particles. It might be suspected that this is the reason for the difference in results obtained with the two initial mixing units. However, inspection of the results shows that this is probably not true. It can be assumed that the chlorine was completely mixed with the wastewater by the second sampling point when the single source was being used. Thus, at the third sampling point the chlorine contact time for all the fluid particles was at least 7 sec. The coliform survival ratio at this point was higher than for the grid initial mixer at the first sampling point (contact time = 5 sec). Therefore, the difference in contact times for individual fluid particles cannot be cited as the reason for the difference in results.

The conclusion drawn from this experiment is that prolonged segregation of the chlorine from the coliform organisms allows the formation

TABLE 2

PHYSICAL AND CHEMICAL ANALYSES OF UNCHLORINATED EFFLUENT

Run No.	Volatile Suspended Solids mg/ℓ	Total Suspended Solids mg/ℓ	Ammonia Nitrogen mg/ℓ	Organic Nitrogen mg/ℓ	COD mg/ℓ	pH
1	46	77	24. 6	7. 6	170	7. 8
2	33	35	15. 7	3. 9	104	

TABLE 3

EFFECT OF INITIAL MIXING ON DISINFECTION OF A PRIMARY EFFLUENT IN A TUBULAR REACTOR

Run No.	Contact Time min	Chlorine Residual mg/ℓ	Coliform Survival Ratio
(1)			
	0. 08	5. 10	0. 88
Single Source	0. 20	6. 30	0. 41
	0. 32	6. 30	0. 45
Multiple-Source Grid	0. 08	4. 85	0. 159
	0. 20	4. 70	0. 056
	0. 32	4. 80	0. 026
(2)			
	0. 08	5. 70	0. 45
Single Source	0. 20	6. 25	0. 37
	0. 32	6. 20	0. 50
Multiple-Source Grid	0. 08	6. 20	≤0. 006
	0. 20	6. 10	≤0. 008
	0. 32	6. 20	≤0. 006

of less bactericidal chlorine residuals from the more bactericidal residuals initially formed. Thus, more rapid initial mixing results in better kills. It is important to note that very short contact times were involved in this experiment, from 5 to 19 sec. This means that if the above conclusion is true, the most bactericidal compounds must exist for only a very short time — certainly less than 5 sec and probably much less.

RAPID INITIAL MIXING AND LONG CONTACT TIMES

Because the experiments described above involved short contact times (<0.3 min) and because an attempt to improve performance in a prototype treatment plant by effecting improved initial mixing failed (see Appendix B), an experiment utilizing the venturi type initial mixing device used in the work of Selleck and Collins and longer contact times (up to 5.2 min) was devised. The initial mixing device was the 1/4-in. PVC tee described earlier.

The tubular reactor consisted of approximately 20 ft of 3/4-in. PVC pipe and approximately 250 ft of 1/2-in. rubber hose. This provided a contact time of 2.0 min. Samples to determine coliform kill were taken at four points along the tubular reactor. A small beaker was filled with chlorinated wastewater from the end of the tubular reactor in order to obtain a sample with a longer contact time, 5.2 min. The residence time of the tubular reactor, 2.0 min, was much greater than the time necessary to fill the beaker, 0.09 min. This minimized backmixing during the filling of the beaker. During the interval that the chlorinated wastewater was in the beaker, it was stirred continuously with a magnetic stirrer.

The data were analyzed by the methods discussed earlier, and the results are shown in Figure 2. The coliform survival ratio, y/y_o, is plotted against Rt where R is the total chlorine residual in mg/l and t is the contact time in minutes. Also shown are results cited above for the 2-in. tubular reactor and those from the work of Selleck [57].

For convenience, two of the initial mixing situations, the 75-gal batch reactor with the paddle mixer rotated at 50 rpm and the 2-in. tubular reactor with the single chlorine injection tube, have been designated as "poor." The other two initial mixing situations, the 1/4-in. tee in the 3/4-in. pipe and the 2-in. tubular reactor with the 13-orifice grid, have been designated as "good." This classification is strictly subjective. While the times of mixing for both "poor" or both "good" mixing situations is probably not the same, it is believed that they are probably sufficiently similar to allow the above classification to be made.

Figure 2 reveals that while rapid initial mixing provided improved performance, i.e., lower coliform survival ratios, at low values of Rt, the "poor" and "good" initial mixing produced the same results

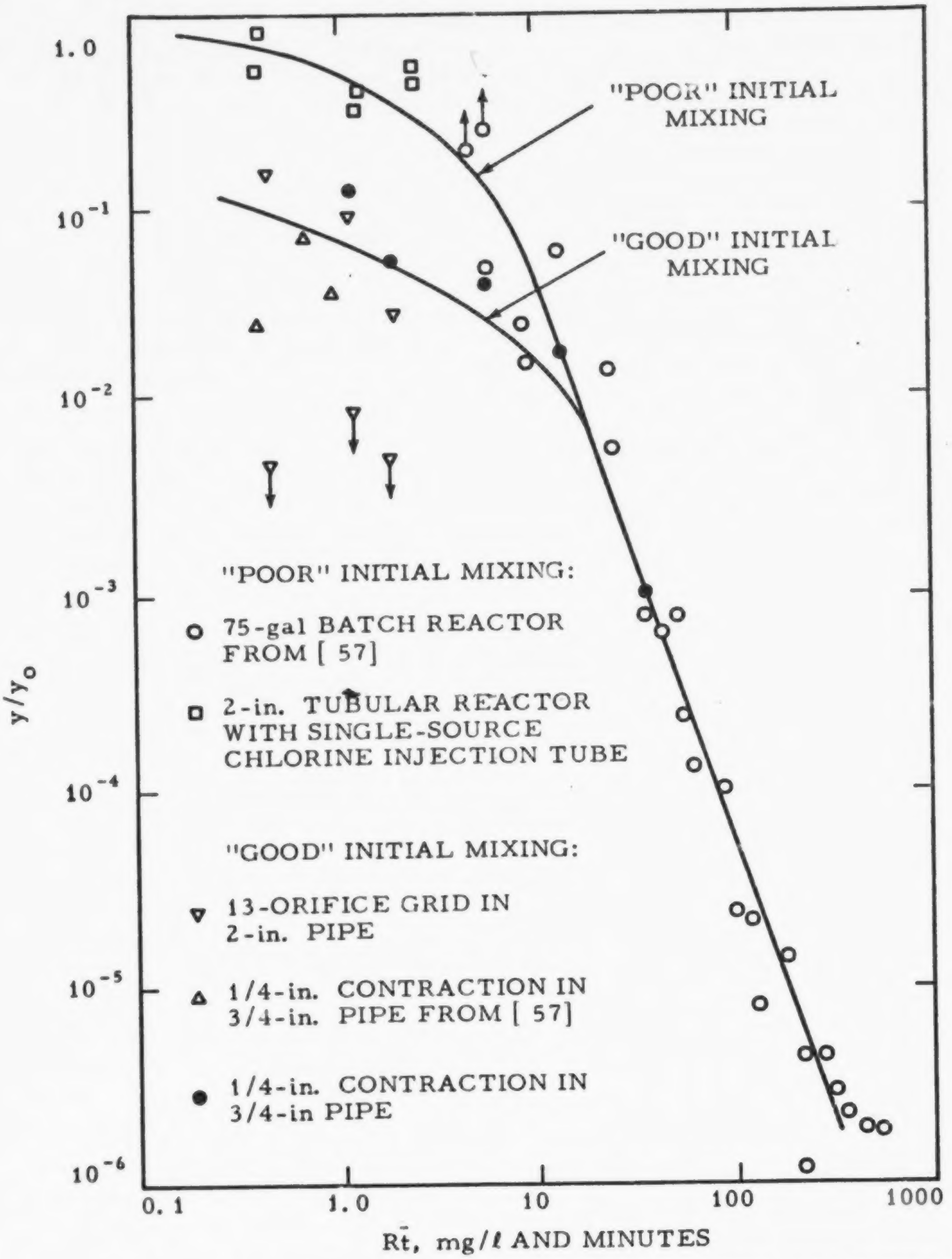

FIGURE 2. PERFORMANCE OF VARIOUS NON-BACKMIXED CHLORINATION UNITS

when $\bar{t}$ was increased with R maintained constant. Thus, in situations where a long pipeline is used to provide contact time for disinfection in wastewater treatment, any reasonably good initial mixing device will probably produce the best obtainable results, those of the batch reactor (see Appendix B).

The reason for the merging of the two curves at the higher values of Rt is unclear. It may be related to varying resistance of the organisms to disinfection. The more resistant organisms, if not killed by the highly bactericidal residuals which are initially formed and which can be utilized under conditions of rapid initial mixing, must be subjected to the same value of Rt as would have been the case if the initial mixing had been relatively slow. Whatever the actual reason, the answer seems to lie in the mechanism of chlorine disinfection and the reactions which chlorine undergoes in wastewater.

It may still be possible to utilize the high initial kill which rapid initial mixing provides. For example, existing plants which have backmixed reactors for chlorination could be improved by installing a chlorine injection device in the pipe, if one exists, leading to the chlorine contact unit. As noted, backmixing seems to be inherently detrimental to chlorination efficiency.

Use of tubular reactors also provides a much better residence time distribution than a CSTR. This is particularly important in chlorination because the coliform kill is so strongly time dependent. Use of a backmixed reactor allows "short-circuiting" of fluid particles with short chlorine contact times and thus a very high concentration of coliform organisms.

APPENDIX B

PLANT-SCALE STUDY OF THE EFFECT OF INITIAL MIXING IN WASTEWATER CHLORINATION

APPENDIX B

PLANT-SCALE STUDY OF THE EFFECT OF INITIAL MIXING IN WASTEWATER CHLORINATION

INTRODUCTION

Because of the success of the initial experiments involving rapid initial mixing and wastewater chlorination (see Table 3 of Appendix A) and also because of the recognized limitations of such small-scale studies, it was decided that a full-scale investigation at a wastewater treatment plant was called for. Although it should be possible to extrapolate the results of model mixing studies and estimate the degree of mixing produced by larger grids, it is difficult to assess the combined effects of mixing, chlorine reactions with impurities present in the waste, and probable coliform kills. With grids much larger than those used in the pilot-scale investigations (in terms of bar diameter and spacing), a much longer time of mixing — time required for the concentration fluctuations to decay to some arbritrarily defined low value — would result. Thus, the mixing might not occur fast enough to allow the most bactericidal chlorine residuals, which may be very short-lived, to act as killing agents. The short contact times involved in the pilot-scale studies also limited their usefulness and prevented their application to prototype systems.

Another reason for full-scale plant tests was that if improved initial mixing were to result in improved performance, the evidence indicating that initial mixing is an important parameter would be much more compelling than if only pilot-scale studies had been made. This would be the case even if the pilot-plant studies had no obvious limitations such as those discussed above.

CHARACTERISTICS OF THE RANCHO CORDOVA WASTEWATER TREATMENT PLANT

The Rancho Cordova Wastewater Treatment Plant is located approximately 15 miles east of Sacramento. It is a secondary plant featuring the Spirovortex activated sludge system. The average flow through the plant is approximately 1. 7 mgd (at the time of day that the tests described herein were run, the flow was approximately 2. 4 mgd).

The Rancho Cordova facility was chosen for the project for several reasons. It was desired that the initial mixing system of the plant be of good design by contemporary standards. It is well known that gross segregation of the chlorine from the waste stream over a period of a minute or longer will give poor results. An example of such gross segregation would be where the chlorine was added to the waste stream by placing the chlorine hose into a large contact basin where the level of turbulence was quite low. Gross segregation can occur and poor performance will result. Backmixing in the initial mixing step is also to be avoided. Selleck and Collins [55] and Selleck, Collins, and White [56] have noted that backmixing, such as may occur in a typical rapid or flash mixer, seems to have an inherently detrimental effect upon the wastewater chlorination process. The alternative to backmixing is a tubular reactor with characteristics as close to plug flow as possible. Thus, to test the grid mixer it was necessary to find a plant where the chlorine was added to the waste stream in a pipe leading from the treatment plant, the pipe comprising the tubular reactor. Such an arrangement was desired for another reason. Samples of chlorinated wastewater must be taken to determine coliform kill and the corresponding contact times should be determined fairly accurately. This is possible in a pipe, but not in most chlorine contact basins where short-circuiting occurs and dead space exists.

The Rancho Cordova plant met these criteria quite well. From the final clarifier, the effluent entered a large box structure by passing over a weir. From there it passed through an 800-ft, 27-in. diameter pipe to a pond. The chlorine injection device was a 6-ft long, 3-in. PVC pipe placed in the bottom of the 27-in. pipe at the point where the flow left the box. The chlorine was injected through 3/8-in. holes, spaced 1-1/4-in. apart along the top of the PVC pipe. It was possible to sample at the point where the 27-in. line entered the pond as it was not submerged. It was also possible to sample at a point 184 ft downstream from the chlorinator.

There were three other criteria for the plant to be used. These concerned installation of the grid. First, it was necessary to be able to tap into the existing chlorine piping system in order to deliver the chlorine solution to the grid. This was fairly easily done at Rancho Cordova. Second, it was necessary to be able to gain access to the point where the grid was to be installed by diverting the flow around this point or stopping the flow. At Rancho Cordova the flow could be stopped for about one hour which allowed rapid installation and removal of the grid. Finally, it was necessary to have a physical configuration such that placing the grid in the pipe could be easily accomplished. This was possible at Rancho Cordova.

After permission was obtained from the County of Sacramento to use the Rancho Cordova plant, the grid was designed and built, and the tests were run.

DESIGN OF THE GRID

The grid used as the initial mixing device in this experiment was designed on the basis of several criteria. First, and most important, it had to provide more rapid mixing of the chlorine solution with the waste stream than did the system which was being used at the treatment plant. This required that the grid bars be as small in outside diameter as possible, that the spacing of the grid bars be small, and that the number of points at which the chlorine was injected into the waste stream be as many as possible.

Other criteria, however, led to design features different from those above. Since at many plants, excessive headloss through the grid could not be tolerated — although at this plant, a headloss of up to 2 ft could have been allowed — the grid bars could not be spaced too closely. Excessive headloss of the chlorine solution flowing inside the grid bars could not be allowed as this would lead to an unequal distribution of chlorine flowing from each of the sources. This made larger diameter grid bars necessary. In order to avoid the possibility of clogging very small orifices, larger orifices were preferable although this meant fewer holes if a reasonably high injection velocity was to be maintained. A high injection velocity was necessary to decrease the effect of chlorine solution headloss inside the grid bars and thus insure uniform chlorine distribution. Finally, the grid had to be reasonably strong to withstand the force of the wastewater flow. This, too, called for larger grid bars. In order to have a grid meeting these criteria it was necessary to sacrifice mixing performance.

A drawing of the grid mixer is shown in Figure 1. Photographs are shown in Figure 2. The grid was constructed from 3/4-in. PVC pipe and fittings. The ratio of the center-to-center bar spacing to the bar diameter, a parameter used in mixing studies, was approximately 3.5, and the solidity, the fraction of the cross-sectional area occupied by the grid, was about 0.48. The main line in the center of the grid was a 2-in. PVC pipe. This allowed the chlorine solution to be distributed evenly to all parts of the grid without excessive headloss. The chlorine injection orifices, were 220 1/8-in. diameter holes on the downstream side of the grid. These did not point directly downstream, but alternated up or down at an angle of approximately 45° from the horizontal. It was believed that this arrangement would improve mixing. The value of n_s was 0.39 in.^{-2}

Based upon a chlorine solution flow rate of 20 gpm, the velocity at which the chlorine was injected into the wastewater stream was 2.4 fps. The existing chlorine diffuser injected the chlorine into the waste stream at approximately 1 fps.

The maximum velocity of the effluent flowing through the grid was approximately 2 fps. From previous studies, the headloss through such a grid at this velocity was approximately 0.8 in. and the total force on the grid was 16 lb. At a velocity of 1 fps, the velocity when the tests were being made, the headloss and force were 0.2 in. and 4 lb, respectively.

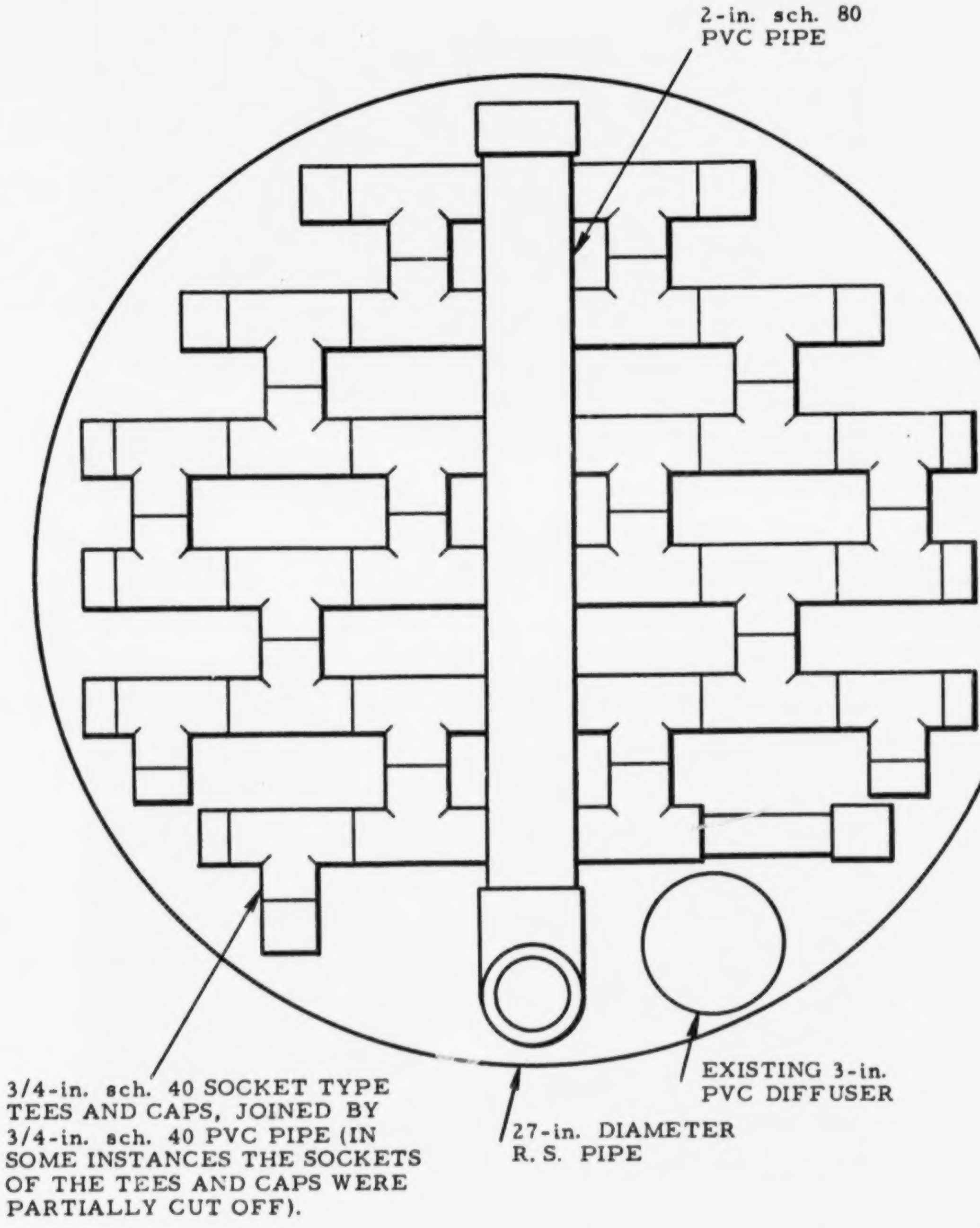
2-in. sch. 80 PVC PIPE
3/4-in. sch. 40 SOCKET TYPE TEES AND CAPS, JOINED BY 3/4-in. sch. 40 PVC PIPE (IN SOME INSTANCES THE SOCKETS OF THE TEES AND CAPS WERE PARTIALLY CUT OFF).
27-in. DIAMETER R. S. PIPE
EXISTING 3-in. PVC DIFFUSER

FIGURE 1. PVC CHLORINATION GRID

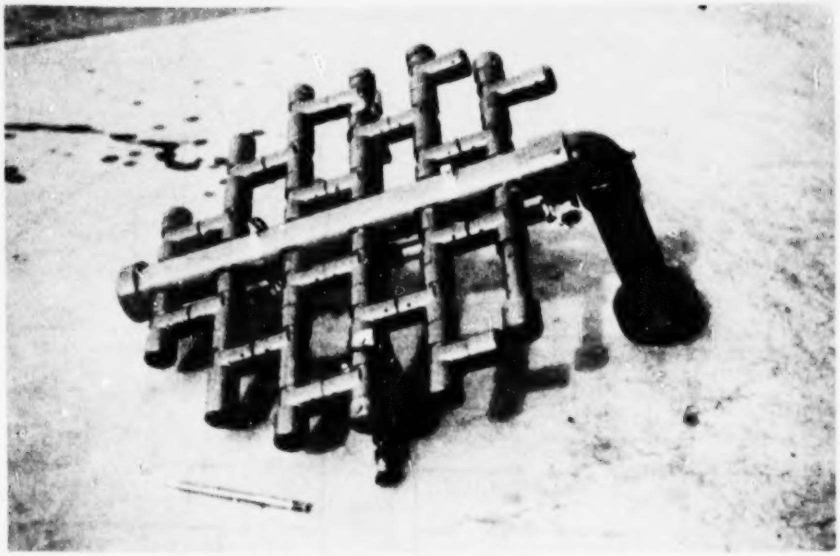

A. FRONT VIEW OF GRID

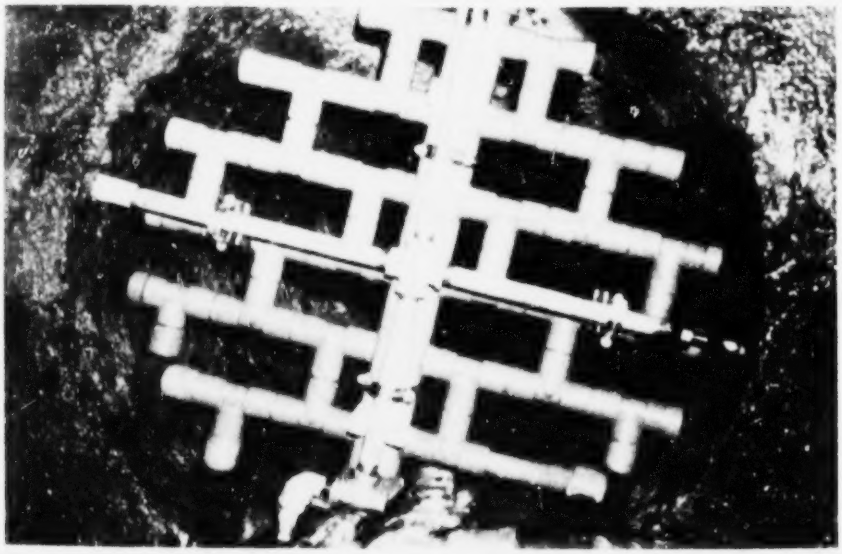

B. GRID IN PLACE IN 27-in. TUBULAR REACTOR

FIGURE 2. MULTIPLE-ORIFICE GRID USED AS INITIAL MIXING DEVICE

The grid was connected to a frame constructed from 1/2-in. iron pipe and fittings. The frame was used to fix the grid in place inside the 27-in. pipe. Jacks mounted on the frame could be extended until the grid and frame were firmly held in place. The advantage in using friction to keep the grid in place was that no permanent brackets had to be installed in the plant, and installation and removal of the grid was quickly and simply accomplished.

EXPERIMENTAL PROCEDURE

A schematic drawing of the chlorination system at the Rancho Cordova Wastewater Treatment Plant is shown in Figure 3. Two runs, one with the grid mixer and one with the pipe diffuser, were made each day for four consecutive days. When the pipe diffuser was being tested the grid was removed to insure that the grid would not interfere or contribute in any way to the turbulence characteristics of the existing arrangement.

The runs were made in the following manner. Each day the first run was made with whichever device had been used last the day before. This meant that it was necessary to stop the flow, de-water the box, and remove or install the grid only once each day. When the flow from the secondary clarifier reached a nearly constant rate, at approximately 1000 hours each day, the chlorine gas flow rate was set to obtain the desired total chlorine residual at the second sampling point. Residuals were measured amperometrically according to the method given by Standard Methods [62]. The residual was varied during the study from approximately 1 to 6 mg/ℓ. When the desired residual was obtained, samples were taken to determine the fraction of coliforms killed. For each determination of coliform concentration, four replicate samples were collected. Samples were taken first in the box upstream from the chlorine injection device to determine the initial coliform concentration, then from sampling point 2, and finally from sampling point 1. Samples for the determination of chlorine residuals were taken. The coliform samples were dechlorinated as quickly as possible with 0.5 mℓ of a 10% solution of sodium thiosulfate. The bacteriological analyses were performed by the Sanitation and Radiation Laboratory, California State Department of Public Health in a mobile laboratory located at the plant site. All bacteriological determinations were made on the basis of four dilutions, using five tubes for each dilution, and following the procedure outlined in Standard Methods.

After samples were taken with the first device, the flow was stopped, the box was de-watered with two gasoline powered pumps provided by Sacramento County, the grid was installed or removed, and the flow was started again. When the flow rate became constant, the sampling procedure was repeated using the other initial mixing device.

Each day a 6-hr composite sample of the unchlorinated secondary effluent was collected. This sample was kept under refrigeration and

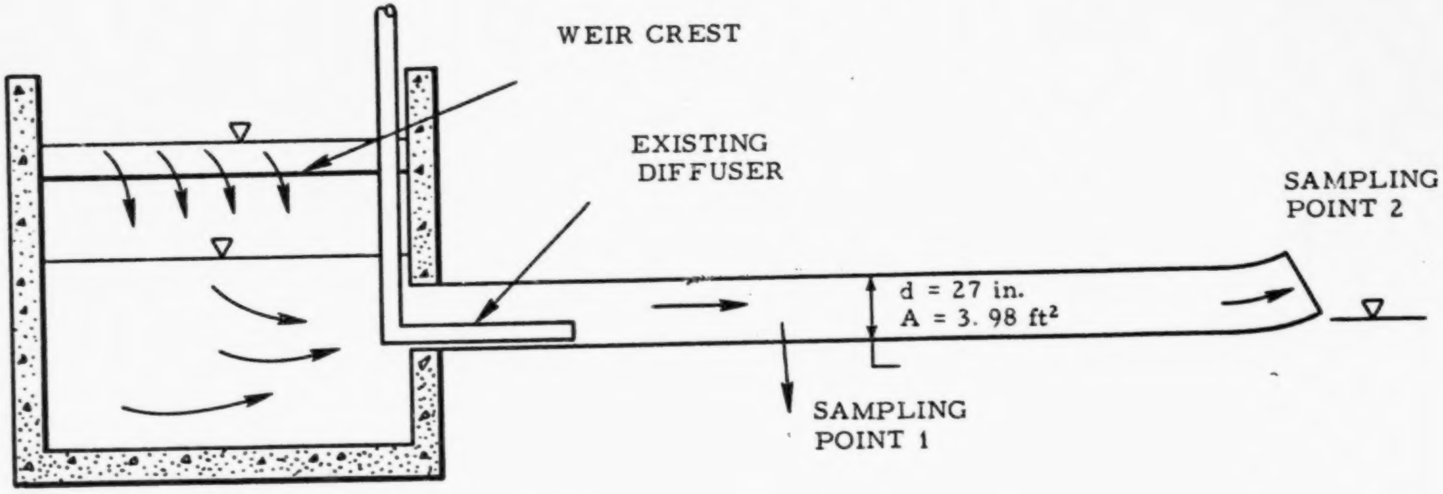
WEIR CREST
EXISTING DIFFUSER
SAMPLING POINT 2
d = 27 in.
A = 3. 98 ft²
SAMPLING POINT 1

FLOW = 2. 2 to 2. 5 mgd ≈ 3. 65 cfs

VELOCITY = 3. 65/3. 98 = 0. 92 fps

PIPE LENGTH = 184 ft to sampling point 1. $\overline{t_1} = \frac{184}{0.92 \times 60} = 3.3$ min

PIPE LENGTH = 622 ft between points 1 and 2. $\overline{t_2} = \frac{622}{0.92 \times 60} = 11.3$ min

$\overline{t}_{Tot.} = \overline{t_1} + \overline{t_2} = 14.6$ min

FIGURE 3. SCHEMATIC DRAWING OF RANCHO CORDOVA CHLORINATION SYSTEM

transported at the end of the day to the Sanitary Engineering Research Laboratory at the Richmond Field Station of the University of California. Determinations were made of the ammonia nitrogen, organic nitrogen, COD, volatile suspended solids, and total suspended solids. The analytical procedures used were those recommended by Standard Methods.

RESULTS

The physical and chemical analyses of the unchlorinated secondary effluent are shown in Table 1. The coliform and fecal coliform survival ratios and the operating parameters are summarized in Table 2. Each bacterial density shown (MPN per 100 mℓ) representes the log mean of four replicate samples

TABLE 1

ANALYSES OF UNCHLORINATED SECONDARY EFFLUENT

Run	NH_3-N mg/ℓ	Org-N mg/ℓ	SS mg/ℓ	VSS mg/ℓ	COD mg/ℓ	Temp °C	pH	
							Unchlor.	Chlor.
1	12.3	3.1	9.0	8.0	54	--	--	--
2	10.8	3.8	4.0	0.0	51	17.0	7.4	7.1
3	13.0	2.8	3.0	0.0	57	18.0	7.4	7.0
4	12.5	3.0	6.0	0.0	46	17.5	7.4	7.1

The results are plotted in Figures 4 and 5. The coliform (Figure 4) and fecal coliform (Figure 5) survival ratios are plotted against Rt, the total chlorine residual in mg/ℓ times the contact time in minutes. These figures show that the multiple-source grid did not improve process performance as was expected. Possible reasons for this are discussed in the next section. A positive result of the experiment is the fact that the slope of the lines in Figures 4 and 5 can be taken as minus 3 on log-log paper. This is the same decay rate that Selleck [57] found for non-backmixed reactors using a primary effluent.

TABLE 2

OPERATING PARAMETERS AND BACTERIAL SURVIVAL RATIOS

Run	Initial Mixing Device	Calc. Contact Time	Flow	Chlorine Residual	Coliform Bacteria MPN/100 mℓ y & y_o	y/y_o	Fecal Coliform Bacteria MPN/100 mℓ n & n_o	n/n_o	Chlorine Residual x Time (Rt)	Chlorine Dosage
		min	mgd	mg/ℓ					mg/ℓ-min	mg/ℓ
1	Grid	0	2.3	0	1.6×10^6	1.0	2.5×10^5	1.0	0	0
		3.2	2.3	3.65	$\leq 4.7 \times 10^3$	$\leq 2.9 \times 10^{-3}$	$\leq 2.0 \times 10^3$	$\leq 8 \times 10^{-3}$	11.7	7.8
		13.9	2.3	3.55	3.0×10^2	1.9×10^{-4}	$\leq 2.0 \times 10^2$	$\leq 8 \times 10^{-4}$	49.4	7.8
	Diffuser	0	2.2	0	1.1×10^6	1.0	$\leq 2.38 \times 10^5$	1.0	0	0
		3.3	2.2	4.2	-	-	-	-	13.9	8.1
		14.5	2.2	4.0	$\leq 4.0 \times 10^2$	$\leq 3.6 \times 10^{-4}$	-	-	58	8.1
2	Grid	0	2.4	0	7.05×10^5	1.0	2.64×10^5	1.0	0	0
		3.0	2.4	4.7	7.3×10^2	1.04×10^{-3}	$\leq 2.0 \times 10^2$	$\leq 7.6 \times 10^{-4}$	12	9.5
		13.3	2.4	4.55	1.2×10^2	1.66×10^{-4}	≤ 25	$\leq 9.5 \times 10^{-5}$	60.5	9.5
	Diffuser	0	2.45	0	1.17×10^6	1.0	2.86×10^5	1.0	0	0
		2.98	2.45	5.05	2.45×10^3	2.1×10^{-3}	$< 2.38 \times 10^2$	$< 8.3 \times 10^{-4}$	15	9.3
		13	2.45	5.05	1.25×10^2	1.07×10^{-4}	≤ 25	$< 8.7 \times 10^{-5}$	65.7	9.3
3	Grid	0	2.55	0	1.3×10^6	1.0	4.5×10^5	1.0	0	0
		2.9	2.55	5.55	1.04×10^3	8.0×10^{-4}	20	4.4×10^{-5}	15.9	10.8
		12.5	2.55	5.70	1.6×10^2	1.23×10^{-4}	≤ 20	$\leq 4.4 \times 10^{-5}$	71.3	10.8
	Diffuser	0	2.5	0	2.64×10^6	1.0	4.5×10^5	1.0	0	0
		3.0	2.45	5.90	1.02×10^3	3.9×10^{-4}	≤ 32	$\leq 7.0 \times 10^{-5}$	17.6	11.2
		12.8	2.5	5.75	4.09×10^2	1.5×10^{-4}	≤ 20	$\leq 4.4 \times 10^{-5}$	73.5	11.0
4	Grid	0	2.6	0	2.01×10^6	1.0	3.06×10^5	1.0	0	0
		2.8	2.6	1.60	5.28×10^5	2.62×10^{-1}	5.67×10^4	1.85×10^{-1}	4.5	4.6
		12.8	2.5	1.80	3.34×10^4	1.66×10^{-2}	$\leq 4.45 \times 10^2$	$\leq 1.45 \times 10^{-3}$	23	4.8
	Diffuser	0	2.4	0	2.6×10^6	1.0	8.58×10^5	1.0	0	0
		3.0	2.4	2.5	3.41×10^5	1.33×10^{-1}	3.84×10^4	4.5×10^{-2}	7.5	5.0
		13.3	2.4	1.85	7.7×10^3	2.96×10^{-3}	$\leq 2.0 \times 10^2$	$< 2.33 \times 10^{-4}$	24.6	5.0

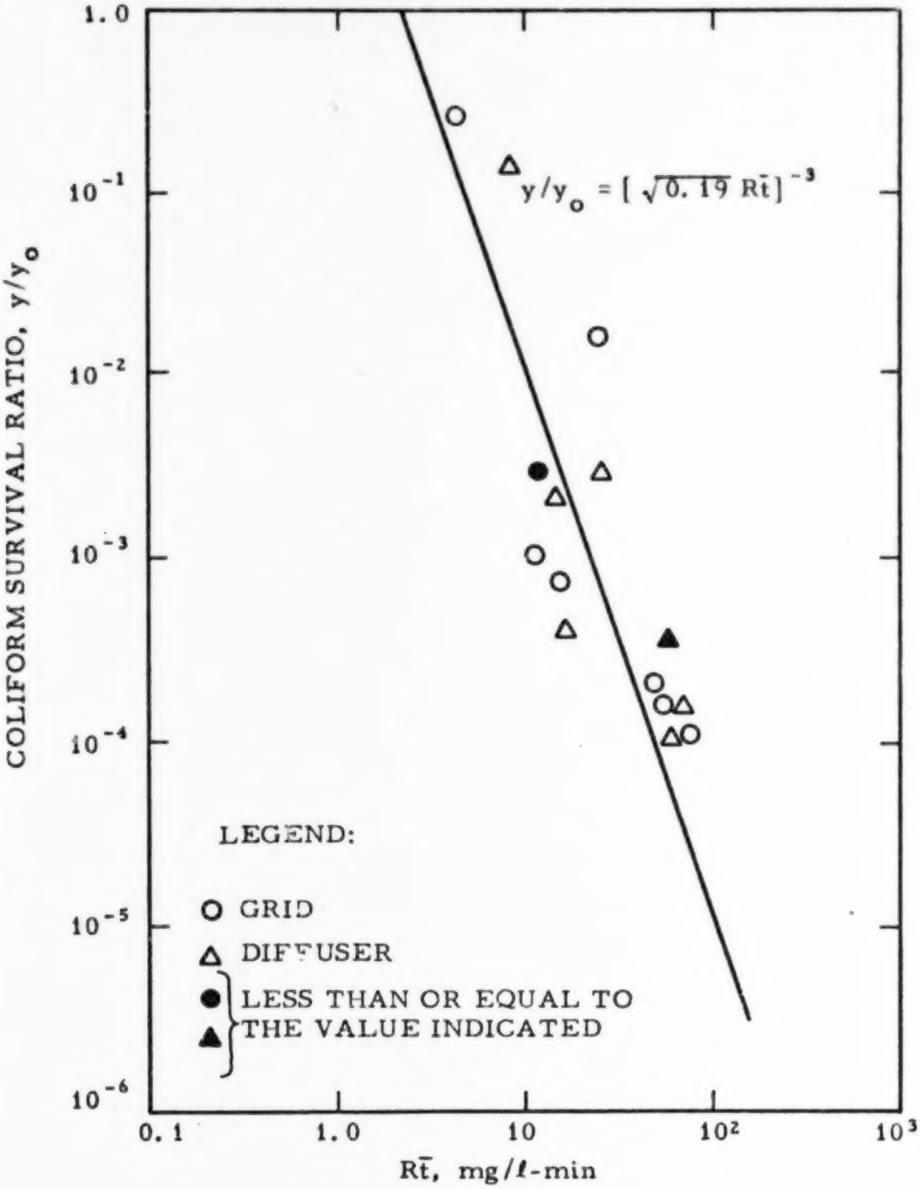

FIGURE 4. COLIFORM SURVIVAL RATIO IN AN ACTIVATED SLUDGE EFFLUENT – EFFECT OF INITIAL MIXING

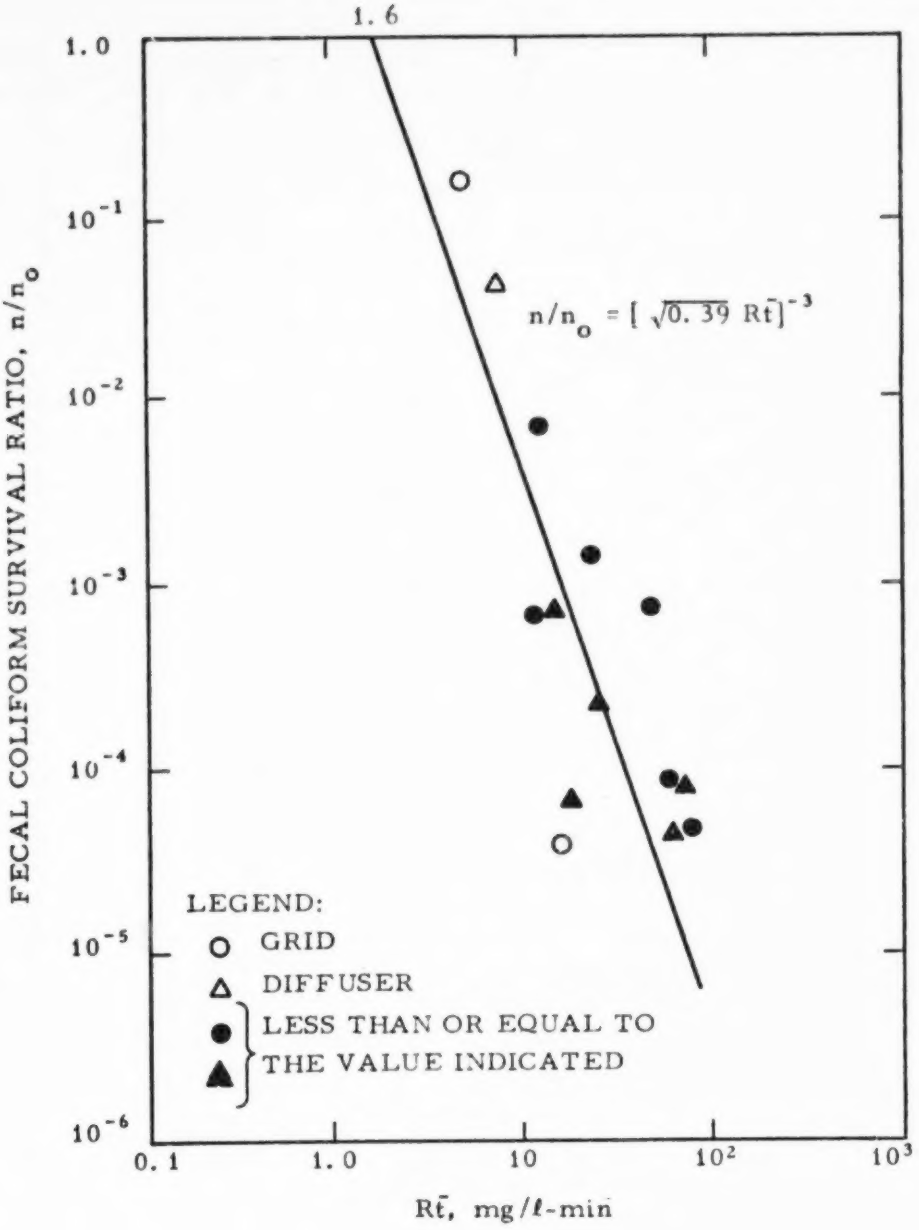

FIGURE 5. FECAL COLIFORM SURVIVAL RATIO IN A CHLORINATED ACTIVATED SLUDGE EFFLUENT – EFFECT OF INITIAL MIXING

CONCLUSIONS

The results of this field experiment, coupled with the previous and subsequent pilot-scale experiments, have led to the conclusions discussed in Appendix A. Specifically, while different rates of initial mixing in a non-backmixed reactor may initially produce different levels of disinfection, at sufficiently long contact times — similar to those found in practice — the results from the various times of initial mixing are the same.

These experiments have shown, however, that while the coliform survival ratio in the effluent of a tubular reactor cannot, in practice, be improved as it had been hoped, it has been found that a tubular reactor is superior to a backmixed reactor for two reasons. First, as noted by Selleck, Collins, and White [56], backmixing apparently results in a chlorine residual with poorer bactericidal effectiveness because of reaction of the chlorine entering the reactor with residuals previously formed. Second, short-circuiting, or the presence in the effluent from the reactor of fluid particles with a very short chlorine contact time, can greatly affect overall performance. A tubular reactor prevents this.

APPENDIX C

COMPARISON OF RESULTS WITH THOSE OF GIBSON

Preceding page blank

APPENDIX C

COMPARISON OF RESULTS WITH THOSE OF GIBSON [11, 26]

Gibson used a square-mesh biplane grid with 1/8-in. grid bars and tracer orifices placed halfway between the grid bar intersections on the upstream side of the bars. This configuration is very similar to that used for one run of this study (see Figure 28, Section VI.) The grid bar diameters were essentially the same and upstream injection was used in both instances. The scalar decay rate should therefore be the same. The values of n_s and $\bar{A}$ were different for the two experiments, but it should be possible to relate the results through use of the mixing model developed in Section VI. NaCl solution was used as the tracer in both studies. A more complete comparison of the parameters of the two experiments is given in Table 1.

The results of the two experiments are shown in Figure 1, with $(a'n_s)/(\bar{A}\alpha'')$ plotted against x/d. Within the accuracy of the measurements, the points for both experiments can be said to fall along the same line. The value of α'' and a for this line are 50-in.$^{-2}$ and 0.86, respectively. In his determination of the scalar decay rate, Gibson obtained a value of a = 0.69. If Gibson's data points were considered separately, a value of α'' much lower than the given value of 50 would result. This, as noted previously, is the result of α'' being very sensitive to slight changes in the slope of the line drawn through the data points.

The fact that the results of the two studies agree to a reasonable extent is important for two reasons. First, it seems to indicate that the probe used in the present study was not excessively large and that a reasonable approximation of the "true" rms values was obtained. It should be noted that the results of both studies may be low; Gibson's because of an inability to measure low wave number components of the spectrum, and those of the present work because of the large probe diameter.

Agreement between the two experiments also serves to further confirm the usefulness of the mixing model developed in Section VI. It was concluded that for a given grid bar diameter and tracer injection system, the results should follow the equation

$$\frac{a'M_s}{\bar{A}} = \alpha''\left(\frac{x}{d}\right)^{-a} \qquad (97)$$

TABLE 1

PARAMETERS FOR MIXING EXPERIMENTS

	Present Study	Gibson
M, in.	0.500	0.625
d, in.	0.125	0.117
M/d	4.0	5.33
Solidity	0.45	0.34
Tracer Source Diameter, d_n, in.	0.0135	0.012
Reactor Cross-Section, in.^{2}	3.14	36.0
Tracer Source Density, M_s, in.$^{-2}$	7.9	5.0
N_{Re_d}	850, 1700, 2550	1,910
A_T, mg/ℓ	50,000	58,000
$\overline{A}$, mg/ℓ	47.5	16.6
Probe Diameter, d_o, microns	75	*
Tracer Injection System	**	**

[*] Not listed. Probe size varied from 10 to 50 microns in Gibson's experiments.

[**] Tracer injected upstream through sources in grid bars placed halfway between bar intersections.

where α'' and a are constants. In Section VI the results of several experiments were compared. In all instances downstream injection was used. Now, reasonable agreement has been found for two experiments which were made in independent studies.

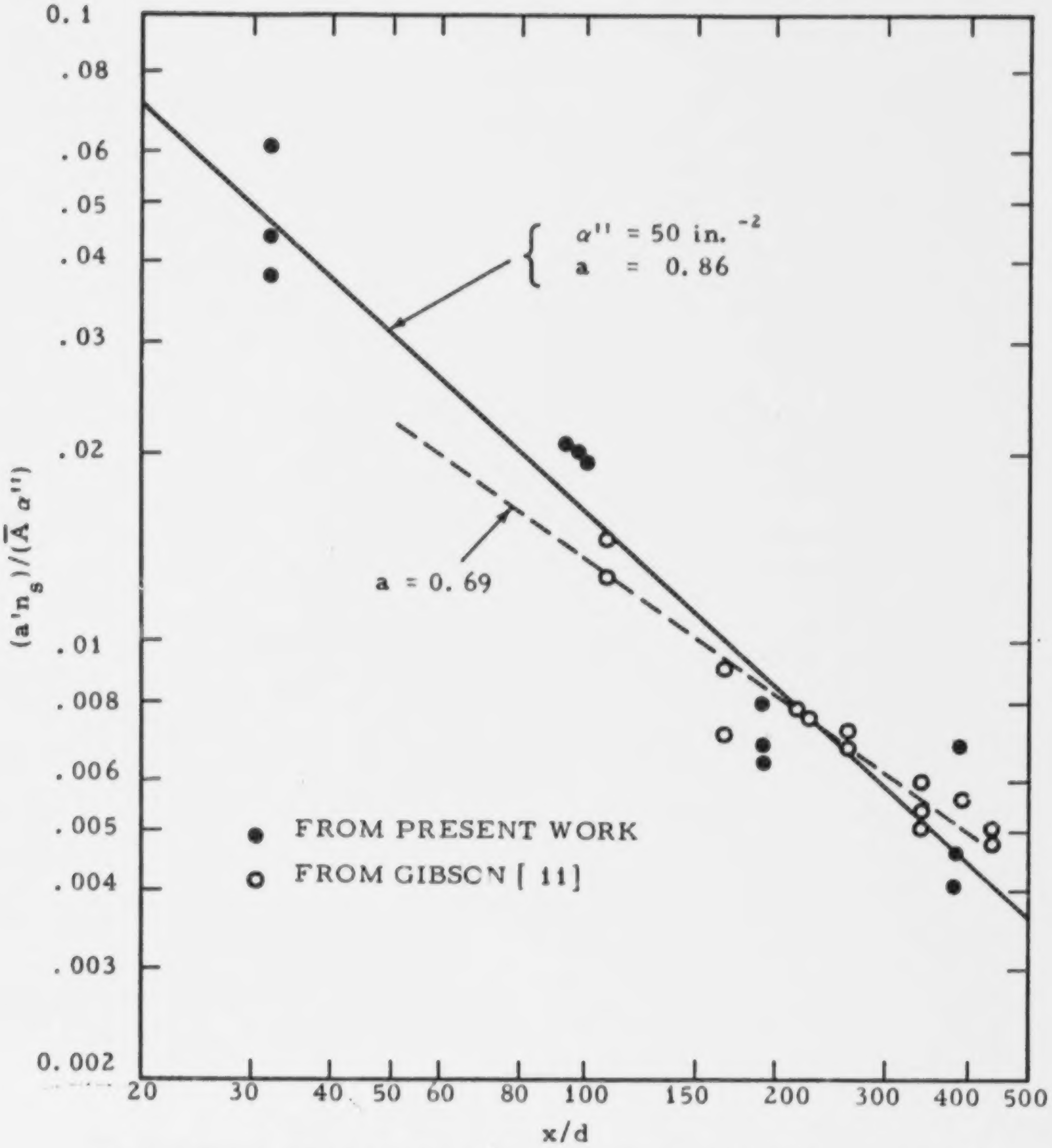

FIGURE 1. SCALAR DECAY DOWNSTREAM FROM A GRID: COMPARISON OF RESULTS FROM PRESENT STUDY WITH RESULTS FROM GIBSON'S STUDY

APPENDIX D

PREDICTION OF MIXING FOR LARGER GRIDS

APPENDIX D

PREDICTION OF MIXING FOR LARGER GRIDS

Although a completely satisfactory method of predicting the time of mixing which can be expected from larger grids has not been developed, it is possible to use the results of the present mixing studies and Corrsin's theory to estimate what the scalar decay curve will be for such grids. Corrsin's equation is

$$\frac{u_1'}{a'}\frac{da'}{du_1'} = \left[\frac{2 + N_{Sc}^{\ -1}}{3(\frac{3}{2})^{2/3}\ (\frac{L_s}{L_f})^{2/3} + 2(\frac{5}{3})^{3/2}\ \frac{\log N_{Sc}}{N_{Re_\lambda}}}\right] . \qquad (54)$$

Assuming Batchelor's turbulence decay law holds ($u' \alpha x^{-1}$), the right-hand side of the above equation is equal to a, the scalar decay rate. N_{Sc} = 700 for sodium chloride, and N_{Re_λ} = 45, the average value for the present work. Putting in these values, Equation (54) becomes

$$a = \frac{2}{3.96\,(\frac{L_s}{L_f})^{2/3} + 0.63} .$$

As mentioned in Section VI, L_s depends on the method of tracer injection (e.g., either upstream or downstream) and L_f is proportional to the grid bar diameter. If it is assumed that L_s/L_f does not vary as the mixing progresses, it is possible to obtain a value of L_s/L_f for an experimentally determined scalar decay curve. With this known, the value of L_s/L_f for larger grids can be estimated and a scalar decay rate can be calculated.

The result of such calculations are shown in Figure 1. The experimental curves for d = 1/4 in. and d = 1/8 in. were taken from Figure 31. From the experimental curve for d = 1/4 in., scalar decay curves were predicted for d = 1/8, 1/2, and 1 in.

For d = 1/8 in. the experimental value of a was 0.4. The predicted value is 0.54. Because of the extensive scatter, a line with a = 0.54 would fit the data almost as well as the line which was used in Figure 31. However, the assumption that α'' is constant places the predicted curve somewhat lower than the experimental curve. A similar calculation using $u' \alpha x^{-5/7}$ as proposed by Frenkiel gave slightly poorer agreement.

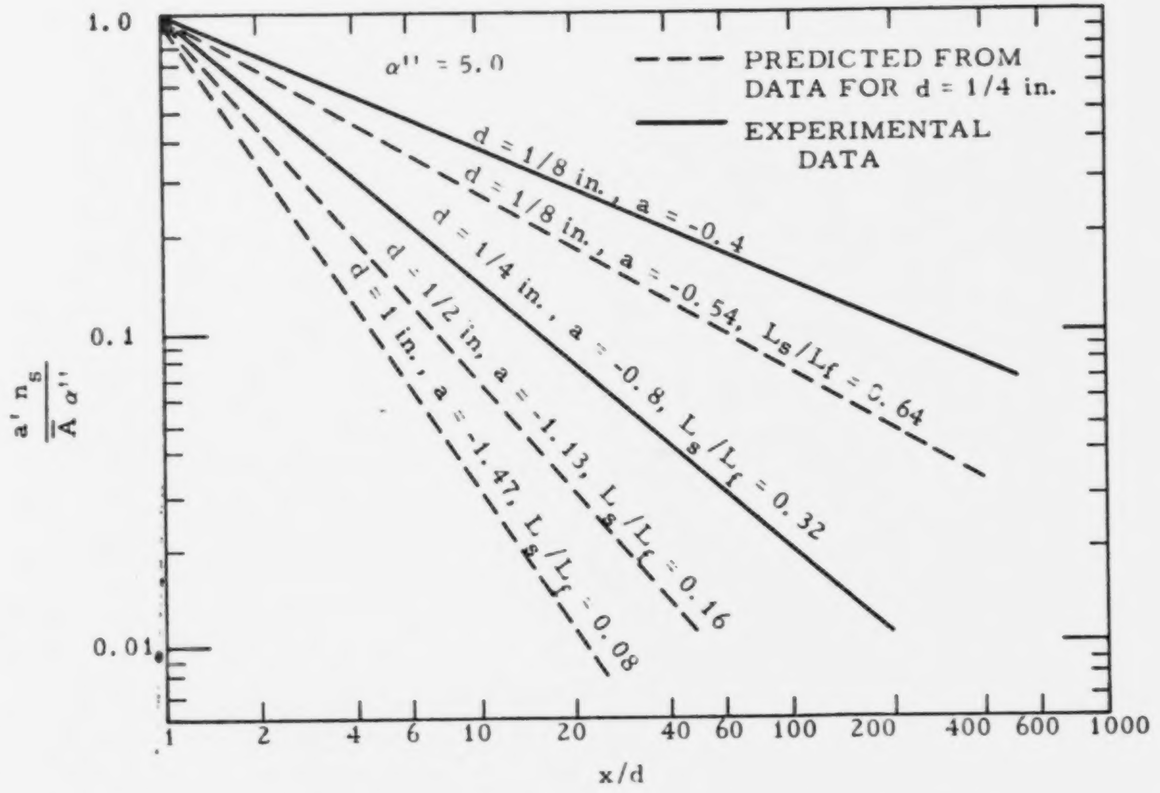

FIGURE 1. PREDICTION OF SCALAR DECAY CURVES FROM EXPERIMENTAL DATA FOR d = 1/4 in.

As no tests were done with grid bars 1/2 or 1 in. in diameter, it is impossible to know how accurate the predicted curves are. However, this graph may be used to estimate the time of mixing to be expected from prototype grids.

SECTION X

GLOSSARY

Symbol	Definition
A	"Point" tracer concentration, mg/ℓ; coefficient in Equation (31); coefficient in Equation (44); reactant in Equation (63); cross-sectional area of conducting medium.
A_1	Coefficient in Equation (30)
$\bar{A}$	Mean component of "point" tracer concentration, mg/ℓ
A_p	Average concentration of tracer mixed with portion of flow during wake-mixing
a	Fluctuating component of "point" tracer concentration, scalar decay rate
a'	rms concentration fluctuation, mg/ℓ
a'_o	Initial rms concentration fluctuation, mg/ℓ
a'_1	Initial rms concentration fluctuation of isotropic scalar field, mg/ℓ
B	Distance from spherical probe which represents volume within which 90% of the total resistance exists, coefficient in Equation (42), reactant in Equation (63)
C	Coefficient in Equation (32), coefficient in Equation (46), Reaction product in Equation (63)
C_D	Drag coefficient
c	Coefficient in Equation (34)
$C(r)$	Scalar correlation function
D_i	Diffusion coefficient of i-fold particles
D_{ij}	Combined diffusion coefficient of i-fold and j-fold particles
D_m	Molecular diffusivity, ft^2/sec

Symbol	Definition
d	Grid bar diameter, in.
d_o	Probe diameter, microns
E	Three-dimensional energy spectrum function, voltage
E_1	One-dimensional energy spectrum function
E_e	Universal three-dimensional energy spectrum function
E_{1e}	Universal one-dimensional energy spectrum function
E_s	Scalar spectrum function
F	Fractional completion of reaction
$f(r)$	Longitudinal correlation function
G	rms velocity gradient, sec^{-1}
g	Acceleration due to gravity, ft/sec^2
$g(r)$	Lateral correlation function
$g(x)$	Function defined by Equation (66)
H_{ij}	Collision frequency of i-fold and j-fold particles in turbulent flow
h_L	Head loss through grid, in.
I_{ij}	Collision frequency of i-fold and j-fold particles due to Brownian motion
I_s	Intensity of segregation
J_{ij}	Collision frequency of i-fold and j-fold particles due to laminar flow
K_A	Aggregation rate coefficient
K_B	Breakup rate coefficient

Symbol	Definition
K_c	Conductivity cell constant
K_L	Head loss coefficient for grid
K_p	Cross-sectional area near each orifice with which the tracer is mixed during wake-mixing
K_w	Coefficient in Equation (92)
k	Wave number, ft^{-1}
k_1	One-dimensional wave number, ft^{-1}
k_B	Batchelor wave number ($k_B = (\varepsilon/\nu D_m^2)^{1/4}$)
k_K	Kolmogoroff wave number($k_K = (\varepsilon/\nu^3)^{1/4}$)
L	Distance between two electrodes of a conductivity probe, in.
L_f	Longitudinal integral scale
L_g	Lateral integral scale
L_s	Scalar integral scale
M	Center-to-center spacing of grid bars, in.
MPN	Most probable number of coliform organisms per 100 mℓ
N	Paddle rotation speed in flocculator, rpm
N_{Re_λ}	Microscale Reynolds number ($N_{Re_\lambda} = u' \lambda_g/\nu$)
N_{Re_d}	Grid bar Reynolds number ($N_{Re_d} = V_M d/\nu$)
N_{Sc}	Schmidt number ($N_{Sc} = \nu/D_m$)
n	Frequency of fluctuations, sec^{-1}
n_1	Number concentration of primary particles
n_i	Number concentration of i-fold particles

Symbol	Definition
n_1^o	Number concentration of primary particles entering flocculator
n_1^m	Number concentration of primary particles in mth compartment of flocculator
P	Power input to flocculator
Q	Flow through flocculator, gpm
Q_M	Mainstream flow rate through tubular reactor, gpm
Q_p	Flow with which tracer is mixed during wake-mixing
Q_T	Tracer injection flow rate, gph
R	Resistance, ohms; chlorine residual, mg/ℓ
R_∞	Resistance measured by a spherical electrode in an infinite conducting medium, ohms
R_p	Resistance measured by probe, ohms
R'	Resistance in parallel with probe, ohms
R_T	$R'R_p/(R' + R_p)$, ohms
R_i	Radius of i-fold particles
R_{ij}	Combined radius of i-fold and j-fold particles
r_o	Radius of single electrode conductivity probe, microns
$\vec{r}$	A vector
S	Grid solidity, i.e., fraction of tubular reactor cross-section covered by grid bars, dimensionless
T	Flocculation chamber residence time, min
T_m	Flocculation chamber residence time per compartment, min
t	Time
$\bar{t}$	Mean chlorine contact time, min

Symbol	Definition
U_i	Instantaneous velocity in i^{th} direction in Cartesian coordinates, fps ($i = 1, 2, 3$)
$\bar{U}_i$	Mean velocity in i^{th} direction, fps ($i = 1, 2, 3$)
$\frac{dU}{dZ}$	Velocity gradient, sec^{-1}
u_i	Fluctuating component of velocity in i^{th} direction ($i = 1, 2, 3$)
u', u'_i	rms velocity fluctuation in isotropic turbulence, fps
V_M	Mainstream velocity in tubular reactor, fps
V, V_r	Reactor volume, ft^3
v	Kolmogoroff characteristic velocity ($v = (\nu \varepsilon)^{1/4}$)
x	Distance downstream from grid, in.
x_o	Apparent origin of rms velocity fluctuations, in.
x_i	Cartesian component of coordinate ($i = 1, 2, 3$)
$\vec{x}$	A vector
y	Most probable number of coliform organisms per 100 mℓ after disinfection
y_o	Most probable number of coliform organisms per 100 mℓ before disinfection
Z	Impedance, ohms
α	Coefficient in Equations (45a) and (86)
α_1	Coefficient in Equation (45)
α'	Coefficient in Equation (89)
α''	Wake-mixing coefficient in general mixing model, Equation (97)
β	Ratio of amount of reactant present to the stoichiometric amount

Symbol	Definition
ε	Rate of energy dissipation
ε_s	Rate of scalar "dissipation"
η	Degree of mixing, Kolmogoroff characteristic length scale
λ_f	Longitudinal microscale
λ_g	Lateral microscale
λ_s	Scalar microscale
μ	Viscosity lb-sec/ft^2
ν	Kinematic viscosity, ft^2/sec
ξ	Voltage
ρ	Resistivity, ohm-ft
σ	Conductivity, mhos/ft

SECTION XI

REFERENCES

1. Rich, L. G. Unit Operations of Sanitary Engineering, New York: John Wiley and Sons, 1961.

2. Hinze, J. O. Turbulence. New York: McGraw-Hill, 1959.

3. Lee, John. "Turbulent Motion and Mixing," Ph. D. thesis in Chemical Eng., Ohio State Univ., 1962.

4. Brodkey, R. S. "Fluid Motion and Mixing," Ch. 2 in Mixing — Theory and Practice, Vol. I, by V. W. Uhl and J. B. Gray. New York and London: Academic Press, 1966.

5. Batchelor, G. K. The Theory of Homogeneous Turbulence. New York: Cambridge Univ. Press, 1953.

6. Taylor, G. I. "Statistical Theory of Turbulence," Parts I-IV, Proc. Roy. Soc., A151:421, 1935.

7. __________. "The Spectrum of Turbulence," Proc. Roy. Soc., A164:15, 1938.

8. Kolmogoroff, A. N. "The Local Structure of Turbulence in Incompressible Viscous Fluid for Very Large Reynolds Numbers," C. R. Acad. Sci. U. R. S. S., 30, 301, 1941.

9. __________. "On Degeneration of Isotropic Turbulence in an Incompressible Viscous Liquid," C. R. Acad. Sci. U. R. S. S., 31:538, 1941.

10. __________. "Dissipation of Energy in Locally Isotropic Turbulence," C. R. Acad. Sci. U. R. S. S., 32:16, 1941.

11. Gibson, C. H. Scalar Mixing in Turbulent Flow, Stanford Univ. Dept. of Chemical Eng. Report SChE-62-001, 1962.

12. Grant, H. L., R. W. Stewart, and A. Molliet. "Turbulence Spectra from a Tidal Channel," J. Fluid Mech., 12:241, 1962.

13. Heisenberg, W. "Zur Statistischen Theorie der Turbulenz," Z. Phys., 124:628, 1948.

14. Batchelor, G. K., and A. A. Townsend. "Decay of Isotropic Turbulence in the Initial Period," Proc. Roy. Soc., A193:539, 1948.

15. Van der Hegge Zijnen, B. G. "Measurement of the Intensity, Intregal Scale and Micro-scale of Turbulence Downstream of Three Grids in Air," App. Sci. Res., 7A:149, 1958.

16. Frenkiel, F. N. "The Decay of Isotropic Turbulence," J. of App. Mech., 15:311, 1948.

17. Corrsin, S. "The Isotropic Turbulent Mixer: Part II. Arbitrary Schmidt Number," A. I. Ch. E. Jour., 10:870, 1964.

18. Moore, F. K. (Ed.) Princeton Series on High Speed Aerodynamics and Jet Propulsion, Vol. IV-Theory of Laminar Flows, Princeton: Princeton Univ. Press, 1964.

19. Saidel, G. M., and H. E. Hoelscher. "Chemical Reactions in the Turbulent Wake of a Cylinder," A. I. Ch. E. Jour., 11:1058, 1965.

20. Kiser, K. M., and H. E. Hoelscher. "Turbulence in the Wake of a Cylinder," Ind. Eng. Chem., 49:970, 1959.

21. Sparks, R. E., and H. E. Hoelscher. "Turbulence and Mass Transport in the Wake of a Cylinder," A. I. Ch. E. Jour., 8:103, 1962.

22. Keeler, R. N. Mixing and Chemical Reactions in Turbulent Flow Reactors, Univ. of California Lawrence Radiation Lab. Report UCRL-7852, 1964.

23. Danckwerts, P. V. "The Definition and Measurement of Some Characteristics of Mixtures," Applied Scientific Research, A, 3:279, 1953.

24. Toor, H. L. "Mass Transfer in Turbulent and Nonturbulent Systems with Rapid Irreversible Reactions and Equal Diffusivities," A. I. Ch. E. Jour., 8:70, 1962.

25. Batchelor, G. K. "Small-Scale Variation of Convected Quantities Like Temperature in Turbulent Fluid — Part I, General Discussion and the Case of Small Conductivity," J. Fluid Mech., 5:113, 1959.

26. Gibson, C. H., and W. H. Schwarz. "The Universal Equilibrium Spectra of Turbulent Velocity and Scalar Fields," J. Fluid Mech., 16:365, 1963.

27. Keeler, R. N., E. E Petersen, and J. M. Prausnitz, "Mixing and Chemical Reactions in Turbulent Flow Reactors," A. I. Ch. E. Jour., 11:221, 1965.

28. Corrsin, S. "Simple Theory of an Idealized Turbulent Mixer." *A.I. Ch. E. Jour.*, *3*:329, 1957.

29. Beek Jr., John, and R. S. Miller. "Turbulent Transport in Chemical Reactors," *Chemical Engineering Progress Symposium Series No. 25*, *55*:23, 1959.

30. Gibson, C. H., and W. H. Schwarz. "Detection of Conductivity Fluctuations in a Turbulent Flow Field," *J. Fluid Mech.*, *16*: 357, 1963.

31. Argaman, Yerachmiel, and W. J. Kaufman. "Turbulence and Flocculation," *Proc. ASCE, JSED*, *96*:223, 1970.

32. LaMer, V. K. "Coagulation Symposium Introduction," *J. Colloid Science*, *19*:291, 1964.

33. Fair, G. M., and J. C. Geyer. *Water Supply and Wastewater Disposal.* New York: John Wiley and Sons, 1967.

34. Langelier, W. F., and H. F. Ludwig. "Mechanisms of Flocculation in the Clarification of Turbid Waters," *JAWWA*, *41*:163, 1949.

35. Rich, L. G. *Unit Processes of Sanitary Engineering*, New York: John Wiley and Sons, 1963.

36. Kim, Wonsuk, H. F. Ludwig, and W. D. Bishop. "Cation Exchange Capacity and pH in the Coagulation Process," *JAWWA*, *57*:327, 1965.

37. Stumm, W., and C. R. O'Melia. "Stoichiometry of Coagulation," *JAWWA*, *60*:514, 1968.

38. Packham, R. F. "The Coagulation Process — A Review of Some Recent Investigations," *Proc., Soc. for Water Treatment and Examination*, *12*:15, 1963.

39. Black, A. P. and Ching-Lin Chen. "Electrokinetic Behavior of Aluminum Species in Dilute Dispersed Kaolinite Systems," *JAWWA*, *59*:1173, 1967.

40. Hahn, H. H., and Werner Stumm. "Coagulation by Al(III): The Role of Adsorption of Hydrolyzed Aluminum in the Kinetics of Coagulation," *Advances in Chemistry Series*, No. 79, "Adsorption From Aqueous Solution," 91, 1968.

41. Stumm, W., and J. J. Morgan. "Chemical Aspects of Coagulation," *JAWWA*, *54*:971, 1962.

42. LaMer, V. K. "Coagulation Versus the Flocculation of Colloidal Dispersions by High Polymers (Polyelectrolytes)," Principles and Applications of Water Chemistry, S. D. Faust and J. V. Hunter, (Eds.) John Wiley and Sons, 1965.

43. von Smoluchowski, M. "Drei Vorträge über Diffusion, Brownsche Molekular Bewegung und Koagulation von Kolloidteilchen, Physik. Z., 17:557, 1916.

44. ___________. "Versuch einer Mathematischen Theorie der Koagulationskinetik Kolloid Lösungen," Z. Physik. Chem., 92:155, 1918.

45. Camp, T. R., and P. C. Stein. "Velocity Gradients and Internal Work in Fluid Motion," J. Bos. Soc. Civ. Engrs., 30:219, 1943.

46. Argaman, Yerachmiel, and W. J. Kaufman. Turbulence in Orthokinetic Flocculation, SERL Report No. 68-5, Sanit. Eng. Research Lab., Univ. of Calif., Berkeley, 1968.

47. Harris, H. S., W. J. Kaufman, and R. B. Krone. "Orthokinetic Flocculation in Water Purification," Proc. ASCE, JSED, 92:95, 1966.

48. Hudson, H. E. "Physical Aspects of Flocculation," JAWWA, 57:885, 1965.

49. Levich, V. G. Physico-Chemical Hydrodynamics, 2nd Edition, New Jersey: Prentice-Hall, Inglewood Cliffs, New Jersey, 1962.

50. Saffman, P. G., and J. S. Turner. "On the Collision of Drops in Turbulent Clouds," J. of Fluid Mechanics, 1:16, 1965.

51. Parker, D. S., W. J. Kaufman, and D. Jenkins. Characteristics of Biological Flocs in Turbulent Regimes, Sanit. Eng. Research Lab., SERL Report No. 70-5, Univ. of Calif., Berkeley, July 1970.

52. Vassilatos, G., and H. L. Toor. "Second Order Chemical Reactions in a Non-Homogeneous Turbulent Fluid," A. I. Ch. E. Jour., 11:666, 1965.

53. Kramer, I. H. "Physical Factors in Chemical Reaction Engineering," Chem. Eng. Sci., 8:45, 1958.

54. Rudolfs, W., and H. W. Gehm. "Chemical Coagulation of Sewage. V — Mixing of Chemicals and Coagulation," Sewage Works Journ., 7:547, 1936.

55. Selleck, R. E., and H. F. Collins. "Disinfection in Wastewater Reuse," Paper presented at the Second Annual Univ. of Calif. Sanit. Eng. Research Lab. Workshop, Tahoe City, Calif., June 26, 1970

56. Selleck, R. E., H. F. Collins, and G. White. "Kinetics of Wastewater Chlorination in Continuous Flow Processes," Paper presented at the 5th International Water Pollution Research Conference, San Francisco, July-August, 1970.

57. ___________. Talk given at the 5th International Water Pollution Research Conference, San Francisco, July-August, 1970.

58. Riddick, T. M. "Zeta Potential and Polymers," JAWWA, 58:719, 1966.

59. Vrale, L., and R. M. Jorden. "Rapid Mixing in Water Treatment," JAWWA, 63:52, 1971.

60. Wilson, G. Work done at Sanit. Eng. Research Lab., Univ. of California, Berkeley, unpublished, 1969.

61. Lamb, D. E., F. S. Manning, and R. H. Wilhelm. "Measurement of Concentration Fluctuations with an Electrical Conductivity Probe," A. I. Ch. E. Jour., 6:682, 1960.

62. Standard Methods for the Examination of Water and Wastewater, 12th Ed., APHA, AWWA, WPCF, 1965.

63. Instruction Manual for 3C66 Carrier Amplifier, Tektronix, Inc., 1969.

64. Baines, W. D., and E. G. Peterson. "An Investigation of a Flow Through Screens," Trans. ASME, 73:467, 1951.

65. Vennard, J. K. Elementary Fluid Mechanics, New York: John Wiley and Sons, 1963.

66. Hahn, H. H., and W. Stumm. "Kinetics of Coagulation with Hydrolyzed Al(III), The Rate-Determining Step," J. of Colloid and Interface Science, 28:134, 1968.

67. Kaufman, W. J. Notes for CE 215A, Univ. of California, Berkeley, 1969.

68. TeKippe, R. J., and R. K. Ham. "Velocity-Gradient Paths in Coagulation," JAWWA, 63:439, 1971.

69. Lee, F. M. The Optimization of Chemical Precipitation-Flocculation of Municipal Wastewater, Ph. D. Thesis, Univ. of Calif., Berkeley, 1972.

☆U.S. GOVERNMENT PRINTING OFFICE:1972 514-149/104 1-3